On the Application and Generation of Subsensory Electrical Nerve Stimulation for the Improvement of Vibration Perception in Patients with HIV-Related Sensory Neuropathy

By David Karpul

For the degree of:

Doctor of Philosophy (MARCS), Western Sydney University,

Doctor of Philosophy Medicine, University of Cape Town

Primary Supervisor:

Associate Professor Paul Breen

Co-supervisors:

Professor André van Schaik,

Associate Professor Jeannine Heckmann,

Submission date:

26 August 2019

WESTERN SYDNEY UNIVERSITY

UNIVERSITY OF CAPE TOWN

IYUNIVESITHI YASEKAPA • UNIVERSITEIT VAN KAAPSTAD

TABLE OF CONTENTS

LIST OF FIGURES

LIST OF TABLES

ABSTRACT

This work investigates the application of Subsensory Electrical Noise Stimulation (SENS) to improve symptoms of HIV-related peripheral sensory neuropathy (HIV-PN). HIV-PN occurs in roughly half of the 5 million people in South Africa with HIV. The disease has been shown to reduce quality of life and increase the risk of secondary ailments. Currently there is no treatment available.

Previously, SENS has shown promise to improve tactile sensitivity in healthy populations and elderly individuals with peripheral neuropathic desensitisation. This work first establishes if SENS can improve the peripheral sensitivity of patients with HIV-PN, and secondly addresses practical aspects of using SENS in a therapeutic context.

The vibrotactile sensitivity deficits of participants with HIV-PN and a matched control cohort is documented and analysed. It is found that HIV-PN participants have reduced sensitivity at all tested vibration frequencies (25 Hz, 50 Hz and 128 Hz), but especially at low frequencies. The interaction with vibration frequency indicates that HIV-PN may interact differently with different types of peripheral mechanoreceptors.

SENS is then applied at four different amplitudes in an attempt to improve perception thresholds of the three vibration frequencies. SENS was shown to generally have a beneficial effect on 50 Hz vibration sensitivity for low SENS amplitudes. It had no effect, or a detrimental effect, at high SENS amplitudes, and also for 25 Hz and 128 Hz vibration frequencies. This work is also the first to document measures of pain with interventions of this type. No clear effects of SENS on sensations of pain were observed, which is a vital outcome if the therapy is to be developed further, since neuropathic pain is a frequent symptom of HIV-PN.

The application of SENS as a practical therapy requires the accurate measurement of the participant's electrical perception threshold, and a wearable device to apply the electrical signal on an ongoing basis. Research into the stability of electrical perception thresholds specifically aimed at subthreshold signals that would improve tactile sensitivity is presented. It was found that these thresholds vary wildly and correlated very little with possible explanatory variables, which introduces a new challenge for the development of SENS in future research.

Currently there are no devices available to apply SENS in non-laboratory settings or for continuous use. The electronic design of a stimulator for using SENS as a wearable intervention is presented and characterised. The circuit is an efficient, low-power voltage to current converter that generates high voltages (120 V peak to peak) from a small, low-voltage rechargeable battery. The design and testing of control and instrumentation circuitry, as well as the addition of various safety and interface features is also documented. The battery life of the circuit is tested to operate for up to 33 hours and the circuit is tested to operate as expected *in vivo*.

The results of this work demonstrate the potential viability of SENS as a therapy for HIV-PN, reveals the variability of electrical perception thresholds, explores the measures of pain for SENS interventions, and provides a complete and thoroughly tested design and implementation of an unparalleled electronic stimulator for non-laboratory environments. The conclusions of this work form both a strong theoretical and practical basis for future SENS intervention research.

STATEMENT OF ORIGINALITY

The work presented in this thesis is, to the best of my knowledge and belief, original except as acknowledged in the text. I hereby declare that I have not previously submitted this material, either in full or in part, for a degree at this or any other institution.

David Karpul

ACKNOWLEDGMENTS

Financial support for this work was received from Western Sydney University, the National Health and Medical Research Council of Australia and the South African Medical Research Council.

I would like to thank my supervisory team, Paul Breen, André van Schaik and Jeannine Heckmann for their contributions, each of whom in their own right were integral to this work. I would also like to thank Sarah McIntyre, Gaetano Gargiulo and especially Gregory Cohen for their constant support.

I also wish to acknowledge and thank Noluthando Primrose Mgwayi who was the field worker during the study with the participants at Groote Schuur hospital. She was absolutely amazing. I'd like to thank Russel Thompson for his help with the statistics. No doubt the thesis would not have been completed without the contributions of the mechanical workshop at UCT Human Biology and the efforts of Charles Harris. Similarly, the efforts of Colin Symons at Western Sydney.

Thank you to my academic mentor Jonathan Tapson. This is all your fault, I think it turned out very well.

Thank you to my parents for supporting me and providing me with the environment to work free of responsibility at the many times of need.

To the neglected group of people in my life who have been so important to this journey, I could write a thesis on how important you are to me, you were always needed, even at a distance. Thank you for your sacrifices and patience: Megan McLaren, Gregory Cohen, Gabrielle Prinsloo, Althea Barry, Shaun and Catherine Matthews and baby Oliver, Cesarina Edmonds-Smith and Holle Wlokes.

Thank you to my fishing buddies for looking after my mental health: Jacob Parmigiani, Emilio Caggiano, Andrew Read, Myburgh van Zijl and Garth Nieuwenhuis.

GLOSSARY AND ABBREVIATIONS

AC	Alternating Current (an electrical signal that changes in amplitude with time, usually with a periodic component). (see DC)
ADC	Analogue to Digital Converter.
ART	Antiretroviral Therapy.
Axon	Long slender nerve fibre that carries spike information/action potentials. (see Spike or action potential)
Boost	A voltage converter that increases the input voltage to a higher level.
BPNS	Brief Peripheral Neuropathy Screening tool.
Buck	A voltage converter that reduces the input voltage to a lower level.
Case-control	A scientific study design where results are compared between two groups of participants exposed to different conditions. (see Crossover)
Compliance	The amount of voltage a current source can provide in order to overcome the load impedance and achieve the desired output current.
Crossover	A scientific study design where results are compared for each subject separately between two conditions. (see Case-control)
DAC	Digital to Analogue Converter.
DC	Direct Current (an electrical signal which does not alter amplitude over time). (see AC)
Distal	Situated away from the head, centre of the body or point of attachment. (see Proximal)
Duty cycle	The ratio of ‘on’ time to ‘off’ time for something that is cycling on and off with a set frequency.
EPT	Electrical Perception Threshold.
Hallux	A person’s big toe.
HIV	Human Immunodeficiency Virus.
HIV-PN	HIV-related Peripheral sensory Neuropathy.
HVCP	High Voltage Current Pump.
HVPSU	High Voltage Power Supply.

Li-Po	Lithium-Polymer battery technology.
Noise	A time varying signal with multiple present frequencies such that a pattern cannot be observed and exact future values cannot be predicted from past values.
PCB	Printed Circuit Board.
PN	Length dependent poly-neuropathy or Peripheral Neuropathy.
PND	Peripheral Neuropathic Desensitisation.
Proximal	Situated closer to the head, or centre of the body, or point of attachment. (see Distal)
SENS	Subsensory Electrical Nerve Stimulation.
Signs	Features of a disease detected through medical examination. (see Symptoms)
Spike or action potential	A spike shaped change in the membrane voltage of a neuron occurring when a neuron is stimulated above its threshold. Spikes travel along the neuron and convey information to subsequent neurons (over simplification).
RMS	Root Mean Square, a measure of the amplitude of a signal over time. (see AC)
SR	Stochastic Resonance.
Symptoms	Features of a disease that are apparent to the patient. (see Signs)
TENS	Transcutaneous Electrical Nerve Stimulation (usually applied at perceivable amplitudes).
TF	Tuning Fork.
TNSr	Reduced version of the Total Neuropathy Screen.
VPT	Vibration Perception Threshold.

FOREWORD

The work that follows is the accumulation of projects and sub-projects completed over a period of years for the singular goal of ultimately intervening to improve tactile sensitivity in patients with HIV-related peripheral sensory neuropathy (HIV-PN).

This foreword introduces the thesis and describes the way in which the various chapters inter-relate. It further acts to highlight the challenges overcome by, and value of the work. Finally, any conventions used in writing this thesis are outlined.

Origins of the work

This thesis originates from previous work conducted by the primary supervisor, Dr Breen from 2012 to 2015, which showed improvements in tactile sensitivity in healthy and elderly participants when using benchtop equipment to stimulate participants' peripheral nerves in a particular manner. The intervention uses Subsensory Electrical Nerve Stimulation and has been dubbed SENS. Little was known about how SENS worked, and consequently which types of peripheral neuropathic desensitisation could be affected. Further, SENS was only known to have an effect while being applied, but no tool existed that was capable of applying it in everyday life.

At a similar time, The University of Cape Town (South Africa) was conducting a follow-up examination of a cohort of patients with HIV. The study sought to document the progression of various physiological parameters prospectively over a period of years after enrolment in an anti-retroviral therapy program. It was very evident that the prevalence of HIV-PN was extensive.

The original project goals where thus firstly, to investigate if Dr Breen's SENS would be effective in reducing symptoms of HIV-PN, and secondly, to research and address limitations that prevented SENS from being used in non-laboratory conditions.

To this end, a partnership between the two universities was formed. Work relating to the question of how to apply the intervention was the realm of Western Sydney University (Australia), and work with the HIV patients was the realm of The University of Cape Town (South Africa).

Chapter descriptions

Chapter 1 presents an extensive analytical review of prior work attempting similar interventions to improve sensory perception. The meta-analysis contained therein examines results from the existing literature in detail, identifying several "holes" in the previous research and where scientific rigor could be improved. Chapters 2, 3, 4, 5, and 6 seek to fill some of those holes, but were not necessarily conducted in sequence, and in many instances the work ran in parallel.

Chapters 2 and 3 document research completed at the University of Cape Town, working with HIV patients diagnosed with HIV-PN, and age matched control participants. It cannot be overstated how unique and challenging this population is to work with, and how fortunate we were to have this opportunity. Both cohorts primarily live in shanty towns, have limited access to technology and for the most part, grew up in a socio-political and economic context where they were denied various human rights including access to education and health care. More than 5 million people in South Africa have HIV, the vast majority of which still live with the adverse effects of Apartheid in their daily lives. Compare this to Australia where there are only 25 000 people with HIV.

We entered into this research with a fair degree of ignorance as to how alien our research was and how difficult it would be to communicate the experimental tasks. In retrospect, our plan to have a young white man (the researcher) in a closed office, doing experiments with black South African women, was a significant oversight considering the social relations in post-Apartheid South Africa. Our saving grace was the expertise and skill of Noluthando Primrose Mgwayi, our fieldworker who recruited our patients and controls, acted as a translator, both in language and culture, and sat in on all the patient testing. The research would have failed without her.

Chapter 2 creates the premise for Chapter 3. In order to intervene to improve tactile sensitivity of patients with HIV-PN, first we must document the effects of the disease on vibrotactile sensitivity compared to a matched control cohort. This work presents the first such documentation with HIV-PN using a double blinded protocol at various vibration frequencies, measuring perception levels in mechanical units which can be repeated by others. Chapter 2 in part has been published in "Brain and Behaviour", an open access peer-reviewed journal [1]. The target audience for this work is those

working in fields linked with neuropathy, as opposed to Chapter 3, which has a target audience of those working to develop this particular class of tactile intervention.

Chapter 3 uses the baseline data collected in Chapter 2 and investigates the effects of SENS in this cohort. It should be noted that even the control, non-HIV participants are sufficiently different from past research that it is uncertain as to whether they will exhibit a response to SENS. This chapter is the first report of the effect of SENS with HIV-PN and also the first to report changes in symptoms of pain in response to this class of intervention. This addresses an important short-coming of past work and will hopefully lead to the inclusion of neuropathic pain assessment in future research attempting to enhance tactile sensitivity in neuropathic populations.

This work has yet to be submitted as a journal publication, but preliminary findings of this work were presented in part at the Australasian Neuroscience Society Annual Scientific Meeting in 2016 [2].

The application of SENS required the measurement of the participant's electrical perception threshold. It was clear during the measurement of the data for Chapter 3 that this threshold did not behave in the stable and easy to detect manner described many times in the literature. We suspected that, through using simple single blinded measurement protocols, along with the strong expectation that this variable was stable, past researchers had placed reality into a preformed mould. Since the stability of the electrical perception threshold is core to the theory of operation of SENS, this justified research into the idea independently of other research questions.

Chapter 4 presents the only known research into the stability of electrical perception thresholds specifically aimed at subthreshold signals that would improve tactile sensitivity. We found that these thresholds vary wildly and correlated poorly with possible explanatory variables. This matched well with observations made when trying to apply these subthreshold signals in Chapter 3, where finding the threshold was like chasing a rabbit in the dark. Indeed, even when found with certainty, in the experiments, mere minutes later, the previously subthreshold signal could become apparent to the participant.

This research raises a big and important flag in the use of SENS and other subthreshold interventions. However, it does not propose a solution beyond recommending further research into the topic.

This chapter was published in part as a paper and presentation at the 2017 39th Annual International Conference of the IEEE Engineering in Medicine and Biology Society (EMBC) [3].

Chapters 5 and 6 present the design of a SENS stimulator for wearable interventions. Part of Chapter 4 characterised the impedance of the connection between the stimulator and the participant. This data demonstrated that high voltages would be needed to apply SENS. The design of a high-voltage stimulator for arbitrary signals, that is also small and battery operated is very challenging. An experienced biomedical electronics-engineer at several points during the design pointed out that aspects of what we were attempting were "impossible". We present the work in the chapter as a clear solution to the problems faced in the design. However, in the academic context it is difficult to bring across just how challenging it was to develop this circuit. The work took three years to develop to completion.

Chapter 5 documents the design of the base circuitry for voltage to current conversion at high voltages from a low voltage battery. The characterisation of the circuit is published in "BioMedical Engineering OnLine" [4]. The design is shown to perform much better than other designs that may compete in a similar design space. Presenting only the voltage to current converter allows other researchers to adapt the design, implementing controlling interfaces appropriate for their needs.

Upon completion of this design block we faced a fork in the road. We could choose to delve into computational neuroscience, in an attempt to use finite element modelling and complex neuron models to further understanding of how the electrical stimulation passes through the skin and tissue to stimulate the sensory axons and enhance the transmission of signal. Or, we could choose to complete the electronic design of the published stimulator. Considering that 1) the electronics had shown such promise to help with future research, extending beyond interventions to improve tactile sensitivity, and 2) the modern research environment holds greater value in producing tangible outputs with real world impact, it was a clear decision that the design should be completed and tested *in vivo*.

Chapter 6 documents the design of control and instrumentation circuitry for the voltage to current converter as well as the addition of various safety and interface features not found in the original design. The battery life of the circuit is tested under various

circumstances to prove how appropriate the device is for applications requiring continuous daily use. Finally, the circuit is tested to operate as expected *in vivo*. The graph in Chapter 6 demonstrating the circuit accurately driving a multi-frequency current signal into 5 participants, together with measured battery life of 18 to 33 hours succinctly demonstrates the ultimate output of years of difficult design work. Chapter 6 in part has been submitted for publication in "IEEE Transactions on Biomedical Circuits and Systems" (TBioCAS). The full design has been handed over to an industrial design firm for modification to convert into a production ready device.

While completing the design it became evident that the original power supply needed to be changed. However, with a multitude of design variables to be balanced, a trial and error process of building circuits would not result in an optimal power supply design.

The parts being used were not readily available in libraries for modelling software such as SPICE. Consequently, to investigate different power supply architectures and optimise the design, a novel circuit-modelling framework was created. The simulations resulted in a regulated power supply that is over 30% more efficient than commercially available solutions. The modelling software developed and the power supply architectures investigated are documented in **Appendix B**.

Thesis conventions

The chapters in this thesis are designed to be read independently of each other. Consequently, a small amount of repetition occurs, especially in the introductions. Further, Chapters 2 and 3 report data from the same parent study and a certain amount of repetition occurs in the description of the methods and participant cohort.

Abbreviations are declared the first time they are used in each chapter regardless of use in previous chapters.

The use of the plural, such as "we", to refer to the author is used on occasion, especially to facilitate the 'active voice' in the written language. Be assured that work I cannot legitimately claim as my own will be clearly highlighted in the text as such.

As there are different types of controls in different parts of the thesis, such as control participants, and control test conditions, the word "control" could become confusing. In most instances the use of the word 'control' will be avoided and a replacement term defined where needed.

I hope you enjoy reading this work. I am very proud of it.

ACADEMIC OUTPUTS ASSOCIATED WITH THIS THESIS

The following is published or submitted academic outputs from this thesis:

The work in Chapter 2 was published in part in "Brain and Behavior":

Karpul D, McIntyre S, van Schaik A, Breen PP, Heckmann JM. Vibrotactile sensitivity of patients with HIV-related sensory neuropathy: an exploratory study. Brain and Behavior. 2018, e01184, doi: 10.1002/brb3.1184

The work in Chapter 3 was presented in part at the Australasian Neuroscience Society Annual Scientific Meeting in 2016:

Karpul D, McIntyre S, Heckmann JM, van Schaik A, Breen PP. On the Application of Subsensory Electrical Nerve Stimulation for the Improvement of Vibration Perception in Patients with HIV Related Peripheral Neuropathy. Australas. Neurosci. Soc. Annu. Sci. Meet. 2016 Abstracts for Poster Presentations, 2016, p. 67.

The work in Chapter 4 was published in part as a paper and presentation in the 2017 Annual International Conference of the IEEE Engineering in Medicine and Biology Society (EMBC):

Karpul D, McIntyre S, Van Schaik A, Breen PP. Measurement of perception thresholds for electrical noise stimuli. Proc. Annu. Int. Conf. IEEE Eng. Med. Biol. Soc. EMBS, 2017, p. 2166–9. doi:10.1109/EMBC.2017.8037284.

The work in Chapter 5 was published in part in BioMedical Engineering OnLine:

Karpul D, Cohen GK, Gargiulo GD, van Schaik A, McIntyre S, Breen PP. Low-power transcutaneous current stimulator for wearable applications. Biomed Eng Online 2017;16:118. doi:10.1186/s12938-017-0409-9.

The work in Chapter 6 has in part been submitted to be published in IEEE Transactions on Biomedical Circuits and Systems (TBioCAS):

Karpul D, Jayarathna T, Cohen GK, Gargiulo GD, van Schaik A, Breen PP. Continuous-current stimulator for transcutaneous wearable applications. Submitted to TBioCAS 2018

1

ANALYTICAL REVIEW ON THE APPLICATION OF SUBSENSORY SIGNALS FOR THE IMPROVEMENT OF PERIPHERAL SENSITIVITY

Peripheral desensitisation is a common problem that is caused by a multitude of prevalent diseases. Currently there are no symptomatic treatments for loss of peripheral sensitivity, however a family of intervention studies over the past 20 years, which applied subthreshold external signals to the limbs, have shown that it is possible to improve sensitivity in some population groups. This review provides meta-analysis of this class of research and suggests future research directions for this form of therapy. 43 studies, and a total of 277 outcome measures met the inclusion criteria and collectively demonstrate that subsensory signals can be used to enhance peripheral sensation in a multitude of settings. We found that improvements in scientific rigour, and scientific reporting are needed. High quality investigations into the mechanisms of the improvement in parallel with investigations into non-laboratory long-term applications are also needed. Overall the methodology shows promise for being developed into an intervention to combat the symptoms of various diseases causing peripheral desensitisation.

1.1 Introduction

Peripheral desensitisation is a common problem that can be caused by diabetes, stroke, alcoholism, HIV, aging and many other conditions. It is estimated that 20-30 million people worldwide suffer symptomatic diabetic neuropathy [5]; approximately 50-85% of stroke survivors have reduced somatosensory performance [6–9]; all people with aging have reduced peripheral sensation [10]; in South Africa, as many as 1.8 million people suffer HIV-related peripheral neuropathy [11].

Length dependent poly-neuropathy, the most common form of peripheral neuropathy (PN), causes reduced tactile sensation primarily in the extremities, and dramatically impacts quality of life. Foot ulceration [12] is common, but not in HIV-related PN, and can result in lower extremity amputation [13]. Plantar sensitivity also affects balance [14–18] and increases the risk of falling [19]. Falls account for the highest proportion of hospital admissions, hip fractures and accidental death in individuals over the age of 65 [16,20,21]. Tactile feedback from the hand is important for maintaining motor control [22–24], and impaired hand sensation reduces the ability to approximate grip force and manipulate objects [25,26]. Ultimately, reduced hand function affects vocation and self-care [27] as well as resulting in reduced use of the hand [28]. Specifically, HIV-related sensory neuropathy has an adverse effect on health related quality of life [29].

Currently there are no treatments for loss of peripheral sensitivity [30]. However, a family of intervention studies over the past 20 years, which applied subthreshold external signals to the limbs, have shown that it may be possible to improve sensitivity in some population groups. These studies sought to improve tactile sensitivity by applying either an electrical current or a mechanical signal to the extremities. The signal itself is low enough in amplitude that the participant cannot perceive its presence (subsensory, subperception, or subthreshold). In each of these exploratory studies the intervention is not shown to continue to have an effect once removed. In this sense the therapy is not meant to treat the underlying condition, but rather to reduce symptoms and enable function while it is in use. Most of these studies prescribe to a common scientific method. First, the intervention or treatment, either a mechanical vibration or an electric current is applied to the participant at different amplitudes to establish the perception threshold of this particular intervention, for this particular participant. The intervention signal is then set to a subthreshold value, usually a set percentage of the

perceptual threshold. Finally, some other functional measure is made with and without the intervention turned on, to establish the interventions influence on the measure. Common output measures are touch sensitivity, or balance performance.

Figure 1 shows a typical application of an electrical intervention for the improvement of tactile sensitivity at the Hallux (big toe). The current is applied across the tibial nerve that sub-serves the tactile receptors of the plantar aspect of the foot [31]. The biological effect of an electrical current injected into a sensory axon is well understood [32–34], but the effect of applying a current through the limb and across the axon is a substantially more complex problem. The manner in which the current distributes in the limb tissue and the effect of simultaneous, and different, currents within the same nerve compartment is not understood, and is beyond the scope of this work. Despite this, several statements can be made about the effect of subsensory stimulation on the biopotentials of the nerve.

A bidirectional current stimulation will cause both hyperpolarisation and depolarisation of the nerve membrane potential in the region of the stimulation. The changing membrane potential is likely to have an effect on the passage of action potentials through the nerves in this region, modifying their timing and amplitude. Further, the stimulation will force the nerve into a different region of its dynamic response, potentially allowing for action potential generation under conditions that would previously have not produced action potentials, and *vice versa*.

Collins *et al.* in 2003 published a functional summary of various intervention methods and outcomes that provides adequate background to the general format of participant testing in this field [21].

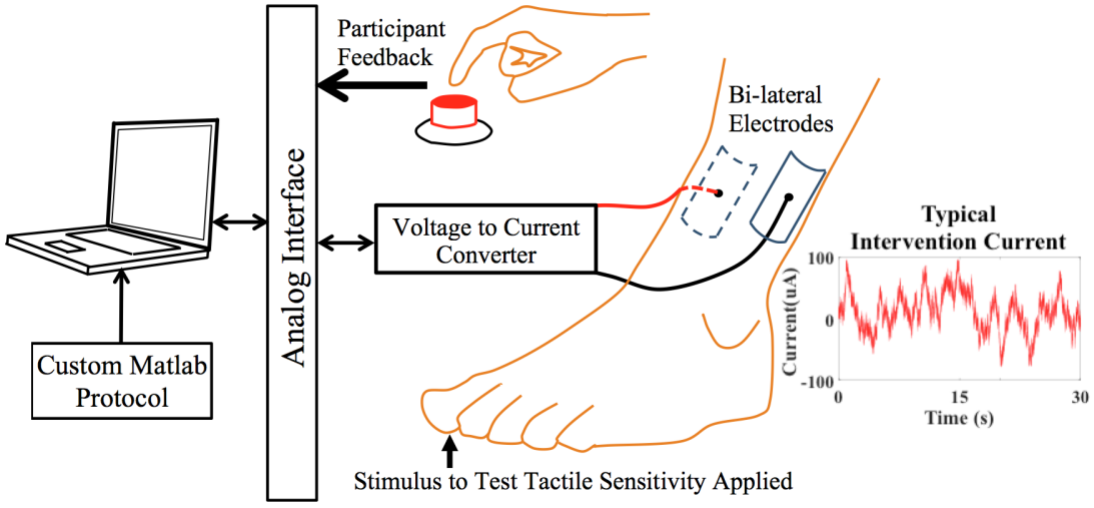

Figure 1. Typical application of Subthreshold Electrical Stimulation proximal to the site where tactile sensitivity is to be tested.

While there is a substantial body of literature, and many different types of interventions and outcome measures used, a cohesive picture of this research field, and where it should head, has yet to emerge.

1.1.1 Scope

This literature review attempts to incorporate all studies investigating interventions using subsensory stimuli to improve peripheral sensation or related measures through *in vivo* experiments published in 2015 or earlier. Studies included for analysis were required to be published in English peer-reviewed journals or presented as part of a published scientific conference proceeding. Studies were searched for using online databases, such as PubMed and Google Scholar and extended to cited and citing articles.

This review does not cover methods of enhancing other sensing modalities such as the vestibular system [35–37], hearing [38,39], sight [39–42] and blood pressure [43]. This review does not cover supra-threshold interventions such as Transcutaneous Electrical Nerve Stimulation (TENS) [44] or chemical interventions such as limb deafferentation [45,46].

In several cases a study is presented in part as a conference preceding and then presented again as a full paper. In these cases, only the fullest presentation of the work

is included for analysis. Additional articles outside of the abovementioned scope are included for discussion but not analysis.

1.1.2 Aims

This review will evaluate and describe the success of these interventions collectively, identify gaps in the literature and discuss the proposed mechanism by which the interventions have an effect on peripheral sensitivity. Further, the general scientific quality of the literature will be evaluated.

This review, unlike many systematic reviews, does not aim to establish any form of medical treatment best practice, but rather to aid in directing future research. Analyses performed are akin to those performed in formal systematic reviews, however are not designed to provide specific numerical outcomes, rather simply portray trends in the literature to possibly guide future work. While the heterogeneous nature of the various study outcomes strictly makes the analysis performed inappropriate, the results can still be informative.

1.2 Origins of subsensory interventions

The first studies to use subsensory interventions in humans for improvement of peripheral sensitivity was Collins *et al.* in 1996, who showed increased ability to detect a mechanical perturbation that was summed with white-noise vibration, and Cordo *et al.* who showed stochastic resonance (SR) in muscle-spindle afferents at the same time [21,47–49].

Earlier work focusing on characterising tactile sensitivity, and the sensory mechanisms through which vibration is perceived in the presence of subthreshold external signals, rather than researching a potential intervention, had also been conducted, but is generally not recognised as the genesis of subthreshold noise interventions [50–52]. The earlier work found that sensitivity was enhanced by signals with the same characteristics, such as a single frequency 70 Hz sine wave vibration “pedestal”, aiding in the detection of 70 Hz vibration stimuli. The studies did investigate the effect of mechanical noise at different near threshold amplitudes but did not find an enhancement of tactile thresholds in contradiction to future work.

Collins showed, in accordance with theory in SR [53,54], that if the intervention noise was too small the participant showed no improvement in tactile sensitivity and if the noise was too large it drowned the perturbation to be detected. This created a classic

inverted “u” shape for the benefit versus intervention amplitude, which held true for many experiments that followed. The term “stochastic resonance” has been called into question, with the term “stochastic facilitation” being motivated as more appropriate [55]. The motivation given is that SR is a specific theoretical model of how added noise can improve performance, but most experimental work only shows that the added noise creates improvements, not that it occurs through the specific mechanism of SR. Despite this, the term “stochastic resonance” is used here to remain consistent with those who reported in their research using this term.

Since then many interventions have been attempted. Table 1 describes each study’s intervention, intervention signal’s frequency characteristics, the outcomes measures and investigated populations. Before proceeding to Table 1, the following text describes how the characteristics of each study were classified for use in the table.

1.3 Classification of existing literature

43 studies, and a total of 277 outcome measures were selected for inclusion in this review. Table 1 summarises the characteristic of each study according to the following criteria.

1.3.1 Intervention signal classification

The interventions used can be categorised using two factors. The first is the mode of the intervention signal (mechanical or electrical). Mechanical interventions take the form of a vibrating element of some description that induces perturbations in the tissue, so as to improve peripheral sensitivity. Electrical interventions take the form of an electric current applied through the skin for the same purpose.

The second factor is the location of the applied intervention signal, distal or proximal. Distal interventions are applied at the site of sensory enhancement and proximal interventions are applied proximal to the site of enhancement.

An example of an intervention that acts proximal to the site of enhancement would be the application of the therapeutic intervention at the forearm, to improve sensitivity at the fingertips. Proximal application allows the extremities to be free of devices while still receiving the benefit distally where sensitivity is of greater importance.

The therapeutic signal itself is a time varying waveform and has a particular frequency spectrum. This can generally be categorised as single frequency (a sine wave, or in one

case a triangular wave), white (noise with a flat frequency spectrum), pink (noise with an inverse relationship with frequency) or 'not given'. Each spectrum can be further described by a frequency bound with lower and upper limits in Hz.

1.3.2 Outcome measure classification

Each study can have several outcome measures. In this analysis we seek to categorise similar output measures in an attempt to reduce the amount of heterogeneity in the subsequent analysis. A full description of each outcome measure is beyond the scope of this work, but any one measure can be more closely examined by reviewing the related article reference in Table 1. Six outcome measure categories were devised.

Detection Tasks (DT) seek to identify a change in sensory threshold by evaluating the participant's ability to detect certain stimuli. Detection tasks include indentation detection, vibration detection, Semmes-Weinstein monofilament detection, two-point discrimination and one-point touch test. In each case a form of threshold is established above which more correct detections occur, and below which fewer correct detections occur. Assessments of variability in the outcome of detection tasks are not detection task output measures themselves but are classified as a proxy measures instead (see Proxy Measures).

Balance Measures (BM) are all measures of postural sway during still standing. These include centre of pressure motion parameters (area swept, total path length, mean centre of pressure (COP) radius, maximum excursion and standard deviation along perpendicular axes); as well as more advanced balance parameters: critical mean square displacement, effective long-term diffusion coefficient and long-term scaling exponent.

Gait Measures (GAIT) are all measures relating to how a person walks and include joint ranges of motion, moments around joints, walking speed, and various stance parameters included ground reaction forces.

Physiological Measures (PHY) are measures that document what is occurring in the internal biochemical or bioelectrical physiology of the participant. These measures include inter-spike timing of single sensory neurons in response to mechanical stimuli (*in vivo*), timing variability of stimulated sensory neurons (*in vivo*), and reaction times of muscle activity recorded with electromyography and electroencephalography measures.

Practical Tasks (PRAC) measure the competency of particular tasks which correlate to everyday activities. These include the nine-hole peg test, the box and block test, texture discrimination test and the timed up and go test.

Proxy Measures (PROX) are outputs indirectly affected by peripheral sensitivity. These include pinch grip, shear force, active range of motion for a joint (not during gait), hand stabilisation time after perturbation, minimal force grasping and variability in other measures such as detection tasks. Some categories, such as balance measures, are a form of proxy task, but for the sake of this analysis they have been considered separately to be more informative to the reader.

1.3.3 Participant classification

Many population groups can benefit from improvement of peripheral sensitivity. The studies presented here investigate healthy younger (HY) individuals, elderly individuals (ELD), post stroke individuals with a peripheral insensitivity component (STR), individuals with ankle instability (ANK), individuals with knee osteoarthritis (OST), single below knee amputees (AMP), and individuals with diabetic neuropathy (DN). One study investigated a subcategory of ELD, elderly fallers, and elderly non-fallers. This distinction is made clear where relevant.

1.3.4 Study design

All studies, with the exception of three, made use of a crossover design where each participant acts as their own control. Hoskins *et al.* 2015 [56], Ross *et al.* 2006 [57] and Ross *et al.* 2007 [58], used a case-control design with two groups of participants, one group receiving the intervention and one receiving a placebo. This is a weaker scientific method for investigating possible interventions. Despite this, these studies have been included for analysis.

1.4 Numerical Analysis

A wide array of data was extracted from each study. In addition to the variables listed in Chapter 1.3, information regarding participant age, gender, the amplitude of the treatment signal, the method of determining the sensory threshold for the treatment signal, details regarding the blinding used in the study and finally the actual outcome measures were captured (see Chapter 1.4.2 for more information regarding the extraction of the study outcome measures). The full raw dataset is available in the folder, “Literature review data” in the digital appendix.

1.4.1 Summary statistics

Table 1 provides a summary of the primary distinguishing characteristics of the included studies. Aside from the works by Collins *et al.*[1] [59–62], most of the studies were small with participant numbers ranging from 5 to 18. There were a similar number of studies investigating mechanical interventions and electrical interventions, and also a similar number investigating distal interventions and proximal interventions (see Table 2). When mode and location are examined in combination, electrical interventions appear to favour the use of proximal interventions, whereas mechanical interventions have a moderate bias toward distal interventions.

Table 1. Classification of 43 studies using subsensory signals *in vivo* to improve peripheral sensitivity listed by publication year. The total number of each output measure is placed in brackets and a '*' indicates statistical significance at at-least p<0.05 was found, suggesting success of the intervention. Participants: HY = Healthy Young, ELD = Elderly, DN = Diabetic Neuropathy, STR = Stroke, AMP = Single Leg Amputee, OST = Knee Osteoarthritis, ANK = Unstable Ankle and n = number of participants. Output Measures: DT = Detection Task, BM = Balance Measure, GAIT = Gait Variable, PHY = Physiological Measure, PRAC = Practical Task, PROX = Proxy Measure.

First Author Year	Mode	Location	Spectrum [Bandwidth (Hz)]	Participants(n)	Output Measures
Collins 1997 [48]	Mechanical	Distal	White [0 30]	HY(10)	DT*(1)
Richardson 1998 [63]	Electrical	Distal	White [0 30]	HY(11)	DT*(1)
Dhruv 2002 [64]	Electrical	Distal	White [0 1000]	ELD(9)	DT*(1)
Gravelle 2002 [15]	Electrical	Proximal	White	ELD(13)	BM*(7)
Liu 2002 [65]	Mechanical	Distal	White [0 100]	DN(8), ELD(12), STR(5)	DT*(4)
Priplata 2002 [18]	Mechanical	Distal	White [0 100]	ELD(16), HY(14)	BM*(16)
Khaodhiar 2003 [66]	Mechanical	Distal	Noise	DN(20)	DT*(3)
Priplata 2003[16]	Mechanical	Distal	White [0 100]	ELD(12), HY(15)	BM*(16)
Wells 2005 [67]	Mechanical	Distal	White [0.125 25], [0.125 50], [25 500], [50 500]	ELD(6), HY(6)	DT*(16)
Priplata 2006 [17]	Mechanical	Distal	White [0 100]	DN(15), STR(15)	BM*(16)
Ross 2006 [57]	Electrical	Proximal	White	HY(2×10), ANK(2×10)	BM(4)
Lee 2007 [68]	Electrical	Proximal	Triangular, 2 Hz	AMP(5)	BM*(4)
Ross 2007 [69]	Electrical	Proximal	White	ANK(12)	BM*(1)
Ross 2007 [58]	Electrical	Proximal	White [not given 1000]	ANK(2×10)	BM*(5)
Hijmans 2008 [70]	Mechanical	Distal	White [25 500]	DN(17), HY(15)	BM*(24)
Collins 2009 [71]	Electrical	Distal	White [0 1000]	HY(12)	PROX(4)

[1] Note that the Collins (Amber) in publications from 2009 onward is a different Collins to in the influential Collins 1997 (James) publication and subsequent studies where he is a co-author.

Galica 2009 [72]	Mechanical	Distal	White [0 100]	ELD(fallers)(18), ELD (non-fallers)(18), HY(12)	GAIT*(9)
Breen 2011 [30]	Electrical	Proximal	Noise	HY(10)	DT*(1)
Collins 2011 [60]	Electrical	Proximal	White [0 1000]	OST(52)	PHY*(3), PROX(1), GAIT(6)
Collins 2011 [61]	Electrical	Distal	White [0 1000]	OST(38)	PROX(2)
Collins 2012 [59]	Electrical	Proximal	White [0 1000]	OST(52)	BM*(7)
Magalhães 2012 [73]	Electrical	Proximal	White [5 2000]	HY(10-11)	BM*(5), PROX*(2)
Kurita 2012 [74]	Mechanical	Distal	White [0 300]	HY(11)	PRAC*(1)
Breen 2013 [75]	Electrical	Proximal	Pink	HY(6-7)	DT*(1), PHY*(1), PROX(1)
Enders 2013 [76]	Mechanical	Proximal	White [0 500]	STR(10)	DT*(2)
Ross 2013 [77]	Mechanical	Proximal	White [0 100]	HY(12), ANK(12)	BM*(10)
Sueda 2013 [78]	Mechanical	Distal	White [0 300]	HY(12)	DT*(1)
Kurita 2013 [79,80]	Mechanical	Distal	White [0 300]	HY(11)	DT*(2), PRAC*(1), PROX*(1)
Ribot-Ciscar 2013 [81]	Mechanical	Proximal	White [0 100]	HY(10)	DT*(1)
Breen 2014 [31]	Electrical	Proximal	Pink	HY(10)	DT*(1), PROX*(1)
Collins 2014 [62]	Electrical	Proximal	White [0 1000]	OST(35)	GAIT*(16)
Hur 2014 [82]	Mechanical	Proximal	White [0 500]	HY(18)	PHY*(1), PROX*(1)
Iliopoulos 2014 [83]	Electrical	Distal and Proximal	White [0 200]	HY(10-12)	DT*(23)
Magalhães 2014 [84]	Electrical	Proximal	White [5 2000]	HY(11)	BM*(9)
Seo 2014 [85]	Mechanical	Proximal	White [0 500]	STR(8-10)	DT(1), PRAC(2)*, PROX(3)*
Keshner 2014 [86]	Mechanical	Distal	White [10 55]	HY(21)	BM*(5)
Hoskins 2015 [56]	Mechanical	Proximal	White [0 300]	HY (4×2)	PRAC*(2)
Lakshminarayanan 2015 [87]	Mechanical	Proximal	White [0 500]	HY(12)	DT*(2)
Lipsitz 2015 [88]	Mechanical	Distal	Not given	ELD(12)	BM*(4), PRAC*(1), GAIT*(5)
Ross 2015 [89]	Mechanical	Proximal	White [0 100]	HY(12), ANK(12)	PROX*(6)
Dettmer 2015 [90]	Mechanical	Distal	White [1 500]	ELD(9), HY(10)	BM*(8)
Wang 2015 [91]	Mechanical	Proximal	White [10 1000]	Not given (5)	DT*(1)
Breen 2016 [92] **reporting on Breen 2011**[30] **and Serrador 2012** [93]	Electrical	Proximal	Pink	ELD(8)	DT*(4)

Table 2. Frequency table characterising the location (distal or proximal) and nature (mechanical or electrical) of the intervention signal in the included studies. One study is counted twice as being both proximal and distal as both interventions were examined. This results in 44 data points for 43 studies. Percentage in brackets.

	Mechanical	Electrical	Total
Distal	15 (35%)	5 (12%)	20 (47%)
Proximal	9 (21%)	15 (35%)	24 (56%)
Total	24 (56%)	20 (47%)	44 (102%)

The vast majority of studies used white noise as their intervention signal usually low pass filtered to 500, 300 or 100 Hz. Only Breen *et al.* made use of pink noise (See Chapter 3.2.3 for more details on the noise signal use by Breen *et al.*).

The studies investigated signal amplitudes ranging from 5% to 90% of detection threshold, with a number of studies declaring their amplitude as "subthreshold" with no percentage or absolute amplitude given. Studies investigating the effect of different subthreshold amplitudes usually found an effect between 60% and 90% of threshold but the best level was study dependant, and in several cases allowed to be participant dependant (*e.g.* [69,73,77,92,94]).

The subsensory nature of the intervention lends itself well to the design of blinded studies. However, blinding was not well reported in the manuscripts with only 4 studies (9%) being definitely double-blinded and a further 8 (19%) possibly being double-blinded, but failing to report so. 16 studies (37%) were definitely single-blinded, with a further 3 (7%) being probably single-blinded, and 9 (21%) being possibly single-blinded, but it was not made clear in the text. Only 3 (7%) failed to provide enough information to infer anything about the blinding used in the study.

Studies needed to establish what the sensory threshold for the intervention signal was in order to ensure the signal was subsensory and to control for relative amplitude of the intervention signal. 9 (21%) of the studies failed to provide a method of threshold determination, or none was used. 15 (35%) are recorded to have used a "self-determined" method, where the participant determines their threshold with no scientific method being applied. 5 (12%) used a single direction method of limits or levels, and 13 (30%) used a method of limits or levels in both ascending and descending modes.

Only one study used a forced choice paradigm to produce the sensory threshold for the intervention signal.

1.4.2 Data extraction for meta-analysis of outcome measures

The Cochrane organisation, known for producing high quality systematic reviews, provides a tool for producing analytical literature reviews, Review Manager (RevMan) [95]. The program can produce various statistical outputs and automated graphics, and requires that for each output measure, that the user provides a signed (beneficial or detrimental) effect magnitude, and a standard error (SE) for this effect.

In the context of this review, we required from each study, the mean percentage change from the control (sham) condition, when applying the subthreshold signal, and the SE of this percentage change. These two outputs must be for paired analysis and not group analysis.

Studies often presented the data in formats inappropriate for this analysis. The most prevalent error was presenting group data instead of paired data, but performing a paired analysis. This took the form of providing the mean of the group of participants in the sham condition, and the mean of the group of participants in the experimental condition for a given output measure, and their associated variabilities, usually standard deviation (SD).

The difference in the means of the groups, is mathematically equivalent to the mean of differences in the paired data, thus the mean effect was easily recoverable. However, there is no perfect way to recover the variability data (SE) from the two group SDs. In these cases standard errors were calculated using the methodology described in [96] from the extracted p-values to infer what the variability must have been to get such a result.

In 128 of 277 output measures, data was extracted from graphical representations using a custom written Matlab program developed as part of this work (See digital appendix folder “Data Extraction Tool”). The program loads a screenshot of a graphic from a paper, allows the user to manually identify the axis and limits, and then allows the export of individual data points contained within the image.

Not every output measure from every study was extracted. Studies often swept various parameters, essentially measuring the effect of many different versions of the intervention. Only the most optimal data of each output measure was extracted (for

example, the outcome for an optimal amplitude of intervention signal, rather than all levels intervention). Only outputs that represented the effect of the intervention over an appropriately matched sham condition were extracted.

1.4.3 Forrest plot analyses

Review Manager was used to produce two different types of meta-analyses. Firstly, we produced analyses of the mean effect of the intervention on each outcome measure category weighted to the level of certainty that each measure affords through its stated variability. This is graphically represented as a "forest plot" for each outcome category, which shows a single data point for outcome measure, and the associated 95% confidence interval.

Calculated study outputs in the meta-analysis were removed if they were considered outliers. This was done to prevent individual studies from dominating the overall analysis, and because outlier studies are less likely to represent the true outcome value, not more. Items with a percentage change from sham of more than 3.5 SD (odds of 1 in 2149) away from the mean of that output type were removed. This was also done for the SE, although items with a large SE have little weight in the analysis. 4 of 141 balance measures, 2 of 66 detection tasks, 1 of 36 gait measures, 1 of 22 proxy tasks and 1 of 7 practical tasks were removed. In addition, 2 of the remaining 137 balance measures, 3 of the remaining 64 detection tasks and 3 of the remaining 35 gait measures with small SEs were also removed because their weighting was greater than greater than 20%, causing the overall results to have a strong bias towards those specific outcomes.

Figure 2 to Figure 10 are the outputs of the forest plot analysis. Studies appear more than once if they have multiple output measures in that category. The overall effect of each study type is shown as a black diamond with width proportional to the confidence interval of the overall effect at the bottom of the figure[2].

[2] In some cases, the width of the black diamond is so narrow that the diamond is barely visible. The mean and confidence interval are represented in numeric form on the left of the figure.

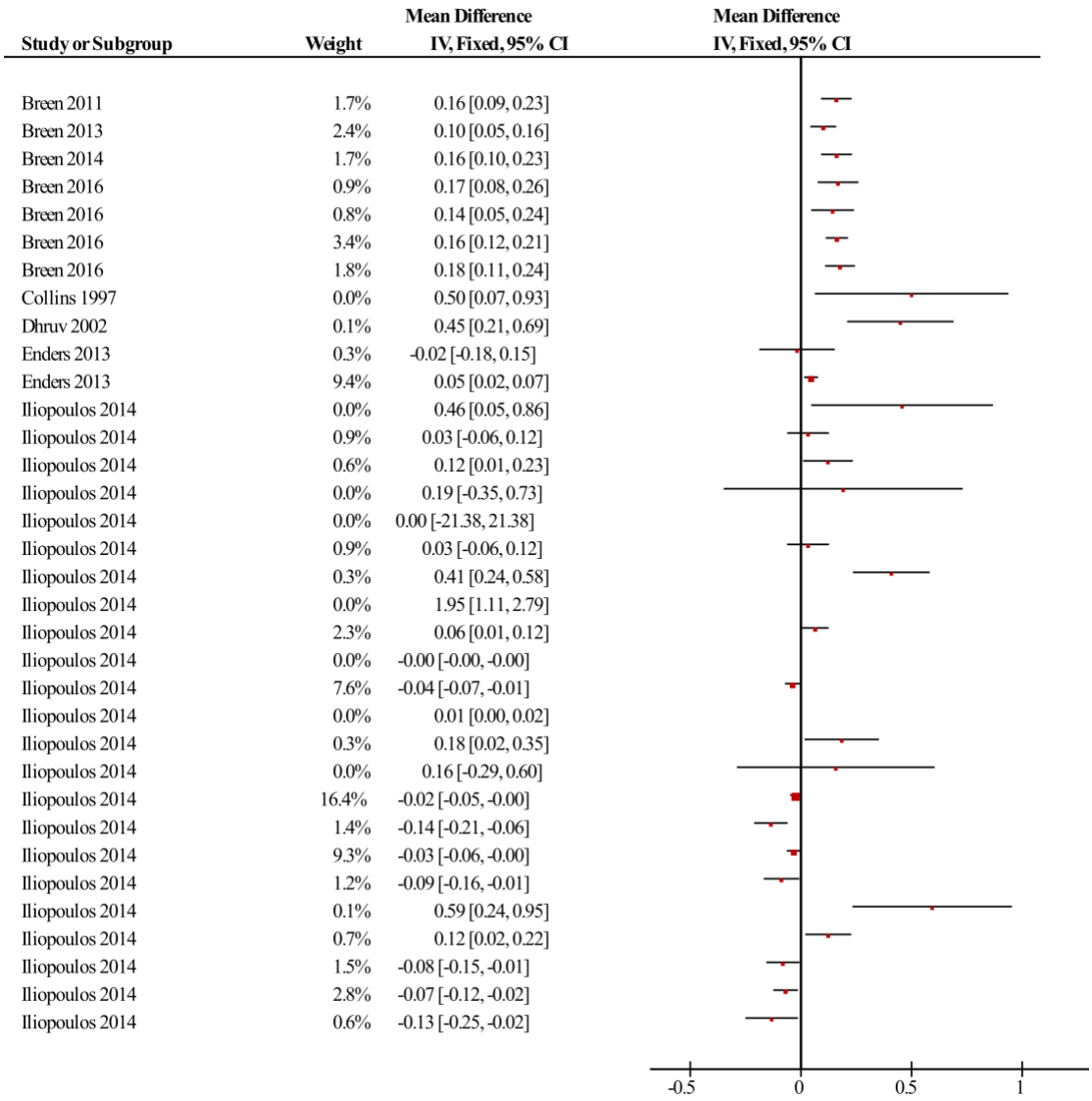

Figure 2. First half of the forest plot for the Detection Task outcome measures listed alphabetically by first author. Outputs are normalised to a fraction of 1 relative to the sham condition. Positive data points represent beneficial effects.

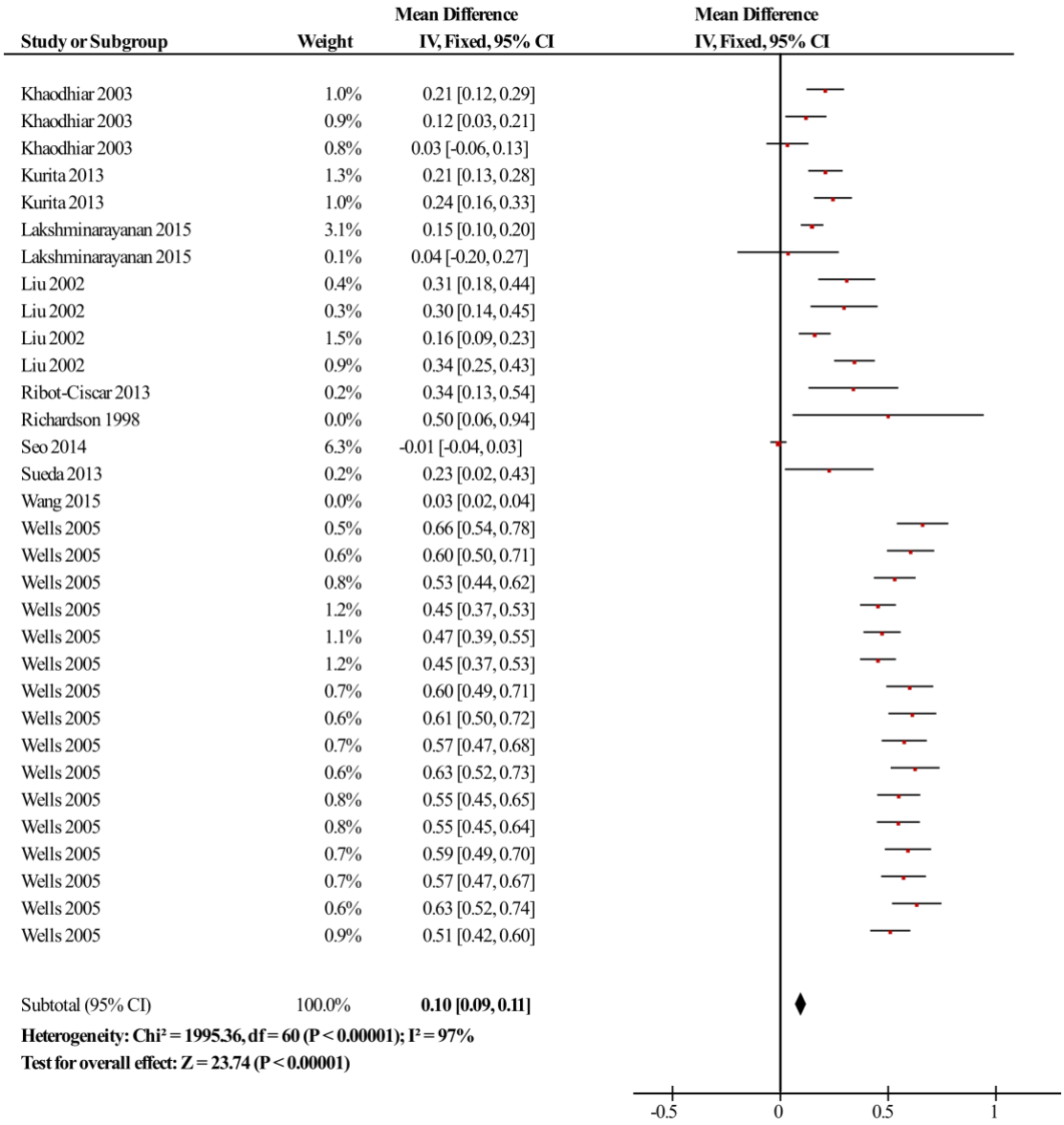

Figure 3. Second half of the forest plot for the Detection Task outcome measures listed alphabetically by first author. Outputs are normalised to a fraction of 1 relative to the sham condition. Positive data points represent beneficial effects. There was a statistically significant beneficial overall effect of 9-11% related to the application of the intervention.

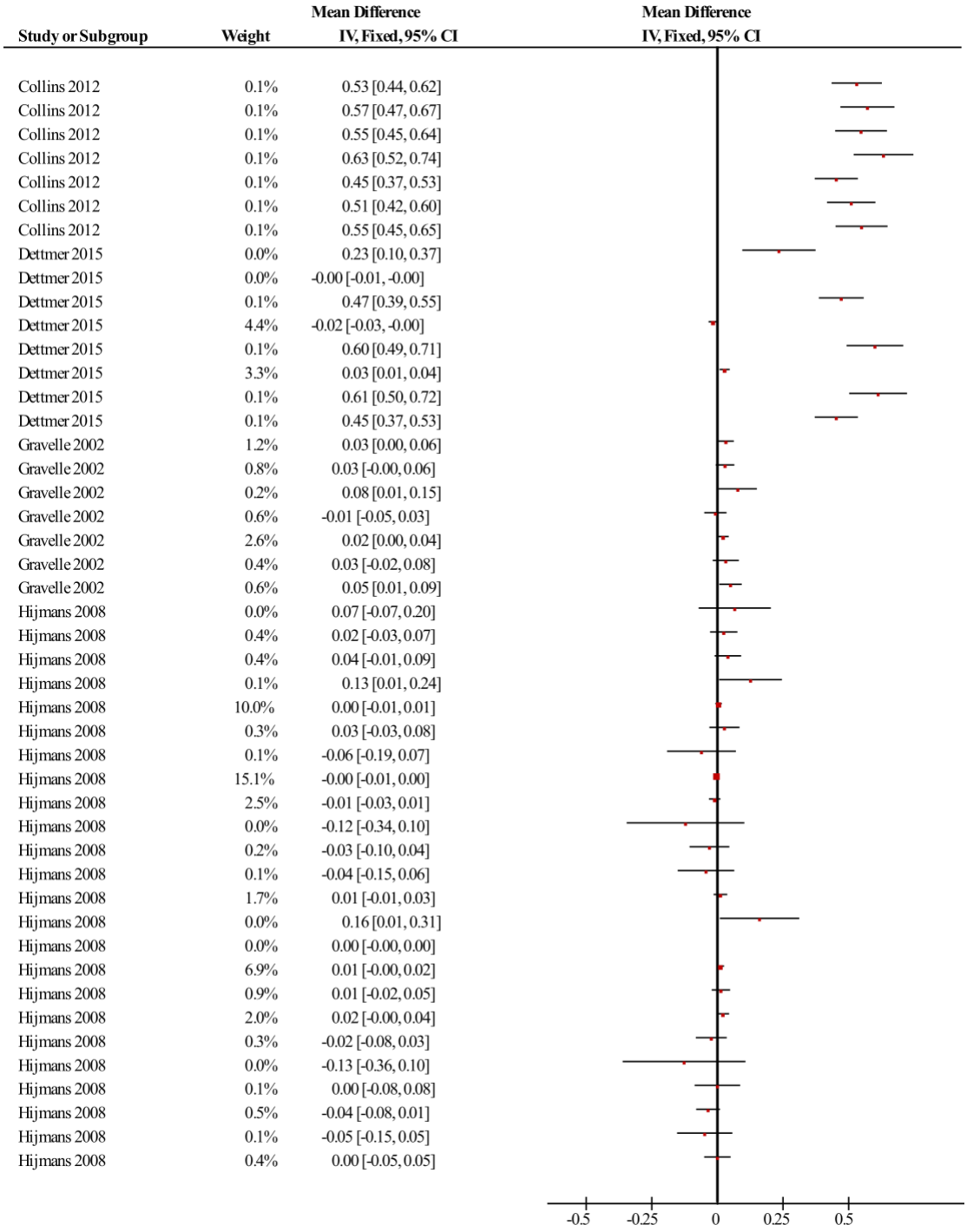

Figure 4. First third of the forest plot for the Balance Measure outcomes listed alphabetically by first author. Outputs are normalised to a fraction of 1 relative to the sham condition. Positive data points represent beneficial effects.

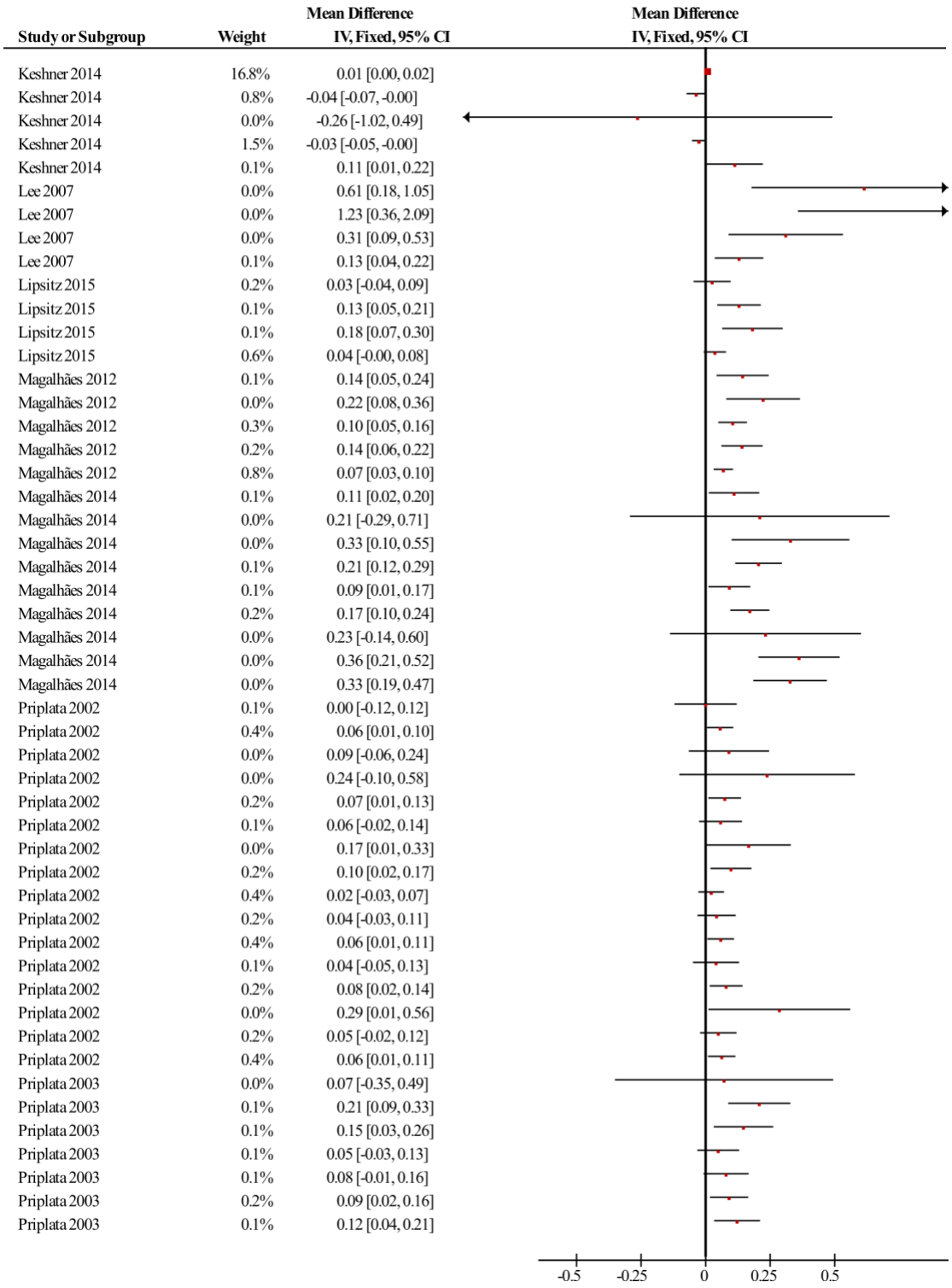

Figure 5. Second third of the forest plot for the Balance Measure outcomes listed alphabetically by first author. Outputs are normalised to a fraction of 1 relative to the sham condition. Positive data points represent beneficial effects.

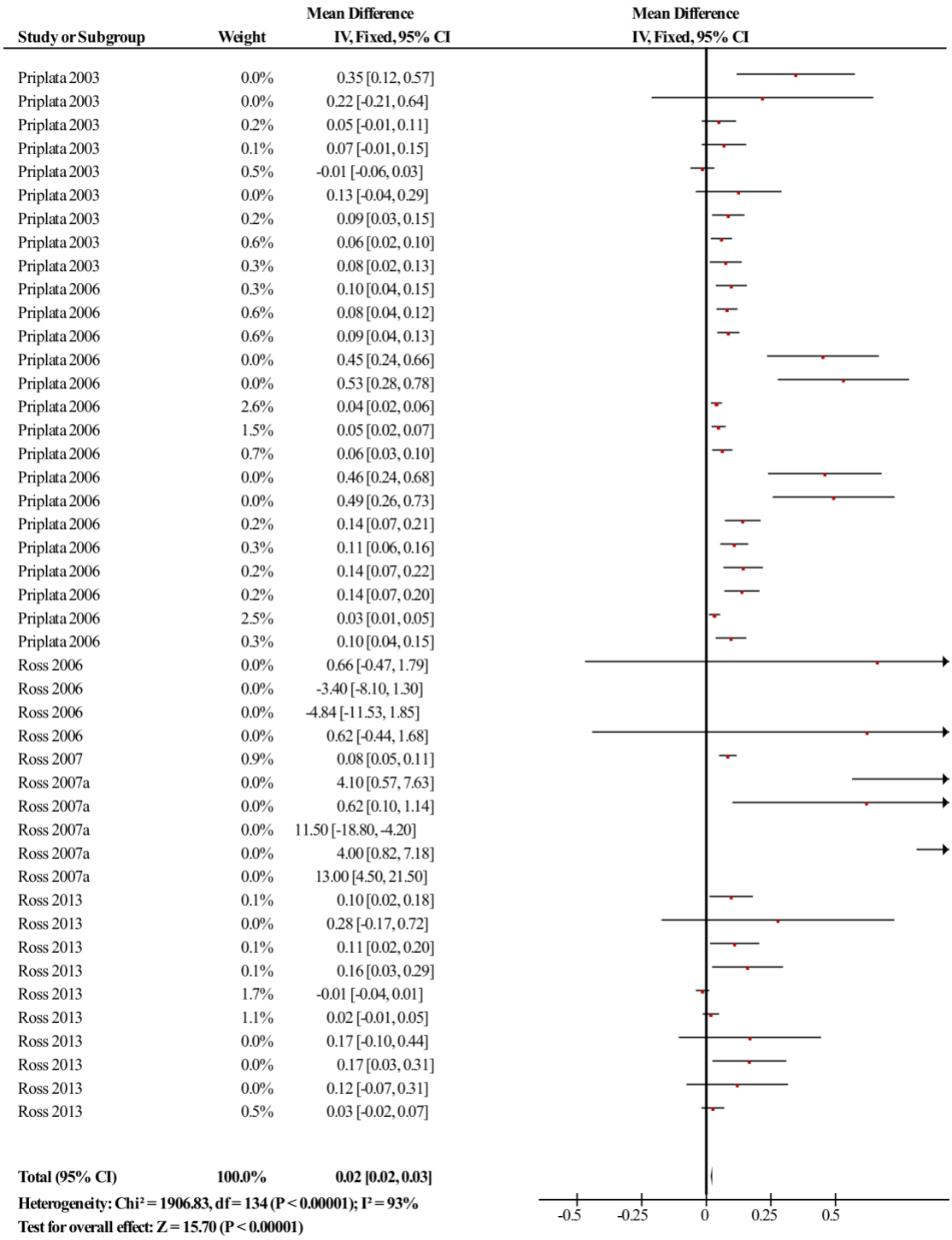

Figure 6. Final third of the forest plot for the Balance Measure outcomes listed alphabetically by first author. Outputs are normalised to a fraction of 1 relative to the sham condition. Positive data points represent beneficial effects. There was a statistically significant beneficial overall effect of 2-3% related to the application of the intervention.

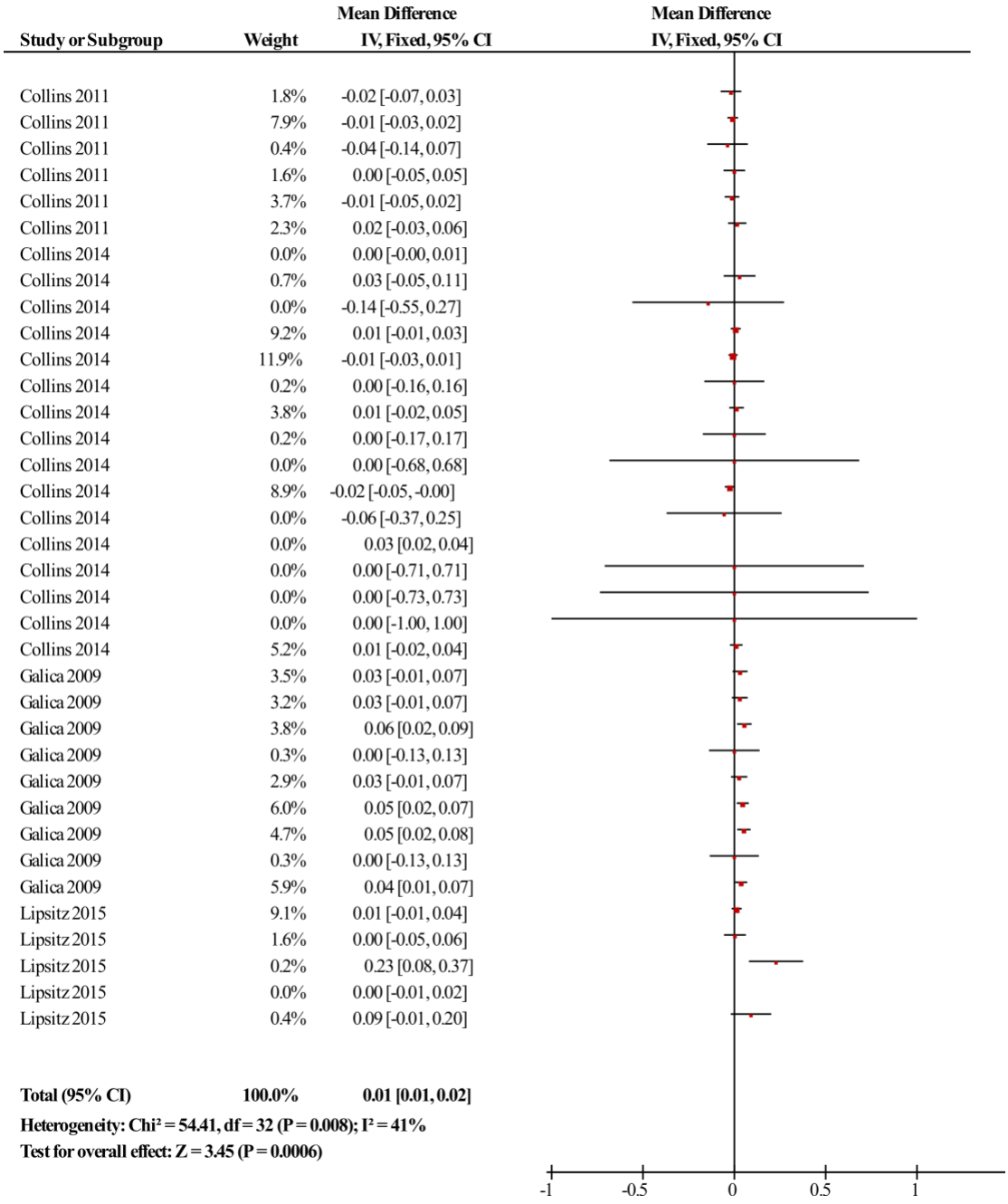

Figure 7. Forest plot for the Gait outcome measures listed alphabetically by first author. Outputs are normalised to a fraction of 1 relative to the sham condition. Positive data points represent beneficial effects. There was a statistically significant beneficial overall effect of 1-2% related to the application of the intervention.

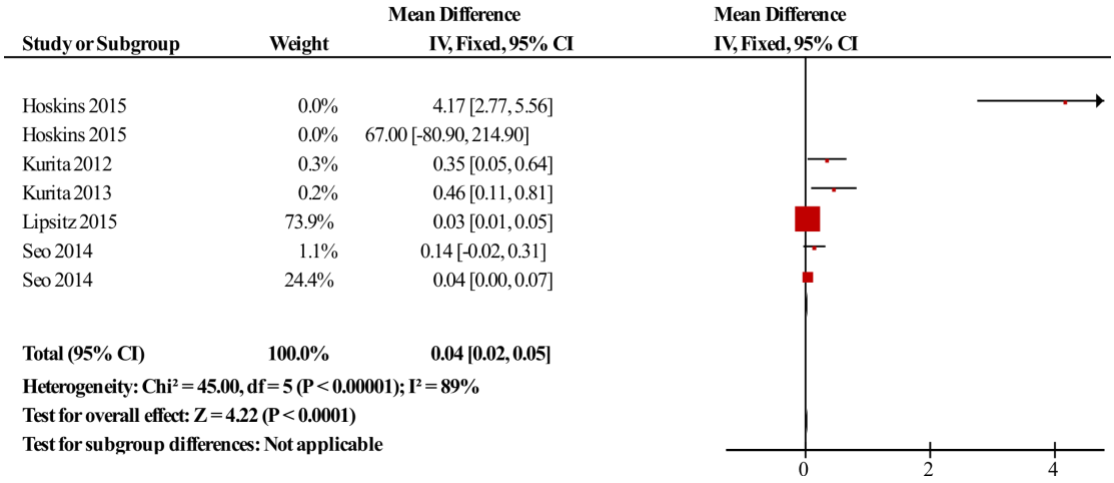

Figure 8. Forest plot for the Practical Task outcome measures listed alphabetically by first author. Outputs are normalised to a fraction of 1 relative to the sham condition. Positive data points represent beneficial effects. There was a statistically significant beneficial overall effect of 2-5% related to the application of the intervention.

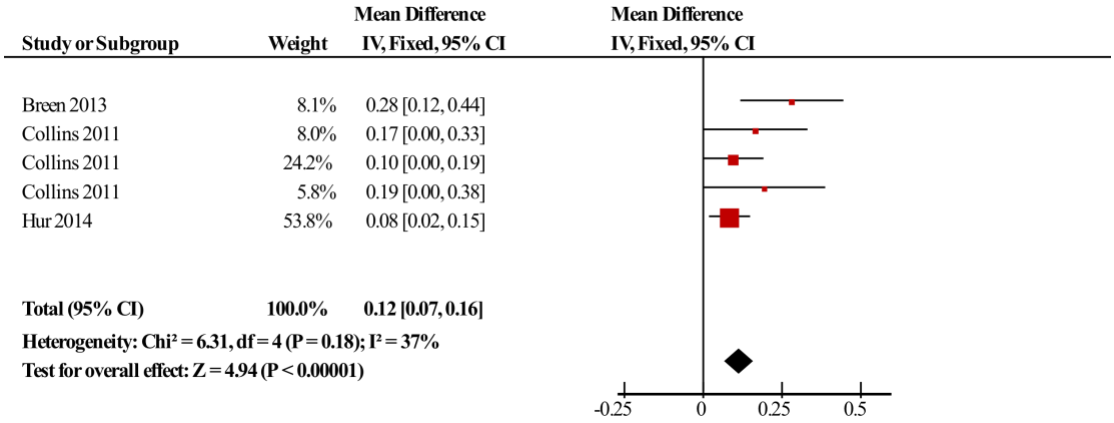

Figure 9. Forest plot for the Physiological Measures listed alphabetically by first author. Outputs are normalised to a fraction of 1 relative to the sham condition. Positive data points represent beneficial effects. There was a statistically significant beneficial overall effect of 7-16% related to the application of the intervention.

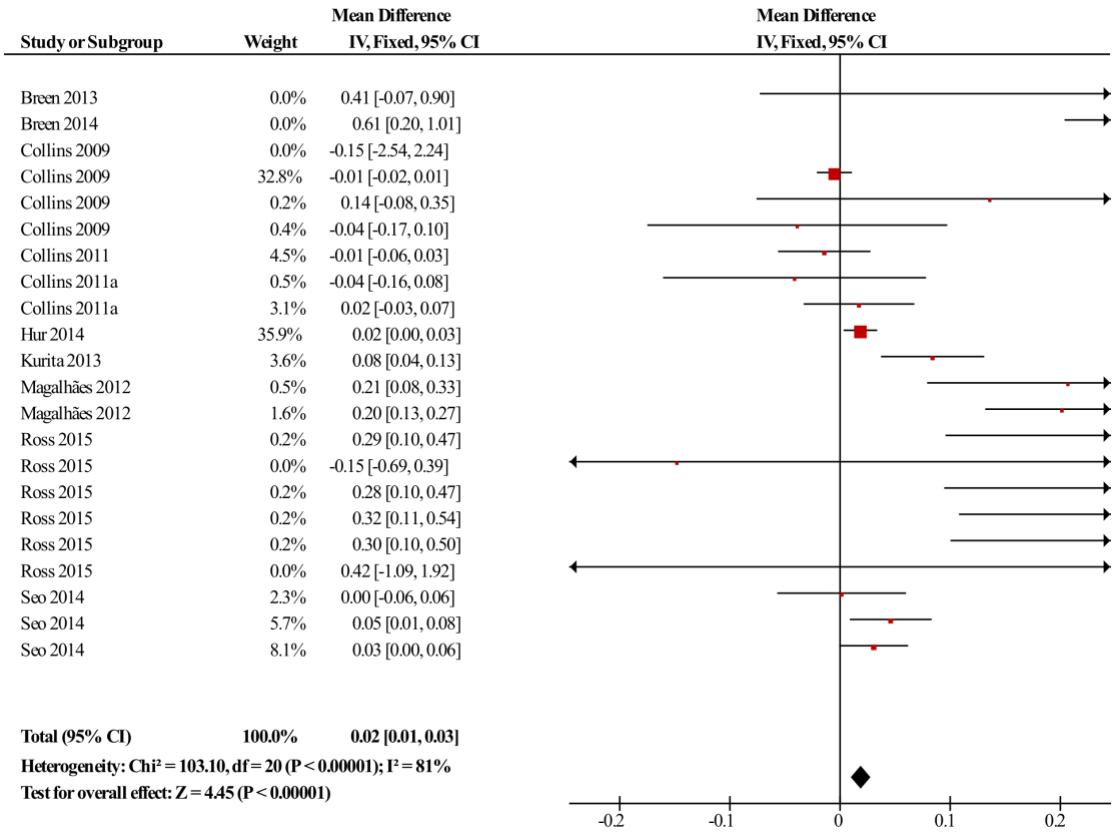

Figure 10. Forest plot for the Proxy Measures listed alphabetically by first author. Outputs are normalised to a fraction of 1 relative to the sham condition. Positive data points represent beneficial effects. There was a statistically significant beneficial overall effect of 1-3% related to the application of the intervention.

The measures of heterogeneity for Gait (I^2 = 41%) and Physiological (I^2 = 37%) Measures indicate that these groups moderately confirm to the notion that they were attempting to measure the same effect and are appropriately grouped. The measures of heterogeneity for Detection Tasks (I^2 = 97%), Balance Measures (I^2 = 93%), Practical Tasks (I^2 = 89%) and Proxy Measures (I^2 = 81%) indicate that these study outcomes are very heterogeneous in nature.

The overall measure of effect indicated a mean beneficial difference of 4% of outcomes relative to the sham condition with 95% confidence interval of 3-4% ($p < 0.00001$), and a high level of heterogeneity (I^2 = 94%).

1.4.4 Funnel plot analyses

The second output of the Review Manager analysis was funnel plots for each output category. Funnel plots are a graphical tool that allows the observation of outlier results and publication bias. If a group of results is measuring the same effect in different studies, one would expect that effects with small SEs to cluster together to represent

the true effect, while effects with large SEs are expected to show more variability in outcome.

Consequently, when plotting effect magnitude on the horizontal axis and SE (inverted, with small values on top and larger values below) on the vertical axis, one expects the data points to form an upward pointing triangle. The position of the point of the triangle represents the true effect of the intervention. Review Manager includes the 95% confidence bounds of this triangle and a vertical line for the weighted output effect for reference.

We expect to see that studies are symmetrically distributed to the left and right of the true effect. If studies appear predominantly to the beneficial (right) side of the triangle, then studies showing a smaller or negative effect have been omitted from the literature and this is evidence of publication bias.

Further, we expect that 95% of the outcomes will lie within the triangle. Studies lying outside of the triangle, especially to the right are likely outlier results that have been influenced by some form of bias.

Figure 11 shows the output of this analysis for the 6 different output categories. Each conforms to a certain extent to the triangular expectation, but with notable biases.

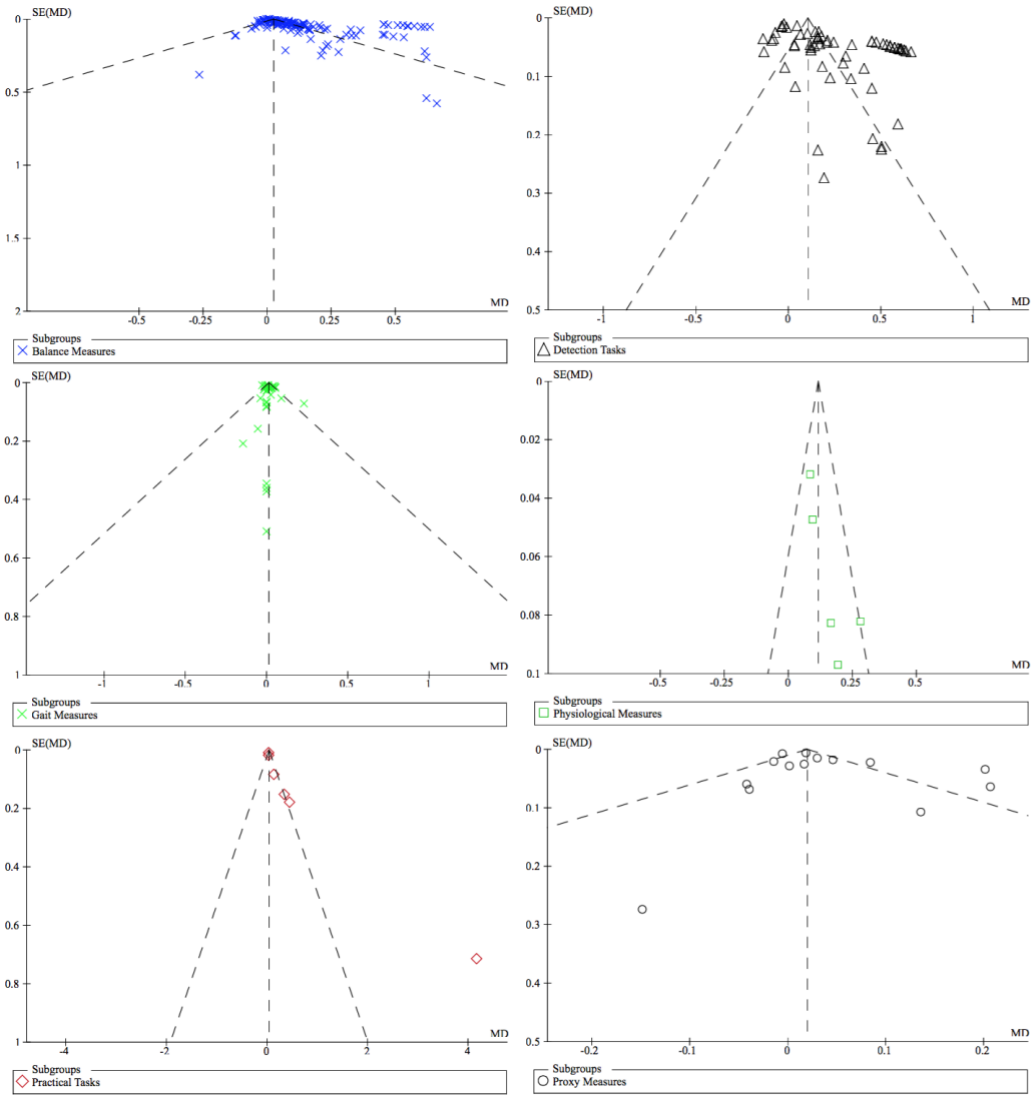

Figure 11. Funnel plots of intervention affect (% change from sham) versus the Standard Error of the measurement for the 6 outcome measure categories. Data points positioned to the right of zero indicate positive intervention outcomes. The dashed line triangle indicates the 95% confidence region for this outcome measure with the centre line being the weighted mean effect.

1.5 Discussion

1.5.1 Extent of effect of interventions

The majority of studies found significant effects for their intervention in at least one of their key outputs. The meta-analysis indicates beneficial effects of 10% for Detection Tasks, 2% for Balance Measures, 1% for Gait Measures, 4% for Practical Tasks, 12% for Physiological Measures, 2% for Proxy Measures, and an overall effect of 4% improvement when all the outcomes are combined. The reason why the mean effects shown here are much lower than those presented in the literature is because most

literature focuses on the outcomes that produced the largest benefit, where here we have analysed all the measured outcomes from each study.

The only work that consistently produced null results was that done by Collins *et al.* [59–62] who failed to find meaningful improvement in output measures of applying electrical SR to the knee compared to the control condition of using a neoprene sleeve, usually in patients with knee osteoarthritis. Interestingly these studies were also the largest of those analysed here (35 to 52 participants versus 5 to 18).

1.5.2 Mechanism of effect

The majority of studies postulate stochastic resonance (SR) as the mechanism of the positive effect observed on peripheral sensitivity outcomes. This is usually meant in the sense that SR is experienced by the sensory end receptors themselves, such as tactile neurons, muscle spindles and Golgi tendon organs. The alternative explanation is that both the sensory signal and the intervention signal are causing some other form of SR more centrally in the spine or brain.

Behaviour of distal interventions does appear to behave in accordance with SR as investigated by Collins (James) and colleagues in multiple papers. Distal, as opposed to central SR as a governing theory of the effect presents three challenges to researchers.

Firstly, it predicts that different intervention amplitudes are required to enhance performance when detecting sensory signals of different amplitudes. This is evidenced by Wells *et al.* 2005 [67] when investigating a sweep of intervention amplitudes for detection of signals at 80% and 90% of detection threshold. Wells *et al.* found that different intervention amplitudes produced optimal results for different sensory signal amplitudes. This makes the design of an intervention for dynamic situations difficult. This point was taken further by Galica *et al.* 2009 [97], when applying an intervention to the feet during gait. Galica attempted to apply varying intervention amplitudes appropriate for each stage of gait. This dynamic intervention amplitude appears to be key to developing that technology into a medical device.

Secondly, the amplitude required relative to the participants threshold may be simple to calculate when the output measure and the intervention are tightly related, for example when applying mechanical noise to affect perturbation detection. However, SR fails to allow for prediction of more complex scenarios. For example, what is the

required electrical signal amplitude to aid for balance enhancement? This cannot be calculated from theory, and has to be measured experimentally.

Finally, classical SR fails to provide explanations for when the intervention is applied proximally. These interventions appear to show a similar enhancement to their distal counterparts. An alternative hypothesis is that despite the added noise not reaching the *perception* threshold of the individual, it is sufficiently strong to activate local sensory organs [87,98]. Action potentials generated by the noise and signal source may combine more centrally (*e.g.* in the spinal cord or somatosensory cortex) to provide central SR [82,99].

The location of the intervention does not seem to have strong effect on the outcome [87], going as far as to show that remote vibratory stimulation at the hand has a similar influence on balance as a vibratory intervention at the feet [100,101]. Further, cross modal SR has been observed where one sensory mode such as audio noise, produces SR in the visual system [102,103]. This implies the signals are mixed centrally.

A further alternative hypothesis postulates that the intervention signal affects the transmission of the sensory signal as it comes past the intervention site, making it more coherent to central perception improving neural synchrony [30,31,76,87,92,98] and reducing spike time variance [75]. This can occur through alterations to the extracellular field enabling transmitted information to improve synchronicity and thus signal amplitude when summed more proximally.

Of course, it is possible that multiple processes combine to generate the observed enhanced response, that is not explained by a single hypothesis. Further work is required to unravel the underlying mechanism, and how this may vary depending on factors such as noise spectrum and location of intervention application.

1.5.3 Scientific rigour

The majority of studies used a crossover study design with at least single-blinding to the intervention condition. This inherently leads to higher quality scientific outcomes than common “case-control” study designs, with interventions where a convincing placebo/sham condition is difficult to generate. However, factors were found that could lead to bias and artefact.

While at least single-blinding is essential, double-blinding is not difficult to include in studies of this nature. Many studies failed to report clearly the nature of their blinding which makes it difficult to assess the scientific quality of the work.

While care was taken to accurately determine the outcome measures of the studies, similar care was not taken to determine perceptual threshold of the intervention. Most studies made it clear that the percentage of threshold of the intervention was important, and that SR, which relies on an accurately determined threshold, was the likely mechanism of effect. However, threshold data was only reported in one study, which showed that there was large individual variability (20%) in vibratory thresholds over 9 tests over three days [88].

The funnel plots shown in Figure 11 allow for an informal assessment of the homogeneous nature of the output measures in each category, the likelihood of publication bias and the frequency of occurrence of outlier measurements. The clustering shown in the detection tasks funnel plot indicates that either these output measures are not comparable, or they were not performed in a consistent fashion. The plots for the other measures show a much more even spread indicating a common effect magnitude.

The bulk of the data points in the balance measures funnel plot lie to the right of the vertical dotted line (which indicates the likely true mean of the intervention effect). This asymmetry to the right is probably the result of publication bias where outputs that showed less effect, no effect, or an adverse effect have not made it to the literature.

Finally, one expects about 5% of the data points to lie outside of the triangle, more than this indicates outlier studies containing some form of artefact. Funnel plots are only strictly appropriate if the data is sufficiently homogeneous. One must be careful not to over interpret the graphs presented here as the analysis indicates a high level of heterogeneity. However, it would seem the data calls for higher consistency in experimental procedures and outcome measures.

Finally, in all cases, cross-over study-data must be analysed in a pairwise fashion using appropriate statistics. However, in many cases, the data was reported as group means and variability for the sham and intervention conditions. This inhibits the ability of the reader to analyse the results and include the data for meta-analysis. Crossover trials must be reported in a fashion appropriate for paired data.

1.5.4 Gaps in the literature

Signal frequency

The analysed studies present little evidence to justify the "shape" and frequency characteristics of the signal. Most agree that "noise" works best because it is more biological and less likely to have learning effects that would reduce its efficacy over time. Little has been done to investigate what types of signals offer optimal enhancement. Trenado *et al.* [104] suggest using a spectrum that includes the frequency ranges of the receptors the intervention wishes to enhance. This is supported by early work that investigated using single frequency stimulation "pedestals" to enhance sensitivity to that frequency alone, and that frequencies outside of the range of the receptor failed to enhance sensation [50–52].

If the effect of the intervention is occurring more centrally, it may be more important to consider the frequency response of the whole neural control loop. This is discussed in some detail in a different paper also by Trenado *et al.* [105].

Little is known about the actual frequencies of the interventions reaching the physiological targets. In most mechanical studies, piezo-electric vibrators are used, which usually have relatively narrow frequency responses. Driving these actuators with white noise is unlikely to produce a white noise vibration response.

A similar argument can be made for electrical interventions. The tissue between the electrodes and the nerve likely acts as a complex and active filter, with the actual voltages and currents reaching the nerves left unknown. Due to physiological time constants, it is unlikely that very high frequencies have a meaningful effect, and consequently the system can be thought to have a low-pass filter characteristic. This is reflected in the 1/f (pink) frequency spectrum choice of Breen *et al.* [30,31,75,92].

While no rationale is given for this design choice by Breen *et al.*, it can be inferred that this signal is more efficient at transferring energy to the nerves than a white noise spectrum, as less energy is dedicated to the potentially inefficient high frequencies. In addition, the pink spectrum is likely to include the mechanical frequency response range of the receptor itself (as discussed above) while not completely excluding higher frequencies that may still create meaningful responses. While it cannot be said that the causal relationship between intervention spectrum and efficacy is understood, pink noise offers the current "best guess".

Long-term effect of treatment

The "wash-out" period of these treatments seems to be immediate, and in short term use there is no apparent learning or adaptation effect [65]. Generally, once you stop applying the signal, the effect does not persist (although this was not the case in at least one study [86]).

The lack of persistence would necessitate that any of these therapies would need to be used in an on-going basis, however, only one study has examined the effect of applying the intervention for more than a few minutes [88], and even here, it is not made clear that the device was left on throughout the day of testing.

It may be desirable to alter the signal characteristics simply to prolong either the duration one can engage with the treatment, or the washout period after the signal is removed. In the former, the signal may either have long-term adverse effects, or the body may learn to ignore the effects of the artificial signal, nullifying the treatment. These long-term characteristics have not yet been investigated, however, some studies have shown consideration towards them in their design. Seo *et al.* 2014 postulate that one of their null results may have occurred as a consequence of prolonged exposure (15-20 minutes) [85]. This outcome emphasises the need long exposure studies.

The effect on perceived neuropathic pain

Sensory neuropathy frequently has a neuropathic pain component. It can be argued that one could predict that these treatments would either improve neuropathic pain, or worsen it. Since pain is so common, it seems an oversight that it has not been questioned alongside the neuropathic populations already investigated.

Non-laboratory trials

To date none of the trials have attempted an intervention in a non-laboratory setting. In a practical environment, aspects such as the size and capacity of power sources, the convenience of use, the manner and durability of attachment and many other factors all play a much larger role in the design of the intervention.

While it is important to lay appropriate groundwork in the laboratory for any intervention, it seems that this field is now ready for non-laboratory trials.

One of the challenges facing research is the development of technology to allow these signals to be applied on an ongoing basis. No wearable continuous electric current stimulators have been developed that fulfil the requirements of these interventions.

Several vibratory solutions have been prototyped and tested [16,17,70,79,80,97,106], but do not appear to have reached to the point where participants can use the device outside of a laboratory setting.

Dose-response ratio

To date no attempts have been made to model exactly how the interventions interact with the diseased physiology, making it impossible to predict for which diseased states particular interventions would work. A very high percentage of participants respond to these interventions but inter-patient variability of the dose-response ratio, and indeed the occurrence of "non-responders" has not been explained.

Detailed physiological and mechanical model

The included studies have not developed a sufficiently detailed model of the physiological and mechanical interactions that cause these interventions to be effective. While SR as a blanket theory appears to fit well, it does not allow researchers to make predictions, such as for what forms of neuropathy these interventions would be effective, or how alterations to the intervention signal would affect various outcome measures.

More studies, such the microneurography studies by Breen *et al.* [75] and Ribot-Ciscar *et al.* [81], exploring the mechanism by which these interventions work would be of great benefit to the field.

1.6 Conclusion

The data indicates this class of interventions represents a real possibility for development into a practical medical device to improve sensation in populations that suffer from peripheral sensory neuropathies.

Future studies should focus on achieving this goal by investigating prolonged exposure in everyday settings, as well as conducting more physiological studies to better understand the mechanism of the interventions so that its parameters can be optimised.

In specific regard to the work of this thesis, no studies investigating the effect of subsensory signals on patients with HIV-related peripheral sensory neuropathy were

found, none of the studies reported on measures of pain, none of the studies investigated the perceptual threshold of participants to electrical noise stimuli, and none of the studies made use of, or researched a device that could apply electrical interventions in a wearable fashion outside of a laboratory setting.

2

VIBROTACTILE SENSITIVITY OF PATIENTS WITH HIV-RELATED SENSORY NEUROPATHY

Prior to conducting investigations into improving the vibrotactile sensitivity of patients with HIV-related peripheral sensory neuropathy in South Africa, it is important that the extent and nature of the sensation loss is first characterised.

The work in this chapter was published in part in "Brain and Behavior":

Karpul D, McIntyre S, van Schaik A, Breen PP, Heckmann JM. Vibrotactile sensitivity of patients with HIV-related sensory neuropathy: an exploratory study. Brain and Behavior. 2018, e01184, doi: 10.1002/brb3.1184

2.1 Introduction

Peripheral Neuropathic Desensitisation (PND) is a common problem with severe consequences (see Chapter 1.1). Over the last 20 years a family of intervention studies have sought to improve tactile sensitivity in healthy and neuropathic populations by applying continuous electrical or mechanical stimulation delivered at amplitudes below the perceptual threshold (*e.g.* [17,48,83,92]). These studies however, have never examined patients with HIV-related peripheral sensory neuropathy (HIV-PN).

More than 5 million people live with HIV in South Africa [107], up to 60% of which suffer from HIV-PN, which may arise as a consequence of the infection or following Antiretroviral Therapy (ART) initiation [108,109]. While there is still no cure for HIV, ART has significantly reduced HIV-associated mortality. In addition, HIV related neurological conditions, such as HIV-PN, have been shown to adversely affect health related quality of life [29]. There is a growing need to find interventions to help this group manage the consequences of HIV-PN. The above mentioned "subperception stimulus" studies present hope that the problem of tactile sensitivity loss in patients with HIV-PN may be addressable. Given that these "subperception stimulus" studies aim to detect subclinical changes in perception thresholds, the measurements used require higher resolution than clinical tools. Before conducting such research, it is important to quantify the tactile sensitivity of patients with HIV-PN and compare the results to healthy matched control participants. This in turn can be used to justify a future intervention with this population.

This chapter provides a detailed description of the vibrotactile sensitivity of individuals with HIV-PN and compares commonly used clinical vibration testing and scoring grades with a more robust double-blinded quantitative vibration perception threshold (VPT) protocol.

2.2 Methods and Materials

2.2.1 Participants

22 HIV-PN participants were recruited consecutively from a cohort of a larger HIV 'inflamm-aging' neuropathy study [110], which monitored patients after enrolment on a government sponsored ART program. These patients were recruited from the HIV clinic at Crossroads Community Health Centre in Cape Town, South Africa. A further 21 control participants (hereinafter referred to as 'non-HIV') were also recruited by a

fieldworker through word of mouth. In the latter stages of recruitment, favour was given to participants that conformed to the age distribution of the HIV-PN participants. All participants were required to sign informed consent provided in either English or Xhosa (Informed consent documents are contained in the digital appendix folder "SENS Ethics").

The informed consent form was composed in English with a Fleish Kincaid grade level of 8.0. The English version was translated into Xhosa by Dilicom Language and Communication, which included a comprehensive translation from English to Xhosa and an independent back translation from Xhosa to English and verification.

This study was approved by the Human Research Ethics Committees of both the University of Cape Town (HREC ref: 838/2015) and Western Sydney University (ref: H11381) (Both HREC approval letters are contained in the digital appendix in the folder "SENS Ethics").

A focused neuropathy examination was performed by a neurologist as part of the larger HIV 'inflamm-aging' neuropathy study (see Chapter 2.2.2). The methods by which this data was collected is described, but it should be noted that it was not collected as part of this thesis work.

The HIV-PN group consisted of individuals with one or more neuropathic signs present in a symmetrical distribution as determined by neuropathy screening. Patients with severe painful neuropathy scoring greater than 6 out of 10 on a visual numeric scale at the time of the screening were excluded from the current study. Non-HIV participants were age and gender matched as a group, self-reported as HIV negative and had a similar demographic background, being recruited from the same geographic region.

All participants were required to be physically able to perform the study tasks, be between 18 and 59 years of age, not be pregnant, have no history of cardiovascular disease or epilepsy, have no implants including pacemakers, not suffer from diabetes or alcoholism, and not be diagnosed with any illness that affects peripheral sensation aside from HIV in the case of the HIV-PN group.

Participants' height, weight, date of birth, foot dominance and self-reported sex were recorded (Appendix D.1).

2.2.2 Clinical neuropathy screening

The Brief Peripheral Neuropathy Screening tool (BPNS) and a reduced version of the Total Neuropathy Screen (TNSr) were used to assess HIV patients for the presence of symmetrical neuropathic symptoms and signs [11,111] (Appendix D.2). Symptoms are defined as features of a disease that are apparent to the patient, and signs as features detected through medical examination.

The BPNS establishes symptoms of pain, numbness, and "pins-and-needles" on a visual numeric scale. It further examines vibration perception in the toes and the presence of ankle reflexes. The ankle reflexes are scored as either normal (2), reduced (3) or absent (4). Vibration perception was assessed using a standard technique of applying the maximally vibrating 128 Hz tuning fork (TF) immediately to the distal interphalangeal joint at the hallux [111]. The final result is given as an ordinal variable indicating the duration for which vibration was detectable: score 0 for >10 seconds, score 1 for 6 to 10 seconds, score 2 for 1 to 5 seconds, and score 3 for no detectable vibration, denoting severe loss of vibration perception.

The TNSr assesses the extent to which neuropathic symptoms and signs progress distally (toes/soles of feet (1)) to proximally (ankles (2), knees (3), hands (4)), with more proximal abnormalities scoring higher (worse). Five categories are examined: sensory symptoms, pin sensibility, vibration sensibility, deep tendon reflexes, and strength of plantar and ankle/toe dorsi-flexion. In addition, proprioception was assessed at the toes, and >20% mistakes (of 10 trials) bilaterally, was categorised as abnormal [109].

The parameters selected from the HIV 'inflamm-aging' neuropathy study [110] for comparison with the VPT (see section 2.2.3) were: date since initiating ART, toe proprioception, BPNS tuning fork test (BPNS-TF), BPNS evaluation of ankle deep tendon reflexes (BPNS-DTR) and the total BPNS score (BPNS-total). Further, VPT was compared with the following outcomes from the TNSr: the distal-proximal extent of reduced abnormal vibration sensibility (TNSr-TF), pinprick abnormalities, reduction in deep tendon reflexes (TNSr-DTR) and the total TNSr score (TNSr-total).

2.2.3 Measurement of Vibration Perception Thresholds (VPT)[3]

Participants were asked to sit in a chair and place their non-dominant foot on a platform as shown in Figure 12. The underside of the big toe was placed over a 20 mm hole in the platform that allowed it to contact the 5 mm ball-bearing-tipped probe underneath.

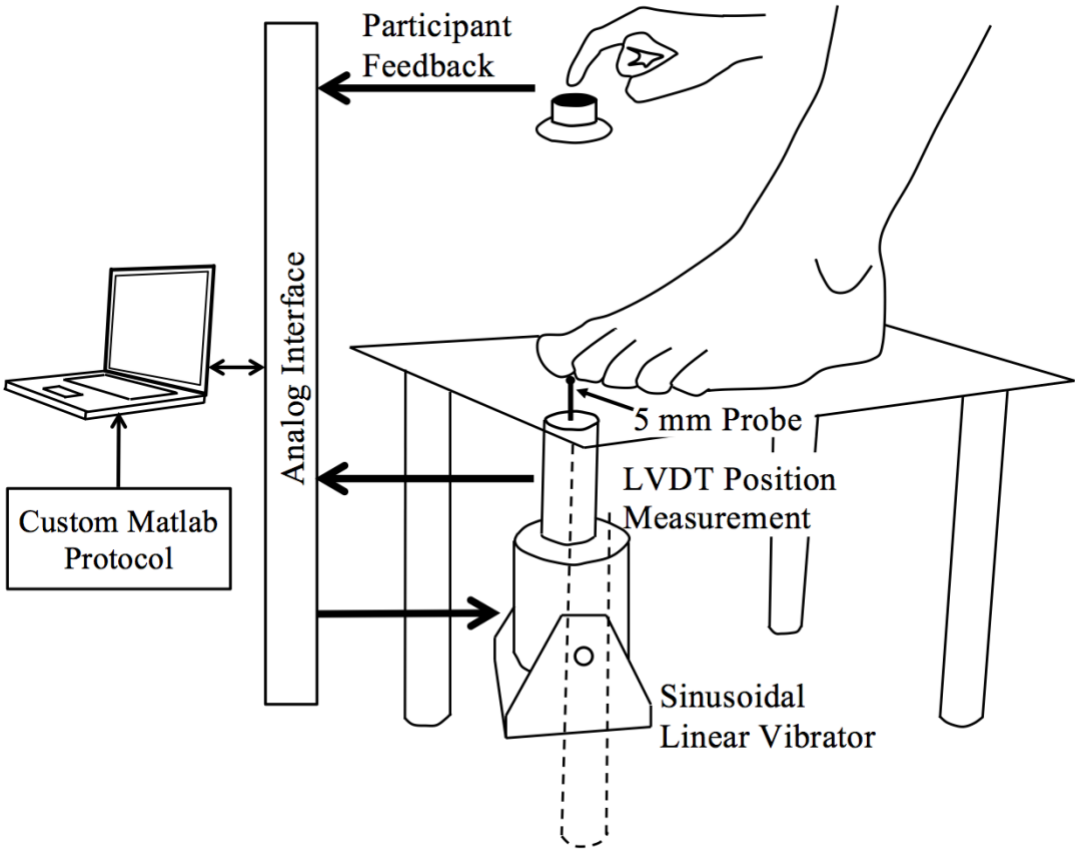

Figure 12. Diagram showing the testing platform and control and instrumentation setup of the vibration sensitivity testing. The platform had a 20 mm hole in its surface through which the probe made contact with the skin.

A 10 mm wide hook-and-loop strap, attached at the left and right edges of the platform in line with the probe, was placed over the toes and was used to keep the foot in place. It also ensured that the hallux was in contact with the probe, depressing the probe by 50 to 150 μm. Adjustments were made during the experiment, if needed, to ensure that contact was maintained in this range.

Figure 13 shows the modified method of limits protocol, which was conducted almost entirely by a custom written Matlab program to ensure double blinding (All program

[3] A full and detailed description of the protocol for measurement of VPT is presented in Chapter 3. Here, only what is necessary for understanding this chapter is presented.

code for this purpose is contained in the digital appendix folder labelled “Hardware and data management system”).

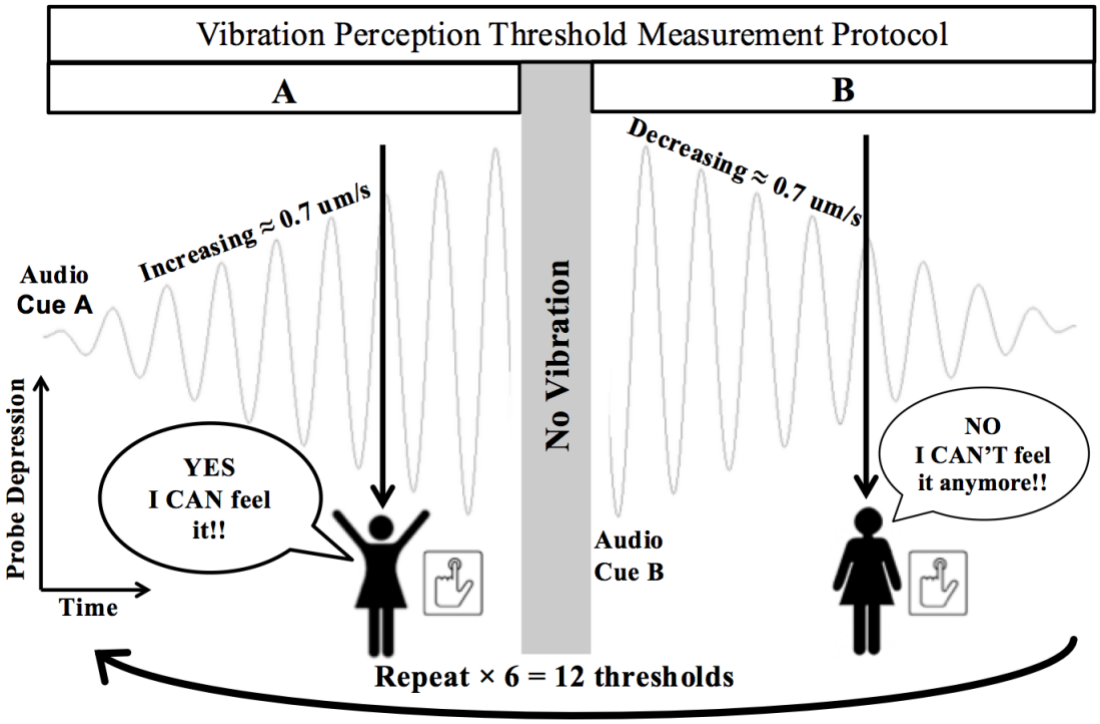

Figure 13. Diagram depicting the testing protocol for vibrotactile threshold testing.

Participants would first hear an easily recognisable audio cue indicating that an “up going” vibration ramp was imminent (See digital appendix folder “Hardware and data management system / DAQ_handlers / ring_up.wav”). The vibration would then start at an imperceptible amplitude and increase until the participant could feel the vibration. The participant was instructed to press a hand-held button immediately upon becoming aware of the vibration. The vibration would then pause for one second, and a different audio cue would sound, indicating the “down going” vibration ramp was imminent (See digital appendix folder “Hardware and data management system / DAQ_handlers / ring_down.wav”). The vibration would then start from a supra-threshold amplitude and decrease toward zero at the same rate as before. The participant would then press the hand-held button as soon as they could no longer feel the vibration. The sequence repeats until a total of 12 thresholds were collected. This would typically take between 5 and 10 minutes depending on the participant’s thresholds and the rate of the ramps. The average vibration amplitude in the 0.5 seconds leading up to the button press was deemed the threshold for that ramp.

The protocol was repeated for three different vibration frequencies. These frequencies were specifically chosen to selectively activate predominantly low frequency mechanoreceptors (25 Hz), predominantly high frequency mechanoreceptors (128 Hz), and a combination of the two (50 Hz). Further, 128 Hz allowed for comparison to traditional tuning fork measurements.

2.2.4 Data analysis

The comparison of the HIV-PN and the non-HIV cohorts was conducted with a two-sample t-test for each continuous variable, and the Fisher's exact test comparing foot dominance.

The effects of various parameters on VPT (all three frequencies), was computed as odds ratios of linear mixed effects models. This technique considers that it is the same participant being measured at each frequency (intra-subject). This allows for greater statistical power than analysing each frequency separately. In text we will refer to testing for a parameter's effect on VPT. In all cases this does not refer to causality, but rather to the manner in which the statistical tests were conducted, with VPT as the outcome measure. Statistics are noted as probability (p), Chi squared value (χ^2) and degrees of freedom (DF).

When testing the correlation between only two variables, such as between a single VPT frequency and a tuning fork test outcome, Spearman rank order tests were used. This tests for a monotonic relationship between the two variables regardless of the shape of the relationship. A positive "Rho" value from the test would indicate that VPT threshold increases with increases in the secondary outcome and *vice versa*. The p-value is the probability of the null-hypothesis that the data was drawn from a zero correlation.

Results are regarded as significant if the p-value is less than 0.05. However, results below 0.15 will also be discussed in context, and may justify further research.

All vibration data was analysed and filtered in Matlab. Two-sample t-tests were calculated in Excel. Fisher's Exact test and Spearman Rank Order tests were calculated in Matlab. Linear mixed effects models were calculated in 'R'.

2.3 Results

2.3.1 Group characteristics

Two of the 22 HIV-PN participants recruited were excluded from the results analysis. One was not able to learn the task, and the other had vibratory thresholds in excess of what the equipment was able to measure (>1000 μm); had severe HIV-PN with absent deep tendon reflexes, unable to perceive vibration sense with the TF at the toes only, altered proprioception at the toes and loss of pin sensibility extending to the knees. One of the 21 non-HIV participants recruited was excluded as their VPT at different frequencies were between 4.3 and 12 standard deviations from the mean of the group, indicating that the participant possibly had undiagnosed sensory neuropathy, and was therefore inappropriate as a control participant.

The two groups consisted entirely of women. The bias towards female predominance is common in sub-Saharan African HIV cohorts [11,109,110]. The HIV-infected group were all virally suppressed on ART (viral loads <400 cps/ml)[110] except one individual (≈4000 cps/ml).

Table 3 shows the participant characteristics. The HIV-PN participants and non-HIV participants were matched for age, foot dominance and height. Matching for age is important since it is expected that age will have an effect on VPT. Weight and BMI were significantly different with the average non-HIV participant's body weight in the obese range (BMI>30) which is common for this demographic [112]. The difference in weight is likely a result of HIV-infection and its treatment causing weight loss [113].

In the HIV-PN group, 18 of 20 had two or more neuropathic signs, and 2 had absent reflexes only. Table 4 shows the outcomes of the various tests performed on the HIV-PN group. In summary, only 2 cases experienced neuropathic symptoms. The neuropathic signs in order of frequency included: 18 had altered/absent ankle reflexes, 14 had reduced distal pinprick sensibility, 10 had altered vibration sensibility by TF, and 7 had altered toe proprioception. Of those with altered vibration sensibility, 50% had altered vibration at the toes only and it extended more proximally in the remaining participants.

Table 3. Participant characteristics (mean and standard deviation in brackets).

	HIV-PN	Non-HIV	P-Value
Age (yrs)	41.6 (7.0)	40.1 (5.1)	0.449
Height (cm)	156.6 (6.1)	159.4 (5.3)	0.146
Weight (kg)	66.9 (13.8)	84.7 (23.0)	0.005
BMI ($kg.m^{-2}$)	27.1 (4.3)	33.2 (8.3)	0.006
Foot Dominance (Right:Left)	19:1	16:3	0.342
ART Duration (years)	8.6 (2.8)	-	-
BPNS-total (0-11)	4.3 (1.1)	-	-
TNSr-total (0-20)	4.9 (2.5)	-	-

BMI: Body Mass Index. ART: Antiretroviral Therapy. BPNS-total: total score of Brief Peripheral Neuropathy Screening tool. TNSr-total: total score of the reduced Total Neuropathy Screen.

Table 4. Frequencies of neuropathic signs for the HIV-PN group. A score of zero indicates "normal" unless otherwise stated. Higher scores indicate more severe signs of neuropathy.

	Test Sore				
	0	1	2	3	4
BPNS-TF	11	7	2	0	NA
BPNS-DTR	NA	NA	2*	6	12
TNSr-TF	10	5	2	2	1
TNSr-DTR	2	6	2	7	3
Proprioception	13	7	0	NA	NA
TNSr-pin sensitivity	6	1	7	5	1

*A score of 2 for BPNS-DTR indicates "normal".

"NA" indicates that this score category does not apply to this test

BPNS-TF and BPNS-DTR: Brief Peripheral Neuropathy Screening tool Tuning Fork and Deep Tendon Reflex evaluation. TNSr-TF, TNSr-DTR and TNSr-pin sensitivity: reduced Total Neuropathy Screen Tuning Fork score, Deep Tendon Reflexes score and pin-sensitivity score respectively.

2.3.2 Comparison of Vibration Perception Thresholds (VPT) between participants with HIV-related Peripheral sensory Neuropathy (HIV-PN) and non-HIV participants

Figure 14 shows a comparison of the HIV-PN group and the non-HIV group at each of the three vibration frequencies. HIV-PN status significantly affected VPT ($p = 0.018$, $\chi^2 = 5.59$, DF = 1) as did vibration frequency ($p < 0.001$, $\chi^2 = 38.71$, DF = 2) *i.e.* sensitivity increased with increases in vibration frequency. Although not statistically significant, an interaction effect between vibration frequency and HIV-PN status on VPT suggests that HIV-PN may affect VPT differently at different frequencies compared to non-HIV participants ($p = 0.064$, $\chi^2 = 5.51$, DF = 2). Post-hoc analysis shows that HIV-PN status had a more detrimental effect on 25 Hz than 50 Hz or 128 Hz.

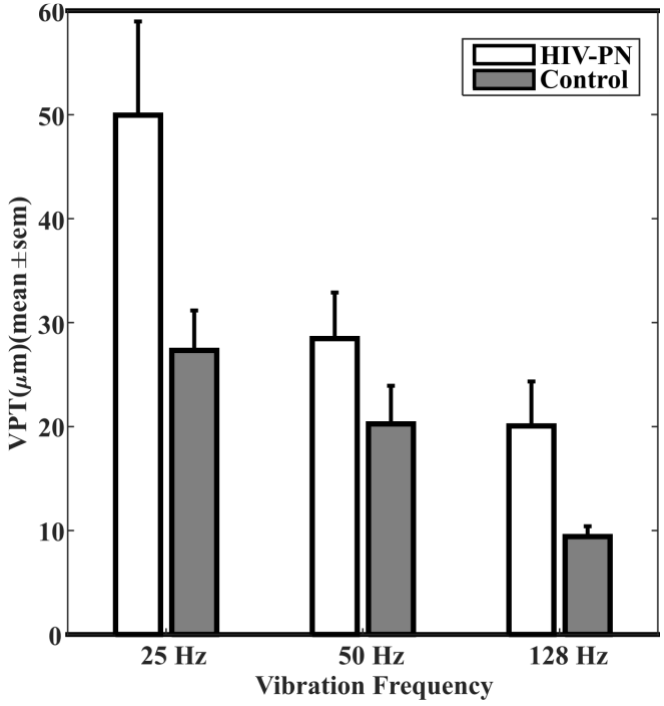

Figure 14. Vibration thresholds of HIV-PN and non-HIV groups at three different frequencies. Sensitivity was reduced in the HIV-PN group at all frequencies (p = 0.018) compared to the non-HIV group.

VPT increased with age when controlling for vibration frequency and HIV-PN status ($p = 0.004$, $\chi^2 = 8.15$, DF = 1). However, age did not interact with vibration frequency ($p = 0.60$, $\chi^2 = 1.03$, DF = 2), or with HIV status ($p = 0.123$, $\chi^2 = 2.38$, DF = 1). VPT did not correlate with participant height when controlling for vibration Hz and HIV-PN status, nor did the interaction of height and either vibration Hz or HIV-PN status have a significant correlation with VPT (p's > 0.57).

While the audibility of the vibration was not recorded, no participants reported being able to hear the vibration. The vibration was only audible to the tester for unusually high amplitudes of vibration at 128 Hz.

2.3.3 Comparison of Vibration Perception Thresholds (VPT) and clinical measures

There was no effect of ART duration on VPT ($p = 0.53$, $\chi^2 = 0.40$, DF = 1), but there was an interaction between ART duration and vibration frequency ($p = 0.038$, $\chi^2 = 6.56$, DF = 2). Post-hoc analysis shows the patients who have been receiving ART for longer have improved sensitivity at 25 Hz. The sensitivity of other vibration frequencies is largely unaffected by the number of years receiving ART.

Figure 15 shows there was no relationship between vibrotactile sensitivity, as measured by VPT at different frequencies, and the grading categories using the 128 Hz tuning fork at the toes (BPNS-TF) or the length-dependent vibration loss (TNSr-TF). We found no significant correlation between 128 Hz VPT and BPNS-TF ($p = 0.76$, rho = -0.08) or TNSr-TF ($p = 0.90$, rho = -0.03). There was no significant effect of any of the clinical measures of large nerve fibre function as graded by BPNS-TF, BPNS-DTR, TNSr-TF, TNSr-DTR, and proprioception on VPT or small fiber function as measured by pinprick sensibility (Table 5, all p's > 0.28). Neither was there any interaction with frequency measurements for large or small fiber function (p's > 0.20).

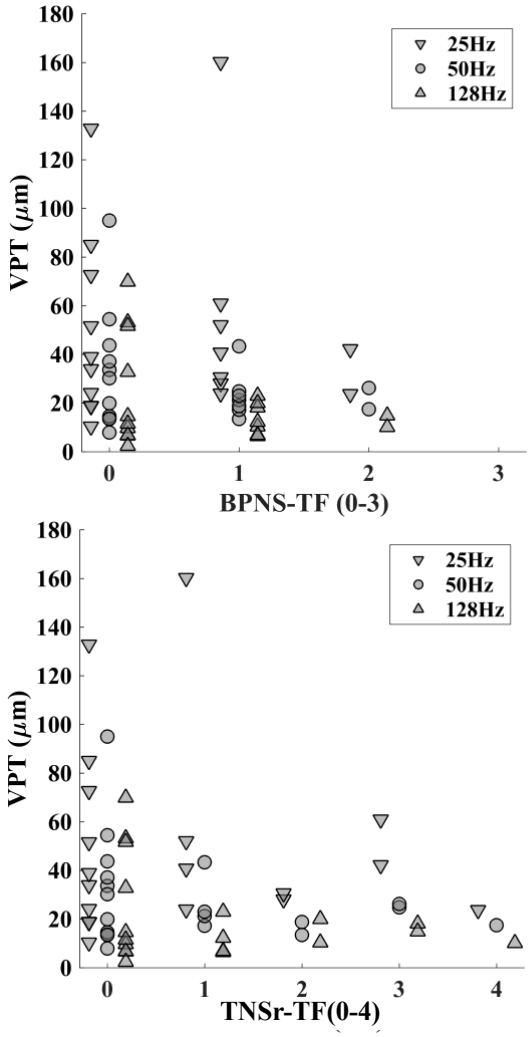

Figure 15. Plot of VPT at three different vibration frequencies versus BPNS-TF (top) and TNSr-TF (bottom) for the HIV-PN participants only. The data's scores are offset slightly for each vibration frequency to improve readability.

Table 5. Statistical outcomes for linear mixed effects models looking at the effect of various clinical bedside tests on VPT at all frequencies. DF = 1 for all main effects of the parameter on VPT, and DF = 2 for interaction with vibration frequency.

	Main effect p (χ^2)	Interaction with frequency p (χ^2)
BPNS-TF	0.41 (0.69)	0.79 (0.55)
BPNS-DTR	0.40 (0.71)	0.98 (0.05)
BPNS-total	0.50 (0.45)	0.96 (0.07)
TNSr-TF	0.34 (0.90)	0.99 (0.01)
TNSr-DTR	0.67 (0.19)	0.90 (0.21)
TNSr-total	0.99 (0.00)	0.80(0.44)
PROP	0.28 (1.18)	0.72 (0.66)

BPNS-TF, BPNS-DTR and BPNS-total: brief peripheral neuropathy screening tool tuning fork evaluation, deep tendon reflex evaluation and total score respectively. TNSr-TF, TNSr-DTR and TNSr-total: reduced total neuropathy screen tuning fork score, deep tendon reflexes score, and total score respectively. PROP: proprioception score. VPT: Vibration perception threshold. P, probability, χ^2, Chi squared value, DF, degrees of freedom.

2.4 Discussion

This study presents vibrotactile sensitivity of a cohort of selected individuals with moderately severe HIV-PN using a robust psychophysics methodology and compares results to clinical screening tools commonly used in the study of HIV-PN. The protocol used here differs from prior work, averages multiple measurements, uses a method of limits in both ascending and descending modes and is double blind, making it more robust than currently available vibration testing. Previous studies using quantified sensory testing (QST) devices in HIV-PN report their results in terms of mean Z-scores based on their cohort controls scores ([114,115]. Therefore, we are not able to compare our results with previously reported HIV-PN groups. Nevertheless, our control group was recruited using similar strategies to previous reports ([114]).

The HIV-PN group had reduced sensitivity, and sensitivity for both groups increased with increase in vibration frequency in accordance with previous research in the area [116]. We would also expect to observe a decrease in sensitivity with increasing age [117]. This was also shown to be the case as age had a statistically significant effect on VPT when controlling for HIV-PN status and vibration frequency. However, the effect of age did not interact with HIV-PN status, *i.e.* HIV-PN patients' and non-HIV participants' VPT was not affected differently by age.

HIV-PN is known to have length dependent properties [108,109], however we found no correlation between height and VPT for either group. Subject heights in the HIV-PN group were normally distributed with a standard deviation of only 6.1 cm, therefore very few participants lay far from the mean to give strength to an analysis of height in this context. Although the lack of correlation should not be over-interpreted in this small sample, the absence of an association signal with height and HIV-PN has been consistently absent in this population [11,109].

BMI was significantly lower in the HIV-PN group. Past work indicates that BMI most likely does not correlate with VPT, but if it does, it is likely to result in increased tactile sensitivity with lower BMI [118–120]. Consequently, it is possible, but unlikely, that the difference in sensitivity between the groups was even larger than the observed difference.

An interesting result would be to find that HIV-PN affects vibration sensitivity of different mechanoreceptor types differently. This could manifest when measuring VPT at different vibration frequencies, as different mechanoreceptors populations have different vibration frequency responses. Indeed Shy *et al.* notes that different stimulation frequencies hold different diagnostic value under varying circumstances (although suggests testing above 128 Hz to more exclusively activate high frequency receptors) [121]. We would observe this effect as an interaction between HIV-PN status and vibration frequency when assessing VPT. This study was statistically powered to find inferences in the primary outcome variables, and interactions require significantly more statistical power. The interaction effect between HIV-PN status and frequency of vibration on VPT ($p = 0.0635$) is not significant, but this should not be interpreted as strong evidence against an effect, given the low power. Calculating the required number of participants sufficient to power the study to determine this outcome is not trivial. It

can be said as a rule of thumb, it is likely that four times the number of participants would be needed.

Previous work has shown that neuropathy symptoms and signs improve for some patients receiving ART over time and worsen for others [109]. We did not find an overall effect of years on ART on VPT, but there was an interaction between ART duration and vibration frequency. Post-hoc analysis indicates that duration of ART was correlated with an improvement in 25 Hz VPT performance. The observed interaction between group (HIV-PN or non-HIV) and vibration frequency, along with the significant interaction between ART duration and vibration frequency is suggestive of a pathology that does not affect all mechanoreceptors similarly.

All clinical measures failed to correlate with VPT. This lack of expected correlation can be explained through several mechanisms. Past results have shown that clinical measures of neuropathy have optimal diagnostic accuracy when combined with each other, including VPT [121,122]. In theory, measures that correlate well with each other would not add additional diagnostic information and it is expected that they test different aspects of the disease or that multiple measures reduce the influence of random variation. Further, excluding patients with severe painful neuropathy may have reduced the strength of the relationship between clinical measures and VPT, although there was no interaction with pinprick, which, like painful symptoms, subserves small fibre function. It is also possible that the clinical measurements lack the resolution to demonstrate continuous relationships. For example, it has been shown that the relationship between the tuning fork vibration time and age only degrades about 5 seconds from the age of 20 to 60 on average [123]. It is therefore unreasonable to expect to see this relationship when tuning-fork time is summarised into 5-second blocks.

A limitation of this study is that the healthy controls did not undergo a neurological screen. This does not invalidate the results, but may have resulted in a smaller difference in VPT between the two groups than if potential control participants with undiagnosed neuropathy were excluded. Testing the control participants for HIV was not part of the protocol for ethical reasons. This omission is common for studies of this nature (*e.g.* [114]).

Since Subsensory Electrical Nerve Stimulation (SENS) interventions have shown promise in improving VPT in the past with other populations that suffer from reduced VPT, it is conceivable that an intervention with SENS would be beneficial to this HIV-PN population and should be explored as an option for therapy. The interaction between VPT at 25 Hz and HIV-PN status, and between years on ART and VPT at 25 Hz suggest that the response to vibration frequency may hold additional diagnostic value over using a tuning fork test only at 128 Hz.

2.5 Conclusion

To the best of our knowledge this work presents the first quantitative, double blind measurement of VPT in patients with HIV-related sensory neuropathy. The results indicate that patients with HIV-PN have reduced vibration sensitivity at all tested vibration frequencies compared to age, height and gender-matched non-HIV participants, and that sensitivity increased with vibration frequency for both groups. Outcomes of tests for interaction with vibration frequency suggest that the pathology in subjects with HIV-related neuropathy does not affect all mechanoreceptors similarly. Future work should increase the number of participants and should include patients with more severe neuropathy. This would allow for a better analysis of interaction effects as well as strengthen the relationship between VPT and parameters that degrade with worsening neuropathic signs and symptoms.

3

SUBSENSORY ELECTRICAL NERVE STIMULATION FOR THE IMPROVEMENT OF VIBRATION PERCEPTION IN PATIENTS WITH HIV-RELATED PERIPHERAL NEUROPATHY

In Chapter 2, the adverse effects of HIV-related peripheral sensory neuropathy (HIV-PN) on vibration perception thresholds (VPT) were demonstrated. Further, the potential of Subsensory Electrical Nerve Stimulation (SENS) as a means of providing much needed therapy for this group was discussed. Here, the effect of SENS on HIV-PN participants and healthy controls is presented.

The work in this chapter was presented in part at the Australasian Neuroscience Society Annual Scientific Meeting in 2016:

Karpul D, McIntyre S, Heckmann JM, van Schaik A, Breen PP. On the Application of Subsensory Electrical Nerve Stimulation for the Improvement of Vibration Perception in Patients with HIV Related Peripheral Neuropathy. Australas. Neurosci. Soc. Annu. Sci. Meet. 2016 Abstracts for Poster Presentations, 2016, p. 67.

3.1 Background

3.1.1 HIV-related peripheral neuropathy

Peripheral neuropathic desensitisation (PND) is a common problem that can be caused by HIV and many other conditions. HIV-related peripheral sensory neuropathy (HIV-PN) is highly prevalent condition which adversely impacts morbidity and no treatment is currently available (see Chapter 1.1 and Chapter 2.1 for more details regarding PND and HIV-PN).

3.1.2 Neuropathic pain

Neuropathic pain is a common complication associated with diabetic PND [5] and occurs in approximately 70% of patents with symptomatic HIV-PN [11]. Sufferers experience paraesthesia (prickling or stinging needles), paroxysmal pain (short shooting electrical attacks), superficial pain (on-going pain, often burning), allodynia (painful response to non-painful stimuli) and hyperalgesia (disproportionate response to painful stimuli) [124]. Symptoms are often worse at night.

The aetiology of painful peripheral neuropathy is not fully understood, but it is accepted that there are several underlying mechanisms. There is evidence from microneurography studies for both the idea that pain may be caused by an absence of proper nerve function [125] and hypersensitivity of the receptors [126,127], leaving it unclear how an intervention increasing tactile sensitivity would affect neuropathic pain.

3.1.3 Interventions to improve tactile sensitivity

Chapter 1 presents a detailed review of a family of interventions that seek to improve sensation by applying a signal (often in the form of multi-frequency noise) to the site where the sensation is to be improved. It is theorised for in the majority of the research that the mechanism of the therapy is stochastic resonance (SR) [128,129].

Research applying these interventions has been performed with participants with a wide array of sensory deficits, but never with participants with diagnosed HIV (see Chapter 1 for a full description of the existing literature). Most studies reported the therapy improved parameters between 5% and 30% for a very high percentage of participants (mostly exploratory studies with $6 \leq n \geq 18$).

Of particular relevance is the work of Breen *et al.* [30,31,75,92]. Breen *et al.* applied electrical current to healthy young participants, proximal to the fingertip [75] and to the

skin medially and laterally, proximal to the malleoli [30,31], and again in the same location in older adults [30,92]. In all cases vibration perception was enhanced by between 10% and 20%.

The intervention noise spectrum used by Breen *et al.* is unique. All other studies have used band limited white noise, but Breen *et al.* used noise heavily weight toward very low frequencies. They have coined this modality "SENS" standing for Subsensory Electrical Noise Stimulation (see Chapter 1 for more details relating to the spectrums used by various studies). Due to physiological time constants, it is unlikely that very high frequencies have a meaningful effect, and consequently the system can be thought to have a low-pass filter characteristic. This is reflected in the choice 1/f (pink) frequency spectrum choice of Breen *et al.*

While no rationale is given for this design choice by Breen *et al.*, it can be inferred that this signal is more efficient at transferring energy to the nerves than a white noise spectrum, as less energy is dedicated to the potentially inefficient high frequencies. In addition, the pink spectrum is likely to include the mechanical frequency response range of the receptor itself (as discussed in Chapter 1.5.4) while not completely excluding higher frequencies that may still create meaningful responses. While it cannot be said that the causal relationship between intervention spectrum and efficacy is understood, pink noise offers the current "best guess".

Since the signal is applied proximally, it is unclear what the mechanism of enhancement is. It could be a form of SR in the sensory axons in the limb. Microneurography data indicates that the mechanism may be related to reduced variability in action potential timing in individual axons, and additional synchronisation of action potentials across parallel multiple axons, allowing a greater cumulative effect when summed centrally [75].

This family of subthreshold interventions has shown great promise in being developed into a device that can help those suffering from PND (see Chapter 1.4 for summaries of the outcomes of studies of this type).

3.1.4 Research goals

SENS has never been studied with HIV-PN or with participants from an African context. The primary goal of this research is to assess the effectiveness of SENS in improving tactile sensitivity of South African HIV-PN patients. The research also seeks

to determine if SENS is effective for healthy participants from South Africa, that have a substantially different background to healthy participants previously researched in other countries.

No prior known work using interventions of this type report on measures of pain, a common symptom of neuropathy in a variety of contexts. The secondary goal of this work is to investigate how SENS effects symptoms of pain.

Finally, the ability of SENS to improve tactile sensitivity has only been investigated for 50 Hz vibration frequency in the past. This works aims to investigate the effectiveness of SENS at lower and higher frequencies that represent a wider spread of mechanoreceptors.

3.2 Methods and Materials

Aspects of the study presented in this chapter overlap with Chapter 2, including the recruitment of participants, measurement of their characteristics, the clinical screening of the HIV-PN participants and the measurement of Vibration perception thresholds. Repetition is avoided, but text which ensures the chapter reads clearly has been repeated for those who read this chapter in isolation.

3.2.1 Participants

22 HIV-PN participants and 21 healthy non-HIV participants were recruited from the same community in Crossroads, Cape Town, South Africa. The non-HIV group has been included for two reasons. Firstly, they act as validation of this particular setup and environment. Should the HIV participants show no effect, it would be natural to question the validity of the experimental equipment and design. By testing healthy participants, the research can be sure that, should SENS not demonstrate an effect in the HIV-PN group, it is a consequence of the population tested rather than the experimental design. Secondly, while several prior studies conduct research investigations of the effect of SENS on healthy participants, it cannot be ignored that the African context is different and sensory perception among healthy participants from the townships of Cape Town may be different to those of Sydney for example. The quality of the research is thus strengthened by comparing the results of HIV-PN subjects with participants who live in a similar context rather than those from other countries.

All participants were required to sign informed consent, which outlined the experimental protocol and exclusion criteria, provided in either English or Xhosa. This study was approved by the Human Research Ethics Committees of both the University of Cape Town (HREC ref: 838/2015) and Western Sydney University (ref: H11381).

A focused neuropathy examination was performed on the HIV-PN participants (see Chapter 2.2.2). The HIV-PN group consisted of individuals with one or more neuropathic signs present in a symmetrical distribution. Patients with severe painful neuropathy scoring greater than 6 out of 10 on a visual numeric scale were excluded from the current study (15% of the total cohort). Those with severe painful neuropathy were excluded for two reasons: because pain may confound the measurement of VPT, and because the hypothesis is that SENS, which aims to improve tactile sensitivity, may also increase perceived pain in these patients.

Non-HIV participants were age and gender matched as a group, self-reported as HIV negative and had a similar demographic background, being recruited from the same geographic region.

Participants' height, weight, date of birth, foot dominance and self-reported sex were recorded. Foot dominance is the foot (left or right) most likely to be used for dexterous tasks. This was measured to arbitrarily standardise which foot was used for VPT measurements.

3.2.2 Study design

In this study, vibration perception threshold (VPT) was evaluated at 50 Hz during the application four different SENS amplitudes as well as a sham condition. Each of the five conditions was tested double blind in a random order for each participant (phase one, Figure 16) to match the work done by Breen *et al*. on other populations [30,31,92,93]. While the study design choice of Breen et al. to test 50 Hz was not explicitly justified, it is a consequence of the test equipment (biothesiometer used) operating only at 50 Hz. Notably, 50 Hz is a vibration frequency that does not exclusively activate only fast acting or slow acting mechanoreceptors [116].

Breen *et al*. found that there was an optimal SENS amplitude for each participant. Consequently, after the 50 Hz testing the most effective SENS amplitude was selected for the second phase of testing (phase 2, Figure 16). The rationale in their research is that once this optimal SENS amplitude is found, that SENS should be applied at this

amplitude for general tactile sensitivity improvement. To test this hypothesis VPT was then evaluated at 25 Hz and 128 Hz vibration frequencies with this best performing SENS amplitude and in a sham condition (for each frequency), in a randomised crossover design. 25 Hz was selected to evaluate predominantly low-frequency mechanoreceptors, and 128 Hz to evaluate predominantly high-frequency mechanoreceptors [116] and to compare results to clinical 128 Hz tuning fork tests [122,123,130].

A constant SENS RMS amplitude was applied throughout each VPT test and the full VPT testing protocol described in Chapter 3.2.5 was conducted for each vibration-frequency and SENS-amplitude pairing. In the text below the 50 Hz vibration frequency trials are individually identified by the amplitude of SENS used (*e.g.* 45µA), whereas the 25 Hz and 128 Hz vibration frequency trials are identified using the vibration frequency and not the amplitude of SENS.

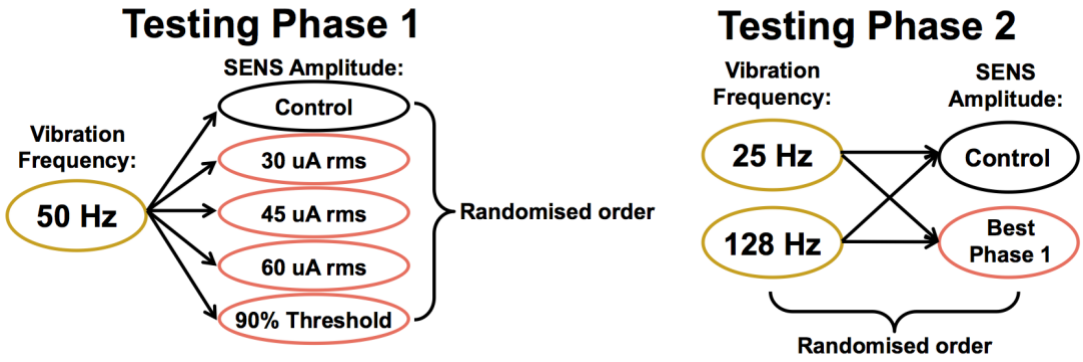

Figure 16. Study design overview. In phase 1, VPT is evaluated for 50 Hz vibration at 4 different SENS amplitudes and one control condition, double blinded in a randomised order for each participant. Upon completion of phase 1, the SENS amplitude associated with the most sensitive VPT relative to the control condition is selected for use in phase 2. In phase 2 VPT is evaluated for 25 Hz and 128 Hz vibration frequencies, each in a control condition, and with SENS (applied at the best performing amplitude from phase 1 for that participant). The four test conditions of phase 2 are completed in a double blinded random order.

3.2.3 Calculation and generation of SENS

In some publications the electrical noise used as "SENS" is referred to as pink noise, or 1/f in frequency characteristic. In reality the noise used in SENS publications is a variation of brown noise with a frequency characteristic closer to $1/f^2$. The waveform is calculated using a random walk algorithm first referred in the context of SENS in Breen *et al.*[75].

Here they describe the generation of SENS as having been produced from equations in [131], which in turn references the book [132]. The equations are included here as reference as they are not easily found in the literature.

The original equation for SENS at any sample point x_i, can be notated as:

$$x_i = C \times x_{i-1} + d_i \quad \textbf{1}$$

where i starts from 1 and x_o is 0, and

$$C = e^{-\frac{\Delta t}{\tau}} \quad \textbf{2}$$

which is a constant between 0 and 1 for positive τ, and d_i is a random value drawn from a Gaussian distribution at step i.

The signal can also be more efficiently generated in vectorised software with the equivalent equation:

$$x_i = C^i \sum_{p=1}^{i} d_p . C^{-p}. \quad \textbf{3}$$

The noise was generated by a custom written Matlab program (See digital appendix folder "Hardware and data management system") and converted to a stimulation current via a digital to analogue converter and an A-M Systems 2200 current stimulator (see Figure 17 for an example waveform). The digital appendix folder "SENS signal generation code" contains examples of how to generate SENS signals in both the iterative and vectorised methods.

The final signal is dependent on the sample interval used. The design choice to generate the intervention signal in this manner was made to match the successful work of Breen *et al.* and consequently the same sample rate of 100 Hz was selected.

3.2.4 Application of SENS and measurement of electrical perception threshold

Signal amplitudes of 30 µA, 45 µA, 60 µA (RMS) and 90% of electrical perception threshold were evaluated.

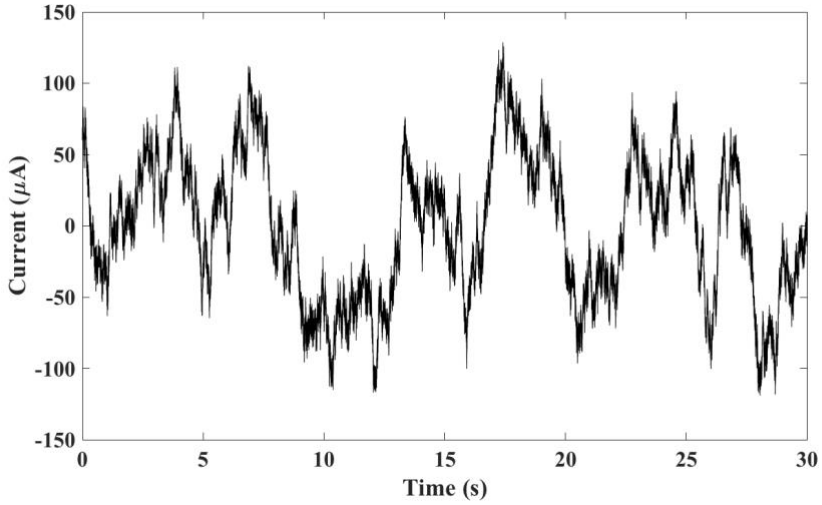

Figure 17. Typical SENS stimulation current waveform.

In order to apply the intervention signal, and establish electrical perception threshold, two Axelgaard UltraStim® Snap SN2040 10 cm × 5 cm adhesive surface electrodes were applied to the skin medially and laterally, proximal to the malleoli on the non-dominant leg (see Figure 18). The non-dominant leg was chosen arbitrarily for consistency. The location of the electrodes was designed to stimulate the tibial nerve that sub-serves the tactile receptors of the plantar aspect of the foot [31]. The electrodes themselves were selected to repeat the work of Breen *et al.* [31]. The manufacturer advertises high quality current density uniformity. Current density uniformity is desirable as it minimises current "hotspots" on the skin which may be damaging to the user.

Electrical perception threshold was established using a single blind method of levels [121]. Threshold was defined as the highest amplitude at which the participant could not feel the electrical stimulation. Given that past studies found the intervention to be effective for currents in the range of 30 to 60 µA, an upper limit of current threshold was set at 555 µA, resulting in a maximum of 500 µA applied when using 90% of threshold. This was done as currents beyond 500 µA are very likely to be supra-threshold at a neuronal level even if not at a perceivable level. Further, currents in the mA range start to risk muscle activation which would confound the measurement of VPT.

3.2.5 Measurement of vibration perception thresholds

To measure vibration perception thresholds (VPT) psychophysics experiments often use a controllable vibration device such as a biothesiometer (Bio-medical Instrument CO., Newbury, OH), neurothesiometer (Horwell Scientific, London, UK) or a custom electronic "tactor" which are driven in ascending and/or descending amplitudes to establish the sensory threshold [133]. The participant is required to indicate when they cannot perceive the vibration as the amplitude is reduced. The amplitude can also be increased from a subperception level to get an ascending threshold. Individual participants can have different decision criteria for identifying the onset or offset of sensation, requiring different levels of certainty. Using both ascending and descending thresholds allows the experiment to control for reaction speed of the participant and the effect of the decision criteria.

Shy *et al.*[121] highlight the importance of double blinding in quantitative sensory testing. Testing VPT inevitably has a psychological component unlike nerve conduction velocity (for example) [121]. Clinical VPT testing and many psychophysics tools such as the Neurothesiometer use single blinding or no blinding at all. This is likely to lead to unreliable or unrepeatable results.

By double blinding the testing, interleaving ascending and descending ramps, calculating the final threshold value controlling for the effect direction (ascending or descending) has on threshold, and performing the test multiple times, the influence of reaction time and many of the biases that lead to potentially unreliable outcomes are avoided [121,134].

To measure VPT, participants were asked to sit in a chair and place their non-dominant foot on a platform as depicted in Figure 18. The underside of the big toe was placed over a 20 mm hole in the platform that allowed it to make contact with the 5 mm ball-bearing-tipped probe underneath.

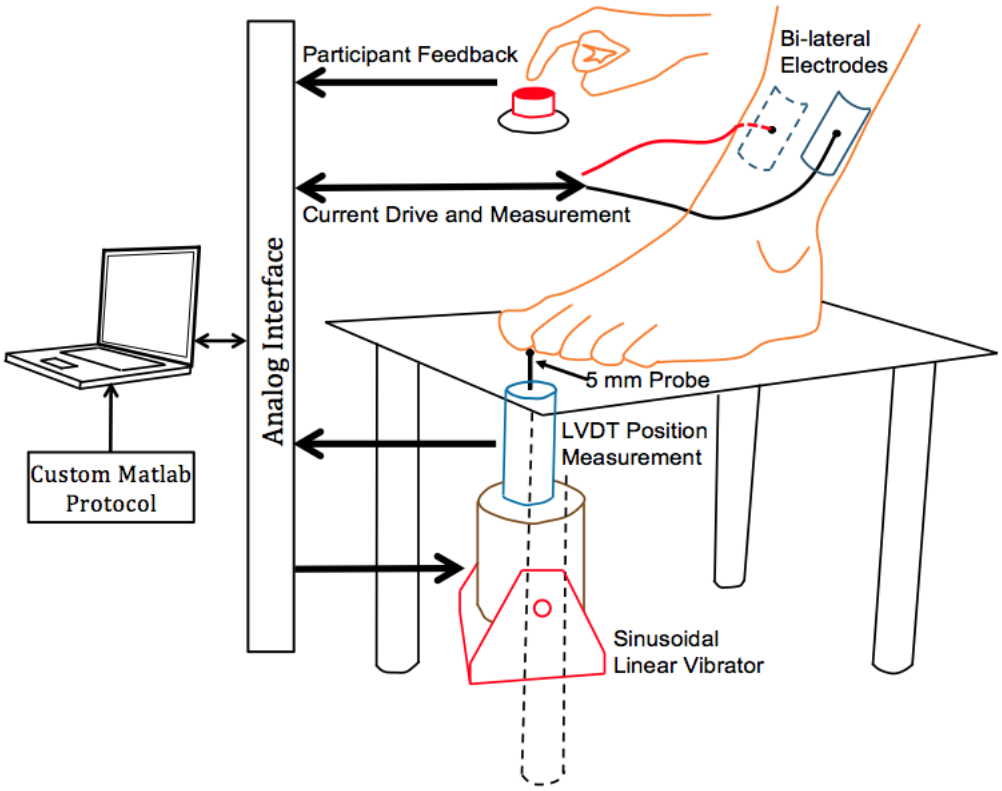

Figure 18. Diagram showing the testing platform and control and instrumentation setup of the vibration sensitivity testing. The platform had a 20 mm hole in its surface through which the probe made contact with the skin.

A 10 mm wide hook-and-loop strap, attached at the left and right edges of the platform in line with the probe, was placed over the toes and was used to keep the foot in place. It also ensured that the hallux was in contact with the probe, depressing the probe by 50 to 150 µm. Adjustments were made during the experiment, if needed, to ensure that contact was maintained in this range.

Figure 19 shows the modified method of limits protocol, which was conducted by a custom written Matlab program with minimal user input to ensure double blinding (See digital appendix folder “Hardware and data management system”).

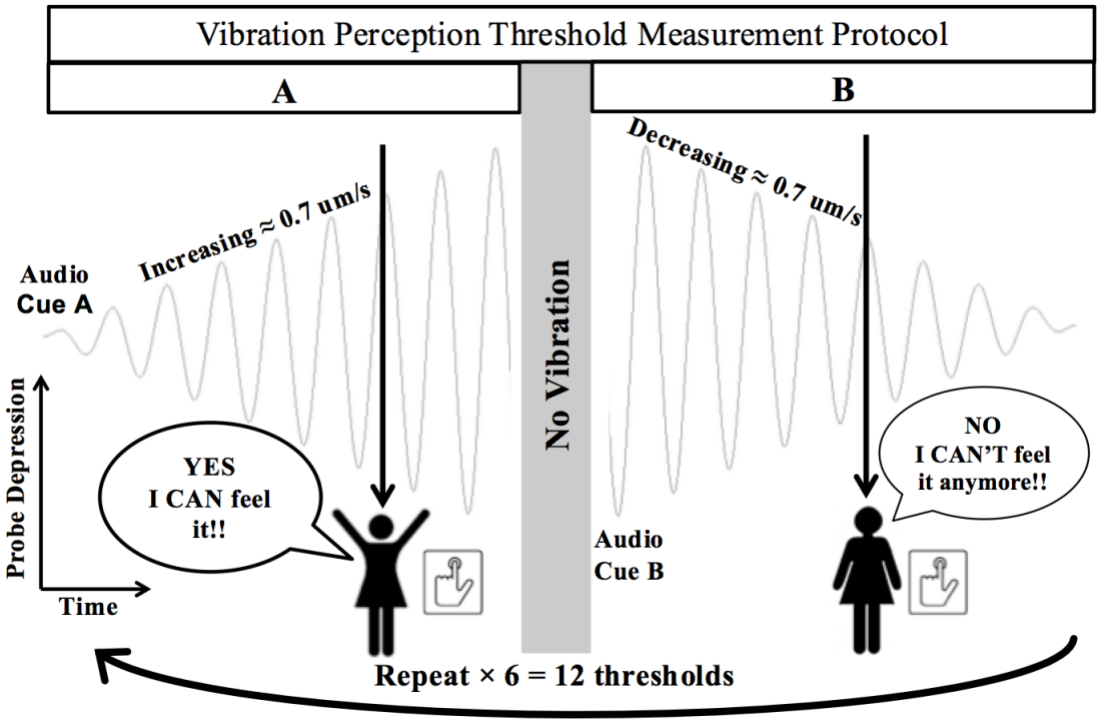

Figure 19. Diagram depicting the testing protocol for vibrotactile threshold testing.

Participants would first hear an easily recognisable audio cue indicating that an "up going" vibration ramp was imminent. The vibration would then start at an imperceptible amplitude and increase until the participant could feel the vibration. The participant was instructed to press a hand-held button immediately upon becoming aware of the vibration. The vibration would then pause for one second, and a different audio cue would sound, indicating the "down going" vibration ramp was imminent. The vibration would then start from a super-threshold amplitude and decrease toward zero at the same rate as before. The participant would then press the hand-held button as soon as they could no longer feel the vibration (see Figure 20).

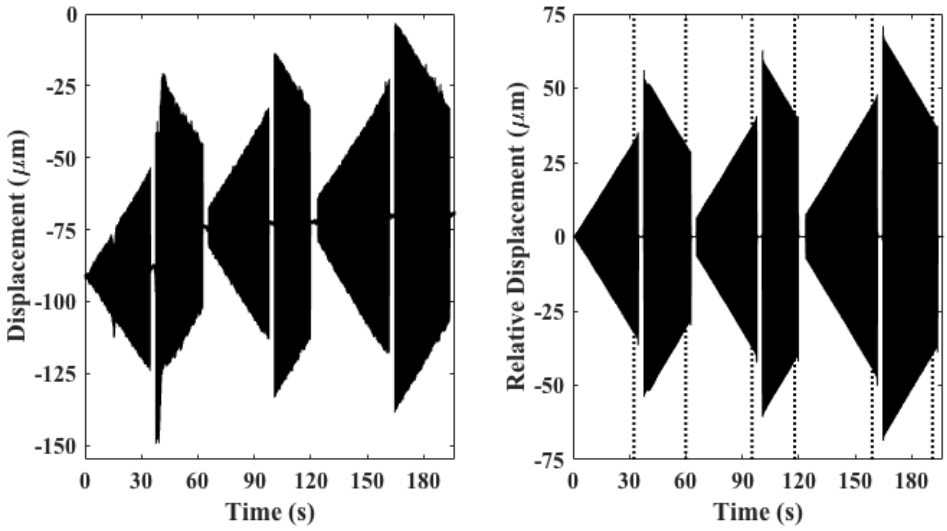

Figure 20. Typical vibration amplitude ramps during a subset of VPT measurement. Left is unfiltered vibration displacement data. Right is the band-pass filtered data with the participant responses marked as vertical dotted lines.

The sequence repeats until a total of 12 thresholds were collected. This would typically take between 5 and 10 minutes depending on the participant's thresholds and the rate of the ramps. The average vibration amplitude in the 0.5 seconds leading up to the button press was deemed the threshold for that ramp.

The subthreshold start value for up going ramps, and the supra-threshold start value for down going ramps was calculated by the computer based on past results for that participant and thus was slightly different each time, creating natural variability in the time to each button press. This can be thought of as increasing the effectiveness of the blinding, as participants, even though unaware of the amplitudes, may want to respond within common time periods if they perceive time-to-response as a predictor of vibration amplitude.

The supra-threshold vibration amplitude was the largest of three possible values: 20% greater than the current threshold estimate, 10 μm greater than the current threshold estimate, or a minimum lead magnitude greater than the current estimate. The lead magnitude was based on the rate of amplitude fall selected for this set of trials, and can be thought of as a minimum time before expected crossing of the threshold. This value was set to 5 seconds with an additional random variability of 0 to 3 seconds for each ramp. The amplitude was limited to 500 μm as this was the limit of the equipment. The

current estimate was calculated as the mean of the preceding thresholds for the current SENS amplitude and vibration frequency pairing.

There was no visual feedback of the vibration amplitude, or explicit measurements of the results available to the investigator or the participant. Only a scale-less representation of the raw measured vibration signal was available to the investigator after each button press to ensure that no errors were being made in the protocol. These errors included responding prior to initiation of vibration, responding long after the amplitude had reduced to zero, or excessive movement artefact. The participant was also permitted to declare that they had responded erroneously. These ramps were noted and were excluded from analysis.

Participants were familiarised with a reduced version of the protocol using only 6 thresholds as opposed to the 12 used in the testing stage. This was done at least once for each vibration frequency, but was repeated until it was clear that the participant was fully competent in the task. This often took many repetitions, which possibly indicates that the task was particularly alien to most participants.

The rate of vibration amplitude increase or decrease was set between 0.7 μm/s and 1.2 μm/s immediately after or during the familiarisation to ensure that the average time to perception was not too long or too short. With such a slow rate, even a several second delay in reaction time by the participant would only result in an error of a few μm in the measurement.

Valid ramps were those where the participant performed the task without error and the offset of the toe remained between 50 and 150 μm with minimal movement artefact. The data was then passed through a zero phase 15 to 135 Hz band-pass filter to further remove movement artefact and electronic noise (see digital appendix folder “Hardware and data management system/Misc/BPF15to135.m” for full filter details).

3.2.6 Measurement of pain

For each test condition, upon completion of the VPT measurement, the participant was asked to rate any symptoms of pain felt during the test in the evaluated limb, in three separate categories, on a visual numeric scale from 0 to 10.

An extract from the SA Brief Peripheral Neuropathy Screening exam (BPNS) was used (see Appendix D.2). Pain was recorded for Pain A: Pain, aching, burning in feet or legs, Pain B: “Pins-and-needles" in feet or legs, and Pain C: Numbness (lack of feeling) in

feet or legs. The scale starts at 0, ‘normal’ (*i.e.* no pain), stipulates 1 as ‘mild’, and extends to 10, ‘Severe’.

3.2.7 Data analysis

The comparison of the HIV-PN and the control cohorts was conducted with a two-sample t-test for each continuous variable, and the Fisher’s exact test comparing foot dominance.

The effects of SENS condition, HIV-PN, the direction of the VPT ramp (ascending or descending) on VPT and separately on symptoms of Pain, was computed as odds ratios of linear mixed effects models. This allows the analysis to use every recorded threshold to gain greater statistical power than a traditional paired comparison. In text we will refer to testing for a parameter’s effect on VPT or pain. In all cases this does not refer to causality, but rather to the manner in which the statistical tests were conducted, with VPT as the outcome measure. Statistics are noted as probability (p), Chi squared value (χ^2) and degrees of freedom (DF). For significant outcomes, the direction of the correlation will be noted.

An additional analysis comparing VPT of the best 50 Hz SENS results (optimal, per participant SENS amplitude) to the 50 Hz sham condition was conducted. Because this data is inherently “cherry picked” a traditional statistical test would provide a skewed result. The probability of the null hypothesis, that SENS had no effect, was evaluated using a Monte Carlo simulation of the experiment [135–137] (see Appendix A for a full description of how this was derived and performed).

Where appropriate data was evaluated for normality using a one-sample Kolmogorov-Smirnov test or KS test. All data subgroups were not statistically significantly different to a normal distribution unless otherwise stated.

All vibration data was analysed and filtered in Matlab. VPT thresholds were log transformed as is traditional for threshold data of this form [50–52,116]. Two-sample paired and unpaired t-tests were calculated in Excel, Fisher’s Exact test was calculated in Matlab and linear mixed effects models were calculated in R.

Power analysis indicated that in a crossover trial we can expect to find a significant result, should one exist, with intra-participant variability of 16% if there is a difference of 15% in the outcome measure for a group size of 20. These figures are in accordance

with predicted intra-participant variability shown in Breen *et al.* for elderly neuropathic individuals using a similar testing paradigm [30,92]. Pain measures are recorded on a scale of 0 to 10, thus it seems reasonable that intra-participant variability and detectable difference in this case will both be the same (≈9%) thus necessitating a minimum sample size of 18.

In general, averaging multiple measurements of the same parameter reduces intra-participant variability by $1/\sqrt{n}$ (where n is the number of measurements made of the same sample set). In our design, we record multiple data points (up to 12 repetitions) for each test condition, much more so than Breen *et al.* (3 repetitions), thus we can expect to see lower intra-participant variability. Adjusting for this, the study is powered to find a difference of 7.5%. Having 20 participants in each group exceeds the groups sizes of other studies in the field by a reasonable safety margin.

Results are regarded as significant if the p-value is less than 0.05. However, results below 0.15 may be discussed in context, and may justify further research.

3.2.8 Exclusion of data

In some cases, data needed to be excluded before analysis. Three participants were excluded entirely, and the reasons for this are discussed in the group characteristics results below (Chapter 3.3.1). Multiple individual thresholds were excluded because the amplitude of SENS did not appear to be below threshold.

When SENS is supra-threshold, it has the effect of inducing a "pins-and-needles" sensation on the skin under the electrode. Since this sensation was documented as part of the pain measurements (Pain B), the participants were asked if the Pain B was under the electrodes or elsewhere. If the participant could feel this sensation, then it is possible that the SENS intervention signal was now supra-threshold (see Chapter 4 for a description of the stability of electrical perception thresholds). It seems best that trials be excluded where SENS was applied, and participants reported any Pain B scores under the electrode, as those trials cannot be said to be blind or subthreshold.

However, some participants reported the sensation even when the SENS signal had been switched off for some time, indicating it may be a placebo effect, possibly caused by psychological priming or just by the presence of the adhesive electrodes. Given the propensity for participants to report Pain B under the electrode when SENS was not

active, trials were only excluded if Pain B was reported at a higher level than the highest of the three sham conditions for that participant.

3.3 Results

3.3.1 Group characteristics

Two of the 22 HIV-PN participants recruited were excluded from the results analysis. One was not able to learn the task, and the other had vibratory thresholds in excess of what the equipment was able to measure (>1000 μm). One of the 21 control participants recruited was excluded as their VPT at different frequencies were between 4.3 and 12 standard deviations from the mean of the group, indicating that the participant possibly had undiagnosed sensory neuropathy, and was therefore inappropriate as a control.

Chapter 2.3 presents a detailed description of the group characteristics. It further analyses how baseline VPT varied between groups and interacted with participant height, age, and for the HIV-PN group, years on Antiretroviral Therapy (ART) and various clinical measures of neuropathy. Here we present a summary of relevant results from that chapter, and analyse the effect of SENS on VPT and pain under different conditions.

The two groups were not statistically significantly different in age, height, gender or foot dominance. Weight and BMI were significantly different with the average non-HIV participant's body weight in the obese range (BMI>30) which is common for this demographic [112]. Past work indicates that BMI most likely does not correlate with VPT, but if it does, it is likely to result in reduced tactile sensitivity with increases in BMI [118–120].

The HIV-PN participants were found to have less sensitive baseline vibration perception at all three vibration frequencies. An interaction with frequency ($P = 0.064$) is suggestive that the HIV-PN participants had particularly poor 25 Hz responses in comparison with the control group. Increasing age was found to correlate with reduced sensitivity. Years on ART correlated with improved sensitivity at 25 Hz only. The two results that applied specifically to 25 Hz suggest that the disease and its treatment have a stronger effect on low vibration frequency mechanoreceptors than other vibration frequencies. Participant height, and all clinical screening outcomes measured did not correlate with baseline VPT (see Chapter 2.3 for further details).

The Electrical Perception Thresholds (EPT) of the groups were not found to be different ($p>0.64$). This result is somewhat corrupted in that EPT were not measured above 555 μA. Four individuals in the HIV-PN group had thresholds in excess of 555 μA, and three individuals in the non-HIV group. Truncating these thresholds to 555 μA, the average electrical perception threshold of the HIV-PN group was 164 μA and 142 μA for the non-HIV group. It was noted for several participants that measuring the EPT was difficult and that there was not a high degree of confidence in the final value. This is reinforced in that during the testing, participants often reported the sensation of the electrical stimulation even when it was below the previously measured threshold for that participant (Chapter 4 addresses this problem, and shows the EPTs are not stable).

3.3.2 Effect of SENS on Vibration Perception Thresholds (VPT)

Figure 21 depicts the effect of SENS on VPT relative to the sham condition for the HIV-PN group and healthy non-HIV control group. Both groups had a statistically significantly beneficial effect of SENS for 45 μA at 50 Hz. Only the non-HIV participants had a beneficial response at 30 μA and 90% of threshold (both 50 Hz). The HIV participants responded with a detrimental effect at 90% of threshold (50 Hz) and non-HIV participants responded with a detrimental effect of SENS in the 128 Hz test condition.

Table 6 provides all the numerical results of the statistical tests for the effects of SENS on VPT. The effect of the direction of the vibration ramp on VPT (ascending or descending) is controlled for. The full numerical outcomes of all the statistical tests is contained in the digital appendix folder “Effects of SENS statistical outcomes”. The full set of individual results is contained in the spreadsheet “Final results.xlsx”, within the digital appendix folder “VPT study data”.

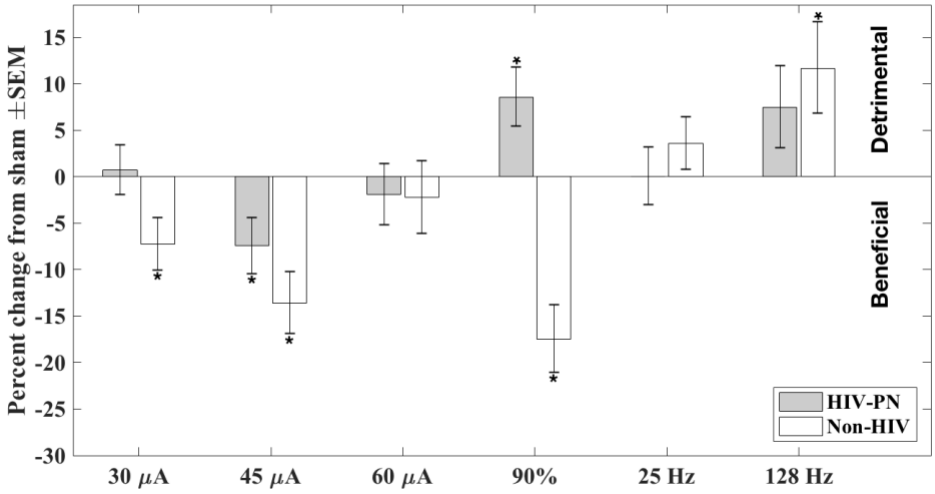

Figure 21. Graph demonstrating the effect of SENS on VPT compared to the matched sham condition for different SENS amplitudes and vibration frequencies. First SENS was tested at 30 μA, 45 μA, 60 μA and 90% perception threshold all for 50 Hz vibration frequencies. Then the best performing 50 Hz SENS amplitude was retested against sham conditions at 25 Hz and 128 Hz vibration frequencies. * indicate results statistically significantly different from zero ($p<0.05$).

Table 6. Statistical results of the effect of SENS on VPT. * indicates significance p < 0.05. All degrees of freedom are 1. Negative percentage changes are beneficial and positive changes are detrimental.

Test Condition	Group	p (χ^2)	Percentage Change
30 μA, 50 Hz	HIV-PN	0.79 (0.07)	0.7
	Non-HIV	0.01 (6.06)	-7.2*
45 μA, 50 Hz	HIV-PN	0.02 (5.58)	-7.5*
	Non-HIV	<0.001 (14.08)	-13.6*
60 μA, 50 Hz	HIV-PN	0.56 (0.33)	-1.9
	Non-HIV	0.57 (0.33)	-2.3
90%, 50 Hz	HIV-PN	0.01 (7.82)	8.6*
	Non-HIV	<0.001 (18.77)	-17.5*
25 Hz	HIV-PN	0.99 (0.0)	0.0
	Non-HIV	0.2 (1.65)	3.6
128 Hz	HIV-PN	0.08 (3.04)	7.4
	Non-HIV	0.01 (6.3)	11.7*

The effect of the direction of the VPT ramp (ascending or descending) was also evaluated. Ascending ramps were found to have a lower threshold than descending ramps at 25 Hz for both groups (p's<0.001), and at 60 μA (50 Hz) for the non-HIV group (p = 0.007).

The effect of SENS was not found to interact with the effect of direction for any test condition (p's > 0.18), *i.e.* there is no evidence to suggest that SENS affected ascending and descending ramps differently.

The interaction of SENS and group (HIV-PN or non-HIV) was also assessed. The effect of SENS was found to be different between the groups for 30 μA (p = 0.043) and 90% (P<0.001) (50 Hz). The remaining conditions were not significantly different between the groups (p's>0.17).

While the audibility of the vibration was not recorded, no participants reported being able to hear the vibration. The vibration was only audible to the tester for exceptionally high amplitudes of vibration at 128 Hz.

3.3.3 The effect of "optimal amplitude" SENS

In Chapter 2.3.2 we found that HIV-PN participants would require an improvement of 45% at 25 Hz, 29% at 50 Hz and 53% at 128 Hz in their VPT scores to match the baseline scores of the healthy control participants. This indicates that even for the best performing SENS condition, tactile sensitivity was not fully restored in HIV-PN participants.

Breen *et al.* [92] found that SENS at 30 μA improved the tactile sensitivity of elderly participants, but not at other amplitudes. They performed an additional analysis asking the question: what if there is not a global optimal amplitude for SENS, what if each participant has a different intervention amplitude that works best for them? They found this to be the case, with a 16.2% improvement in performance when the best outcome for each participant was cherrypicked from the data. It is possible that by performing a similar analysis, the effect of SENS on HIV-PN can be shown to be larger than the 7.5% seen above, if applied at an optimal amplitude.

The study design presented here served only to answer this same question regarding optimal SENS amplitude for 25 Hz and 128 Hz vibration frequencies. The amplitude of SENS that worked best at 50 Hz for each participant was tested at 25 Hz and 128 Hz vibration frequencies, double blind, against new sham conditions. There was no effect of SENS at 25 Hz, and SENS was actively detrimental for the non-HIV participants at 128 Hz.

To replicate the finding of Breen *et al*. we extract the best response to SENS for any of the 50 Hz test conditions for each participant separately. Figure 22 shows the response of this new category compared to the sham 50 Hz condition. To test for a statistically significant effect, conventional statistics require the study design to have a separate sham condition matched to each amplitude of SENS at 50 Hz. However, matching the design of Breen *et al.*, this work only had one sham condition for all 50 Hz tests. This results in a statistical bias discussed extensively and solved in Appendix A.

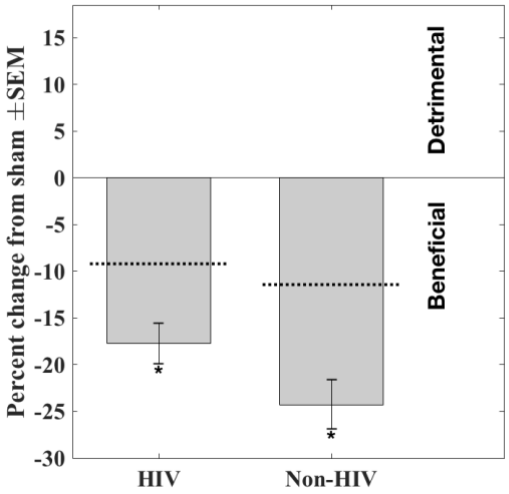

Figure 22. Effect of SENS on VPT at 50 Hz vibration frequency, for an amplitude of SENS optimally individualised for each participant. The dotted lines indicate the boundary of statistical significance as determined by Monte Carlo simulation (see Appendix A).

Monte Carlo simulation indicated that the effect of SENS seen in Figure 22 was statistically significant for both the HIV-PN group and the non-HIV group, and was not the consequence of the study design. Table 7 provides the numerical results of the analysis. The p-value is the output of odds ratios of linear mixed effects models (see Chapter 3.2.7), and suffers from the selection bias created when picking only the best outcomes. The simulated 5 percentile p-value is the limit under which the p-value must fall in order for the optimal SENS condition to be said to have a statistically significant effect at 5%.

Table 7. Experimental and simulated outcomes of statistical tests with the "optimal" SENS condition.

	Effect of optimal SENS on VPT	Simulated 95 percentile effect of optimal SENS on VPT	p-value	Simulated 5 percentile p-value
HIV-PN	-17.8%	-9.2%	4.54e-13	1.26e-5
Non-HIV	-24.3%	-11.4%	6.22e-15	8.93e-6

Since the biased "p-value" is smaller than the "simulated 5 percentile p-value" SENS can be said to have had a beneficial effect on VPT in both groups in this condition. The effect seen on the HIV-PN group for optimal SENS (17.8%) is very similar to that seen by Breen *et al.* on elderly individuals (16.2%).

3.3.4 Effect of SENS on pain

The data recorded for pain was very sparse, with most participants reporting no pain in many conditions. Because the data is so sparse, all non-zero pain data is presented here and identified per participant rather than creating summary data, although some summary data is still provided at the end of the analysis. HIV-PN participants are identified as 'H' followed by a unique identifying number, and all non-HIV participants are identified with a 'C' followed by a unique identifying number. The identifiers remain consistent throughout this chapter.

In Table 8, Table 9 and Table 10 the data for symptoms is reported as "sham" : "SENS" for each test condition. Because only one sham condition was recorded for the four 50 Hz vibration frequency test conditions, that sham data is repeated for each 50 Hz column. In a small number of cases participants reported measures as being a range of consecutive outcomes, *e.g.* '6' or '7'. In these cases, the data was summarised as the midpoint *e.g.* '6' or '7' becomes '6.5' in the data analysis.

Table 8 presents the results for the only two HIV-PN participants and one non-HIV participant who reported any sensation of "pain, aching, burning in feet or legs" during the VPT testing. Participant H1 reported the pain over the top of the foot and at the back of the lower leg. H2 reported pain below the ankle for one trial. The tester noted for that trial: "Same place as numbness. I think she reported pain, she meant numbness,…". The participant did report numbness in other trials. Notes from the trials of C1 indicate: "very difficult to get number off scale. Estimates vary wildly." And that the pain varied from lameness on the foot, to cramps, that were not painful, above the electrodes below the knee, and on the front of the tibia.

Table 8. Participants reporting "Pain, aching, burning in feet or legs" above zero for any test condition, on a scale of 0 (normal) to 10 (Severe). Data shown as 'sham' : 'SENS' conditions. No pain reported in either condition is noted as '-'.

ID	30µA	45µA	60µA	90%	25 Hz	128 Hz
H1	6:5	6:4	6:6	6:6	3:4	3:6
H2	-	-	-	-	0:4	-
C1	1:0	1:2	1:2	1:0	-	0:3.5

Table 9 present the results for participants who reported any sensation of “Pins-and-needles" in feet or legs” during the VPT trials. Most participants reported the sensation under the electrodes. These trials are included here only where the sense under the electrodes was equal or lower than during the sham conditions. Where the sensation was reported exclusively under the electrodes is marked with a “†” symbol in the table. The notes from the individual trials indicate:

- The rating of ‘5’ given by H3 in the 50 Hz sham condition was originally rated as a ‘10’, but was lowered after it was explained to the participant the severity of a ‘10’ rating.
- C2 felt the sensation in the whole foot, but slightly stronger under electrodes.
- C3 felt the sensation up the shin above the electrodes for 50 Hz sham trials, and behind the heel for 45 μA trial, and only at the start of the trials for both the 45 μA trials and the 25 Hz trial.
- C6 could feel pins-and-needles during testing and after the VPT test as well.

Table 9. Participants reporting "Pins-and-needles" in feet or legs" above zero for any test condition, on a scale of 0 (normal) to 10 (Severe). Data shown as 'sham' : 'SENS' conditions. No symptoms reported in either condition is noted as '-'. 'NA' indicates a trial was excluded. "†" indicates the sensation was noted to be under the electrodes and nowhere else.

ID	30µA	45µA	60µA	90%	25 Hz	128 Hz
H1	-	0:3	0:3†	-	-	3†:4
H2	-	-	-	-	-	0:2
H3	5†:0	5†:0	5†:0	NA	NA	NA
H4	-	0:1†	-	-	-	3†:0
H5	1†:0	1†:0	1†:0	1†:1†	-	-
H6	NA	-	0:1	-	NA	NA
C2	3:1†	3:2	3:1†	NA	1†:3	NA
C3	1:2	1:2	NA	NA	0:1.5	NA
C4	NA	-	NA	0:3	-	-
C5	0:1	-	NA	NA	NA	NA
C6	-	-	NA	NA	-	0:1

Table 10 presents the results for the participants who reported any sensation of "Numbness (lack of feeling) in feet or legs" during the VPT testing.

In general, the reporting of numbness seemed unreliable, which is not unexpected since the participant is sitting for a long period with their leg and foot completely stationary. The notes for the individual trials indicate that:

- H2 felt numbness below ankle.
- H4 felt numbness below the ankle and under the foot. For the 25 Hz trials it was also above the electrodes and could feel the numbness outside of the testing period.
- H7 felt the numbness in foot.
- H8's rating of '5' is for a cold sensation that could not be classified as Pain A or Pain B, located around the electrodes. The sensation went away between

trials. The rating of '3.5' was also not explicitly for numbness, as the participant had difficulty describing the sensation and said it to be like vibration under the foot.

- H10 felt the numbness on top of foot.
- For C1 the numbness is noted as lameness on top of the foot. The '6' rating of C1 is noted as "very difficult to get number off scale. Estimates vary wildly.".
- C6 felt a little numb on the toe, and noted that the 25 Hz vibration felt different to the other frequencies.
- C7 felt the numbness covered the whole foot during and after the VPT tests.
- C8 felt numbness outside of testing period as well as during the VPT test. The 50 Hz control condition denoted as sensation of cramps and not numbness. The sensation of numbness for the 25 Hz condition was felt under the foot.
- C9 felt numbness along front of leg from above the electrodes and down, and felt it was stronger during the testing.
- C10 reported a sensation of coldness as numbness during trial at the toes only.
- C11 felt numbness on the leg.

Table 10. Participants reporting "Numbness (lack of feeling) in feet or legs" above zero for any test condition, on a scale of 0 (normal) to 10 (Severe). Data shown as 'sham' : 'SENS' conditions. No symptoms reported in either condition is noted as '-'. 'NA' indicates a trial was excluded.

ID	30μA	45μA	60μA	90%	25 Hz	128 Hz
H2	1:0	1:0	1:0	1:3	5:0	-
H4	2:0	2:0	2:2	2:0	5:4	2:3
H7	-	-	-	-	8:7.5	-
H8	-	-	0:5	0:3.5	0	0
H9	-	-	0:3	NA	NA	-
H10	-	-	NA	NA	1:0	-
C1	0:1.5	0:6	0:1	-	1:0	0:2.5
C6	-	-	NA	NA	0:1	-
C7	-	-	-	-	5:0	-
C8	3:0	3:0	3:0	3:0	2:0	NA
C9	-	-	NA	NA	0:3	-
C10	-	0:1	-	-	-	-
C11	-	-	0:1	NA	-	-

The effect of SENS on each the three measures of pain were assessed for each test condition for the HIV-PN and non-HIV groups. No effects of SENS on pain were found (all p's>0.14).

The effect of group (HIV-PN or non-HIV) on pain scores, and the interaction between group and SENS on pain scores was also analysed. No effects were found (p's>0.13). This is to say that pain level was not affected by the group a participant was in, nor did SENS have a different effect on pain for the different groups.

Table 11, Table 12 and Table 13 summarise the pain outcomes. Table 11 shows the number of participants who reported any amount of each kind of symptom in the sham condition. The table indicates that very few participants reported pain in the baseline measurement, but comparatively more indicated "Pins-and-needles" or numbness in both the HIV and non-HIV cohorts.

Table 11. Number of participants who experienced pain in the sham condition.

ID	Pain	Pins-and-needles	Numbness
HIV	1	4	4
non-HIV	1	2	3

Table 12 shows the number of participants who experienced more severe symptoms in the sham condition than in the SENS condition. High numbers would indicate that SENS may have had a role in reducing the severity of symptoms. The table indicates, in accordance with the statistical analysis, that there were very few occurrences where SENS improved symptoms, and there was little difference in the response between the groups. This does not present strong evidence that SENS has a beneficial effect on reported symptoms.

Table 12. Number of participants who reported more severe symptoms in the sham conditions than the SENS condition. Data displayed as "number of HIV participants" : "number of non-HIV participants".

ID	30μA	45μA	60μA	90%	25 Hz	128 Hz
Pain	1:1	1:0	0:0	0:1	0:0	0:0
Pins-and-needles	2:1	2:1	2:1	0:0	0:0	1:0
Numbness	2:1	2:1	1:1	1:1	4:3	0:0

Table 13 shows the number of participants that experienced more severe symptoms in the SENS condition than in the SHAM condition. High numbers would indicate that SENS may have had a detrimental effect on symptoms. The table indicates, in accordance with the statistical analysis, that there were very few occurrences where SENS worsened symptoms, and there was little difference in the response between the groups. This does not present strong evidence that SENS has a detrimental effect on symptoms in either group. Together, Table 12 and Table 13 provide reasonable evidence that even if SENS has an influence on symptoms of pain, it is not sufficiently strong to be measured in this context.

Table 13. Number of participants who reported more severe symptoms in the SENS conditions than the SHAM condition. Data displayed as "number of HIV participants" : "number of non-HIV participants".

ID	30μA	45μA	60μA	90%	25 Hz	128 Hz
Pain	0:0	0:1	0:1	0:0	2:0	1:1
Pins-and-needles	0:2	2:1	2:0	0:1	0:2	2:1
Numbness	0:1	0:2	2:2	2:0	0:2	1:1

3.4 Discussion and Conclusions

This work presents the first known data assessing the effect of SENS on patients with HIV-PN, and the first data exploring the effect of SENS on perception thresholds for vibration frequencies other than 50 Hz. Finally, it presents the first known data on

symptoms of pain when using a subthreshold intervention signal for the purposes of enhancing tactile sensation.

The results present evidence that SENS can improve tactile sensitivity in this population without increasing perceived peripheral neuropathic symptoms, but also indicate that SENS has limitations that need to be further explored before it can be implemented as a clinical intervention for participants outside of the research environment.

The primary goal of this study is to assess the effectiveness of SENS in improving VPT of HIV-PN patients and healthy controls participants.

3.4.1 Efficacy of SENS for 50 Hz Vibration Perception Thresholds (VPT)

SENS improved tactile sensitivity of both groups at 50 Hz when SENS was applied at an optimal amplitude for each person. SENS was also effective in improving 50 Hz vibration sensitivity when applied at pre-set low amplitudes (45 μA RMS for both groups, and 30 μA RMS for the non-HIV group). This is mostly consistent with past research by Breen *et al.* which had a similar experimental design, but a different population group [92].

There are several unexpected results. Firstly, that both groups responded positively to SENS at 45 μA and not 30 μA as in previous work. It has been established here, and in previous work that the best amplitude of SENS is participant specific. With such low participant numbers in previous work (n = 8) and here (n = 20) it is not surprising that there is variability in this outcome. What is important is that it was low amplitudes of SENS that worked globally over the groups. In a potential therapeutic use of SENS, it may not be practical to measure the optimal amplitude of SENS for each user or apply the signal at a percentage of the electrical perception threshold (EPT). In this case, having an amplitude of SENS that works for all participants, even suboptimally, may be a practical solution.

The second unexpected result was the response to SENS at 90% of EPT. In these circumstances one could expect the stimulation at this amplitude to be effective, since 90% of threshold in subthreshold interventions has been shown to be effective in many prior studies. This was the case for the non-HIV participants. One could also argue that it should not be effective, since electrical thresholds were very high and consequently 90% of EPT for most participants was a much higher amplitude than what has worked in the past. This was the case for the HIV-PN group. It is certainly unexpected that the

non-HIV participants would respond so strongly to such a high amplitude of SENS, and that the HIV-PN group would have such a different response to the non-HIV group. This, and that EPT between a healthy group and a group with known tactile deficiencies were not found to be different, call into question the validity of the EPTs measured for the HIV-PN participants. The data provides little explanation for this result and further exploration is recommended.

3.4.2 Efficacy of SENS for 25 Hz and 128 Hz Vibration Perception Thresholds (VPT)

The research also investigates the effectiveness of SENS at previously unresearched vibration frequencies. An unexpected result was that SENS applied at the amplitude that created the most benefit for 50 Hz vibration was actively detrimental for the non-HIV group, and possibly detrimental for the HIV-PN group ($p = 0.08$) at the high vibration frequency (128 Hz). Further, SENS had no significant effect at the low vibration frequency (25 Hz) making results fairly consistent for both groups.

There are three possible explanations for this result. It could be a result specific to these population groups. This is unlikely since the 50 Hz results are relatively similar to previous research outcomes. It could be that the whole paradigm of using subthreshold electrical stimulation has a different effect on low and high frequency mechanoreceptors. This too is unlikely since 50 Hz does not represent a set of mechanoreceptors that respond exclusively to frequencies in this range, but rather a combination of both high a low frequency receptors [116], suggesting a positive response to 50 Hz should translate at least to either higher or lower frequencies of vibration, and possibly both.

The most likely reason is that the combinations of the spectrum of the SENS signal itself and the electrical filtration of that signal when passed through the tissue to the nerve axons carrying the vibration signals, results in an intervention that has a frequency response curve. It is difficult to measure this response noninvasively, without the use of tools like microneurography. The shape of this curve could start off near zero for low vibration frequency signals, and has a peak beneficial response somewhere in the range of 50 Hz, and then becomes actively detrimental to higher vibration frequency signals. The hypothesis that altering either the amplitude or the spectrum of SENS could

result in a different frequency response curve is testable and should form part of future work.

Regardless of what the reason for the discrepancy in response at different vibration frequencies is, the result sheds light on the mechanism of SENS. In most subthreshold interventions, the mechanism is said to be stochastic resonance (SR). This rationale is often maintained when the intervention is applied proximally to the intervention site. However, the model of classic SR does not predict that the extent of the enhancement should be sensitive to vibration frequency. It is therefore likely that SENS does not operate through SR. Chapter 1.5.2 offers alternative explanations found in the literature for enhancements seen through the application of SENS-like signals.

The results regarding vibration frequency dependence represent a very important finding. If SENS is to be used to improve quality of life, it must improve tactile sensitivity for a wide range of tasks. Further research must be done into this frequency response and strategies for overcoming this limitation.

3.4.3 Effect of SENS on symptoms of pain

The secondary goal of this work is to investigate how SENS affects symptoms of pain. Previous SENS studies and other subthreshold studies have not investigated the effect of the intervention on perceived pain. If these interventions, which improve tactile sensitivity, also increase the amount of pain perceived in neuropathic populations, it could severely limit the use of SENS as therapy. Conversely, should SENS reduce the amount of pain experienced, it would become strong motivation for the further investigation of SENS as therapy.

There was no evidence to suggest that SENS exacerbates existing “Pain, aching, burning in feet or legs” or causes it to occur when none previously existed. Neither was there evidence to suggest that SENS alleviated symptoms of pain. The qualitative description of pain for the three participants was not consistent between them, further re-enforcing the idea that SENS does not have an effect on neuropathic pain.

Similar results occurred for symptoms of “Pins-and-needles” and “Numbness (lack of feeling) in feet or legs”. While many more participants reported these sensations, the data was still very sparse and demonstrated no consistent anectodical or statistical pattern that would imply that SENS impacted the scores reported for these symptoms.

The exception to this was the sensation of “Pins-and-needles" that was frequently reported as being felt under the electrodes, and was likely a result of SENS being applied at a supra-threshold level. This does present a problem for the application of SENS as therapy, since it appears that EPTs cannot be relied upon to remain stable.

No statistical difference in any of the three measures of pain were found between the groups, *i.e.* it cannot be said that the HIV-PN participants experienced more pain than the non-HIV group in these circumstances. This is likely a result of excluding HIV participants with high levels of neuropathic pain. This reduces the external validity of the result and must be noted as a limitation when stating that SENS likely does not cause pain in HIV-PN patients.

3.4.4 Limitations of this study

A limitation of this study is that the healthy, non-HIV participants did not undergo a neurological screen or HIV testing, and consequently may have suffered from undiagnosed diseases that affect VPT. One potential control participant was excluded for this reason. That there was a significant difference in baseline VPT between the groups indicates that it is unlikely that the results were compromised by this limitation. Further, participants were recruited from an area where HIV awareness campaigns are prominent and HIV testing is freely available.

Participants with severe painful neuropathy were excluded from the HIV-PN group and this limits the extent to which we can claim the results apply to HIV-PN participants with severe painful neuropathy. However, given that the results indicate SENS did not have an adverse effect on pain, this evidence can be used to justify the inclusion of participants with severe painful neuropathy in future studies.

The reports of “Numbness” and “Pins-and-needles” were generally noted as being unreliable. It is possible that a more robust protocol investigating pain would have led to more consistent results and that simple numeric scales are insufficient. A more significant limitation is that the study did not evaluate the effect of SENS on noxious stimuli. Thus, it cannot be said if SENS has an hyperalgesic effect.

EPTs were found to be unstable, and therefore the results of SENS at 90% of threshold can be called into question. The stability of these thresholds is investigated further in Chapter 4.

The ultimate goal of this field of work is to provide a therapy to improve the symptoms of HIV-PN. Showing an improvement in VPT is an important step towards that goal, but it is ultimately a laboratory measure used as a proxy for overall tactile sensitivity. Research should eventually progress to assessing performance in functional tasks and reduction of known risk factors for health-related quality-of-life, such as falls.

Finally, pain and VPT was only assessed over a period of a few minutes at a time. The effect of SENS when used for extended periods remains unstudied. This is likely a consequence of the technology to apply SENS as a wearable device being unavailable. Chapters 5 and 6 attempt to address this problem by developing the electronics required for a wearable SENS stimulator.

3.4.5 Clinical implications for the use of SENS as therapy

SENS continues to show promise to be developed into a therapy for patients suffering peripheral neuropathic desensitisation. Here we showed that past results of VPT benefit also apply to HIV-PN. Results also indicate that SENS is unlikely to have an adverse effect on neuropathic pain, which could have been a big stumbling block in its use as therapy.

However, while SENS was shown to be beneficial for 50 Hz VPT, it was not shown to benefit 25 Hz or 128 Hz VPT. This casts doubt on its ability to be beneficial for functional tasks and reducing risk factors. The reasons for this are unknown and more research should be conducted into the spectrum of both the SENS signal itself and the physiological mechanism of the benefit it provides, so that it may be optimised for a wider range of tactile benefit.

The largest benefit in VPT observed with SENS for the HIV-PN participants was 17.8% improvement at 50 Hz for individualised optimised SENS amplitudes. This represents roughly half of the gap in baseline VPT performance between the HIV-PN group and the non-HIV control group. Whether this difference is clinically significant should be investigated.

Future work should include participants with higher levels of neuropathic pain and should focus on investigating the effect of SENS on the perception of noxious stimuli, the effect of SENS on different vibration frequencies and the physiological mechanism of the effect of SENS.

4

MEASUREMENT OF PERCEPTION THRESHOLDS FOR ELECTRICAL NOISE STIMULI

Subsensory therapeutic signals often rely upon the application of a mechanical or electrical signal at amplitudes that are a particular percentage of the participant's perceptual threshold. The ability of one to detect the perceptual threshold, and for it to remain stable is vital to the operational paradigm of these interventions.

The work in this chapter was published in part as a paper and presentation in the 2017 Annual International Conference of the IEEE Engineering in Medicine and Biology Society (EMBC):

Karpul D, McIntyre S, Van Schaik A, Breen PP. Measurement of perception thresholds for electrical noise stimuli. Proc. Annu. Int. Conf. IEEE Eng. Med. Biol. Soc. EMBS, 2017, p. 2166–9. doi:10.1109/EMBC.2017.8037284.

4.1 Introduction

Richardson *et al.* were the first to demonstrate the use of Subthreshold Electrical Nerve Stimulation (SENS) to improve peripheral sensitivity *in vivo* in humans [63]. SENS has since been shown to successfully improve sensitivity and related outcome-measures in multiple populations (see Chapter 1 for a full description of existing literature).

The therapy consists of two surface skin electrodes driving current into the participant near where sensitivity is to be enhanced (*e.g.* the fingertip), or proximal to the enhancement site (*e.g.* lower leg for improvement at the big toe) (Figure 23). The current usually has the spectral characteristics of 'white' or 'pink' band limited noise, and a carefully chosen amplitude between 60% and 90% of the participant's electrical perception threshold (EPT).

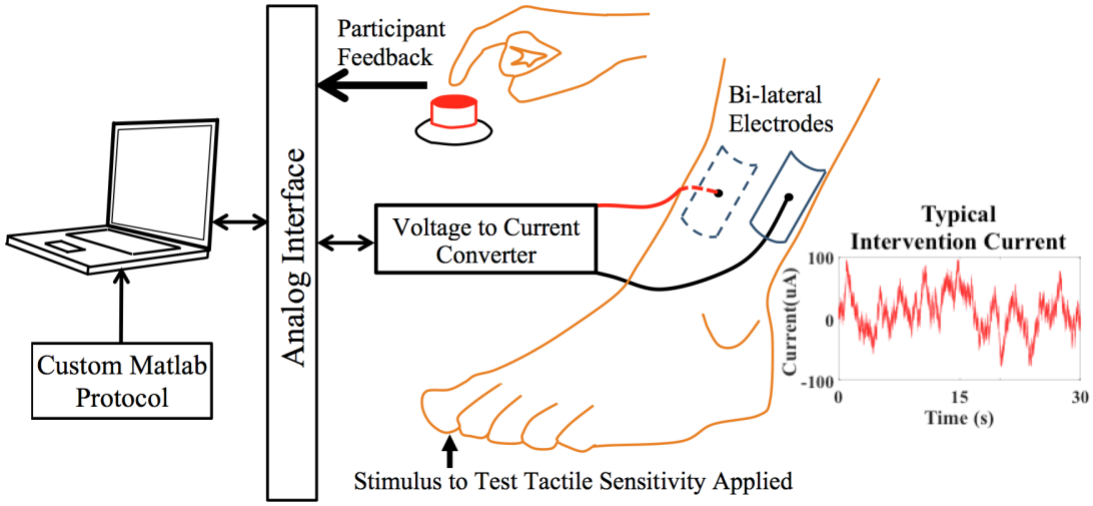

Figure 23. Typical application of SENS proximal to the site where tactile sensitivity is to be tested.

In this chapter the therapeutic signal is referred to as the "intervention" or just SENS. This is not to be confused with the "stimulus" which is the signal to be detected by the participant, thus demonstrating increased sensitivity. When implementing a SENS experiment, first the intervention signal is treated as a stimulus, and its perception threshold is established. The intervention amplitude is then set to some pre-determined subthreshold value.

Chapter 1.5.2 presents a detailed discussion of the potential mechanisms of effect for interventions of this type. In most interventions of this type, the amplitude of the intervention relative to the perception threshold of the intervention signal is regarded as important. Wells *et al.* demonstrated that both the intervention and the stimulus

amplitudes affect the efficacy of the intervention (in this case for vibratory noise) [67]. The effect is maximal when the intervention amplitude, relative to both the perception threshold and the amplitude of the stimulus, are appropriately matched. A smaller stimulus would require a larger SENS amplitude and *vice versa*.

Regardless of the method employed and the underlying mechanism, it is clear that controlling the SENS amplitude relative to the EPT is vital to allow the intervention to function optimally. Despite this, little focus has been dedicated in the literature to methods used to determine EPTs and the factors that influence their variability. The SENS studies cited in Chapter 1 determined EPTs using "self determination", a method of levels or limits, or failed to provide information on the matter. The studies gave no indication that this aspect of the experiment was double blinded. The actual EPT or variability data were not provided. This is understandable since EPT was not meant as an outcome measure in these studies.

A major drawback to using the method of limits for measuring perceptual thresholds is that it can be biased by the decision criterion adopted by the participant when uncertain whether the stimulus is present. A participant who adopts a liberal criterion may indicate she detected the stimulus when uncertain, while a more conservative participant may wait until she is more certain. If the two participants had identical sensitivity for detecting the stimulus, the liberal observer would appear to have a lower threshold. Furthermore, the criterion adopted can change during testing, and can be influenced by a desire to perform well or to please the experimenter, or by impatience or boredom. In order to measure sensitivity independently of response bias, a 'two-interval forced choice' (2IFC) paradigm was employed. This involves participants judging which of two successive time intervals (indicated by audio cues) contained the stimulus. 2IFC is a psychophysical procedure commonly used in perceptual science (see Chapter 4.2 for more details regarding 2IFC).

In most SENS applications little attention is given to the characteristics of the electrode skin interface, however, the electrode impedance, surface areas and connection quality have a large effect on the voltage applied to the skin as well as the current density and distribution in the tissue. Most studies simply cite the total current applied (*e.g.* 60 μA RMS [92]) since measuring electrode characteristics and current density is either difficult or impossible in some circumstances.

Rosell *et al.* investigated electrode impedances at ten placements around the body [138]. They found significant differences in impedance at difference locations, especially at frequencies below 100 kHz, which includes the frequencies used for SENS.

Bîrlea *et al.* performed a study that investigated participants who wore electrodes for seven days without removal and monitored the changes in impedance over time [139]. They found 14% decrease in the resistance of the surface electrode connection and a 15% decrease in the resistance of the underlying tissue. They also found a reduction in the capacitance of the connection after exercise, but not over the week. This experiment has implications for a final therapeutic version of SENS as a product that may be worn on a long-term basis. If impedance and SENS threshold are related, and impedance changes over time, then it is vital that this be considered when adjusting SENS amplitude during long-term use.

Bîrlea *et al.* modelled the impedance formed between the stimulation electrodes as a network of a single small resistor (r) in series with the parallel combination of a large resistor (R) and capacitor (C) (Figure 24). 'r' is typically in the order of 2 kΩ, and can be thought to roughly represent the resistance of the limb itself. 'R' and 'C' are usually in the order of 20 kΩ to 60 kΩ and 30 nF to 600 nF and represent the resistance and capacitance of the electrode connection to the skin respectively. At high frequencies and in pulsatile applications, 'C' effectively shorts out 'R' and thus 'r' dominates the impedance of the network. However, close to DC conditions, 'C' is open circuit and 'R' dominates.

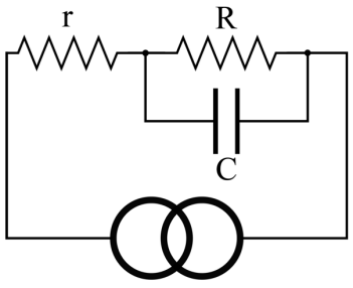

Figure 24. Effective network impedance of two electrodes connected to a human appendage driven by a current source.

McAdams et al. review the effects of electrode site preparation on the network impedance [140]. It is noted that when the stratum corneum, or more generally the epidermis is partially eroded by abrasion or aggressive cleaning, R can be reduced

‘dramatically’ and ‘C’ increases. While this is desirable for isolated experiments, this is not desirable as a long-term solution to the problem of contact impedance, as this form of electrode site preparation can be damaging to the skin.

This chapter describes an experiment designed to examine the effects that electrode location and characteristics have on EPT. The effects of signal frequency characteristics on EPT are also examined. Finally, the stability of EPTs under consistent conditions is also evaluated.

4.2 Methods

The experimental protocol was approved by the Human Research Ethics Committee of Western Sydney University and conformed to the Declaration of Helsinki. We investigated the SENS perception thresholds in two healthy participants, one female aged 34 and one male aged 30.

4.2.1 Experiment setup

EPTs were determined for every permutation of the following variables:

- Electrode Location – electrodes pairs were medially and laterally placed, proximal to either the left ankle or the left wrist. Referred to as ‘Ankle’ or ‘Wrist’.
- Electrode type – Axelgaard UltraStim® Snap SN2040 10 cm × 5 cm rectangular electrode, Axelgaard UltraStim® Snap SN2020 5 cm × 5 cm square electrode, and BIO Protech electrode T716 standard round ECG electrodes, approximately 2 cm diameter were used. Referred to as ‘Large’, ‘Medium’ and ‘Small’ respectively.
- SENS frequency characteristics – either Gaussian white noise or pink noise (with a 1/f characteristic), both low-pass limited to 250 Hz in software. Referred to as “White” and “Pink” respectively.

This made for 12 experiments per participant. A further 5 permutations, making use of only the Large and Medium electrodes, were then selected at random to be repeated in both the Pink and White conditions making for 10 repeated trials in total.

The participants were single blinded to the SENS frequency characteristics, which was always tested in consecutive but randomly ordered pairs. Participants were not blinded to the electrode location or type.

The experiments were run using a custom Matlab program interfacing through a NI USB 6218. The current was generated using Digitimer DS5 bipolar constant current stimulator. Participant responses were acquired via push buttons connected to the NI USB 6218.

4.2.2 Electrical perception threshold determination

EPTs were measured using the 'two-interval forced choice' (2IFC) paradigm. Participants were asked to attend to two successive 1-second intervals, indicated with an audio cue. They were told that the electrical stimulation would be applied throughout one of these two intervals, and not the other. Their task was to indicate which interval contained the stimulus (Figure 25). This means that any bias to respond 'first' or 'second' is independent of performance on the task, since the stimulus was presented equally often in each of the intervals.

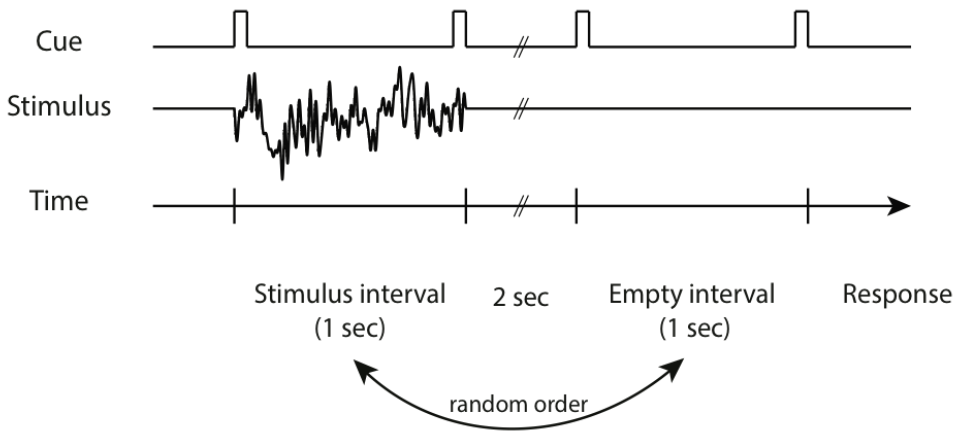

Figure 25. Illustration of the two-interval forced choice paradigm. Audio cues indicated the start and end of each time interval. Illustration by co-author Sarah McIntyre [134].

Repeatedly presenting a stimulus at different intensity levels produces a psychometric function relating stimulation level and detection performance.

In order to efficiently estimate the threshold, we used a Bayesian adaptive psychometric procedure known as QUEST [141–143], implemented in Psychtoolbox-3 for MATLAB [144]. For each threshold estimate, 44 trials were conducted. The intensity of the electrical stimulation was fixed for the first 4 trials, and determined by the QUEST algorithm for the remainder. An example experiment using this procedure is illustrated in Figure 26. We defined the threshold as the intensity at which the stimulus would be correctly identified for 82% of trials (the default setting for the quest toolbox). The prior threshold estimate was set to 200 μA rms and the final threshold was given

by the mean of the posterior distribution function. The QUEST algorithm adapts the test level to best extract information about the threshold on each test. Incorrect answers carry more weight as a false negative is relatively rare, whereas a false positive (a correct answer when the participants could not detect the signal) occurs 50% of the time.

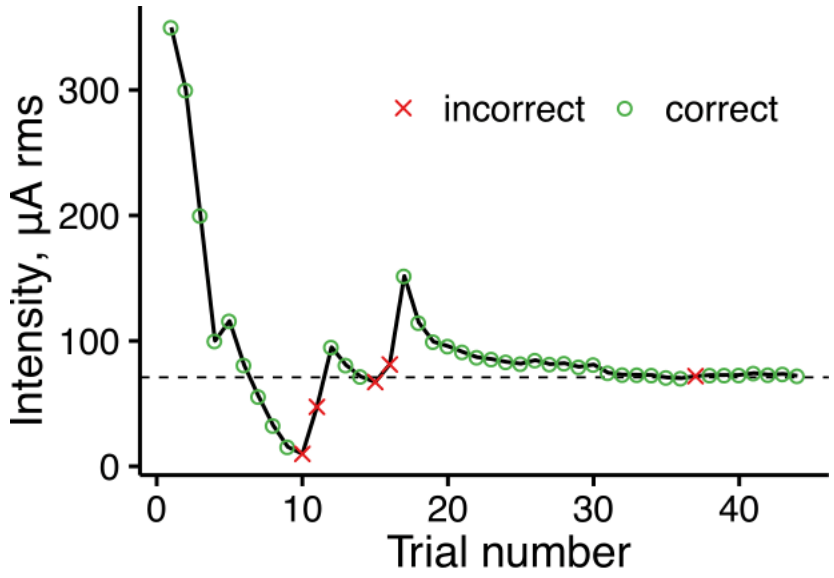

Figure 26. An example of the sequence of trials in a threshold estimation experiment. After the first four trials, the intensity of the electrical stimulation (in µA rms) was determined by QUEST based on performance on previous trials. The final estimate of the threshold is shown as the dotted line (71 µA rms). Correct and incorrect responses are indicated as circles and crosses. Figure by co-author Sarah McIntyre [134].

4.2.3 Electrical impedance determination

After every EPT determination the electrical impedance of the electrode-skin combination was measured. This was not done for the ten additional repeat trials.

A custom written Matlab program interfacing with an Agilent digital signal generator, which in turn drove the current generator, created a sinusoidal current, approximately 210 µA rms through the electrodes and limb. The frequency was varied logarithmically in 39 steps from 10 Hz to 10 kHz. The resulting current (measured over a series resistor) and driving voltage were measured using an Agilent digital oscilloscope, interfaced by the Matlab program.

The effective network component values were then calculated by using a least squares fit of the model of the resistor network shown in Figure 24 to the 40 resulting total impedance values for each test condition. This resulted in estimations of ‘r’, ‘R’, and ‘C’ for each associated threshold determination.

4.3 Results

4.3.1 Electrical perception determination

The EPT of the initial test under each condition is shown in Figure 27. A repeated measures ANOVA indicated that threshold was not associated with electrode type, participant, or location (p's > 0.6), but was associated with SENS frequency characteristic ($p < 0.01$). When controlling for electrode type, participant, and location, frequency characteristic caused an average reduction of 117 µA RMS when changing from white to pink noise.

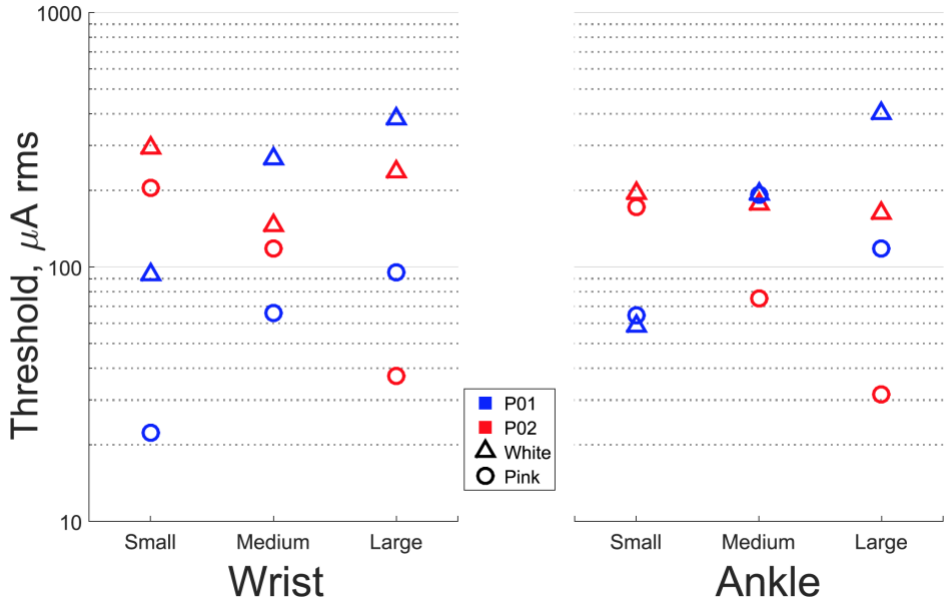

Figure 27. Plot of electrical perception threshold for explanatory variables of electrode type, electrode location, participant, and noise frequency characteristics.

Figure 28 shows the percentage change in EPT when thresholds were re-measured under the same condition on a different day. Despite controlling for location, electrode type, participant and SENS frequency characteristics, changes in excess of 650% occurred, with an average change of 195.8 %. Most changes being positive indicates that the underlying distribution is asymmetric, and there is a higher probability of data accruing above the mode than below it.

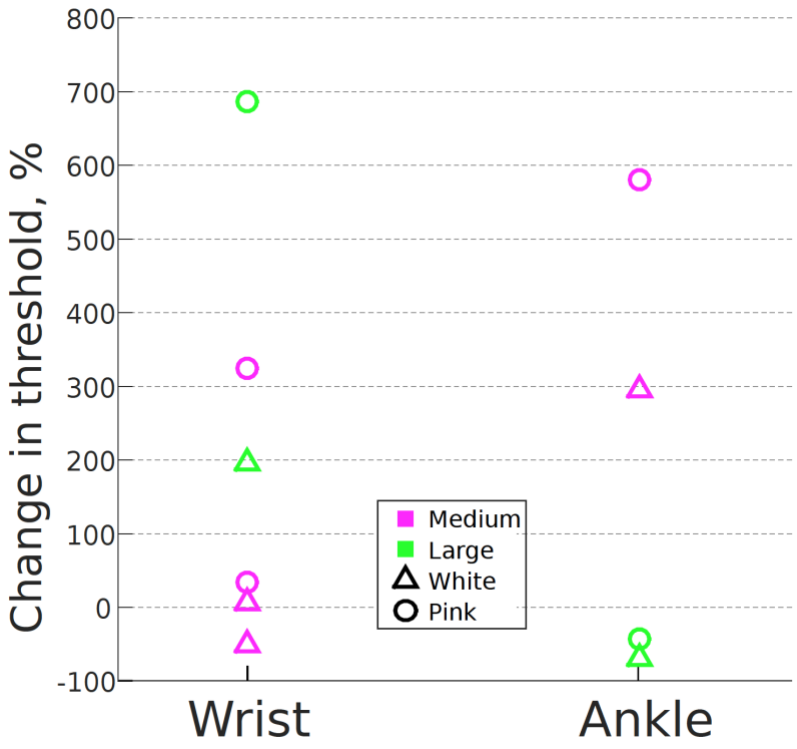

Figure 28. Plot of the percentage change in electrical perception threshold when re-tested under the same participant, frequency characteristic, location, and electrode type conditions.

4.3.2 Impedance measures

Figure 29 shows 'r', 'R', and 'C' plotted against the associated EPT. While participant level and electrode level clustering can be seen in parts of the graphs, no clear correlations between any of the three impedance outcomes and perception threshold emerged, even when controlling for participant or electrode type.

The mean 'r^2' for the multiple fits of the network model to the 40 voltage and current data points for each impedance measurement was > 0.99 indicating an excellent fit to the data. 'r^2' in this context refers to the statistical strength of the fit, and not the square of the resistive component 'r'.

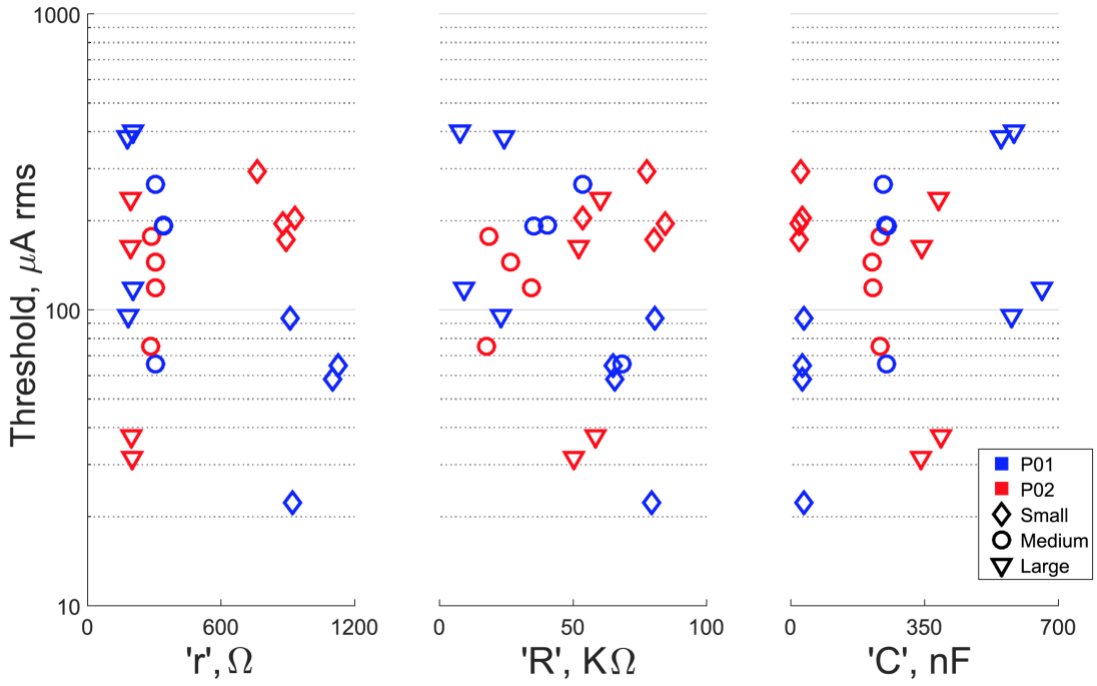

Figure 29. Plot of the three impedance measures for the electrode-limb combination vs. electrical perception threshold.

Single factor ANOVA's testing the effect of electrode type on r, R, and C, indicated all three were significantly associated (each $p < 0.001$). This is not an unexpected result and serves to confirm the hypothesis that electrode type affects the impedance of the network.

4.4 Discussion and Conclusion

EPT varies much more widely than originally thought (Figure 27), under a variety of conditions. We considered participant, electrode type, electrode location, the network impedance of the electrode-limb combination, and the frequency characteristics of the applied current as possibly explanatory variables. Of these only the frequency characteristic of the applied signal was shown to reliably influence EPT. This is usually held constant for a given application and would not serve to reduce EPT variability in practice.

Figure 28 shows how EPT varies when measured a second time, when controlling for the variables measured here. The magnitude of these variations far exceeds the precision with which the intervention threshold is supposedly controlled in SENS studies.

Together, these data indicate that not only is EPT highly variable, but that the explanatory variables measured here do little to explain this variability. This presents a very serious conundrum for the application of classic stochastic resonance in this context. Stochastic resonance requires precision control of the amplitude of the intervention relative to the sensory threshold of the intervention signal. If the EPT is indeed a moving target, or even not a target at all, this may prohibit the use of SENS for stochastic resonance purposes. However, these interventions have been shown to have beneficial effects despite the instability of EPTs. This further illustrates that the underlying mechanism is unlikely to be Stochastic Resonance (SR).

The failure of the explanatory variables investigated here to correlate with EPT indicates that other factors are more instrumental in determining the variability. Future work should focus both on how to implement SENS without the need for a stable threshold, and investigate other factors that may influence the threshold.

4.5 Acknowledgments

While all scientific work is collaborative to some extent, in particular this work was created in collaboration with co-author Sarah McIntyre (SM) [134]. SM constructed the QUEST procedure using a publicly available toolbox within Matlab for measuring perceptual thresholds in this context and conducted some of the statistical analysis.

5

LOW-POWER TRANSCUTANEOUS VOLTAGE TO CURRENT STIMULATOR FOR WEARABLE APPLICATIONS

While there are multiple exploratory studies published on how Subsensory Electrical Nerve Stimulation (SENS) can be used to improve sensation, these studies all use large benchtop equipment to provide the stimulation signal.

This chapter documents the design of the base circuitry for voltage to current conversion at high voltages from a low voltage battery so that SENS can be applied as a wearable device.

The work in this chapter was published in part in BioMedical Engineering OnLine:

Karpul D, Cohen GK, Gargiulo GD, van Schaik A, McIntyre S, Breen PP. Low-power transcutaneous current stimulator for wearable applications. Biomed Eng Online 2017;16:118. doi:10.1186/s12938-017-0409-9.

5.1 Background

Peripheral neuropathic desensitisation is a prevalent condition which adversely affects morbidity, and there is no available treatment (See Chapters 1.1 and 2.1 for details on the prevalence and effects of peripheral neuropathic desensitisation).

Chapter 1 describes a family of exploratory studies that seek to improve tactile sensitivity in these populations. A subset of these interventions use Subsensory Electrical Nerve Stimulation (SENS) as their intervention, a particular form of which is investigated in Chapter 3. SENS-type interventions usually take the form of a continuous signal, typically band-limited white noise, which is applied at amplitudes between 60% and 90% of perception threshold. The interventions have shown no ability to have lasting effects once removed, thus necessitating a wearable version for continuous use. This methodology is contrary to previous interventions that applied supra-threshold signals in an attempt to create lasting effects, such as Transcutaneous Electrical Nerve Stimulation (TENS) [145]. Chapters 1, 3 and 4 all make contributions to the understanding of the mechanism of the effect of SENS.

Studies have not yet progressed to experiments outside of laboratory conditions but there is scope to start investigating more long-term application and to adapt the interventions for the practical considerations of everyday use. While the majority of previous experiments investigated the application of a vibratory intervention, the electrical stimulation variant would in theory allow a smaller, cheaper, and lower power solution.

Electrical stimulator designs with similar constraints often make use of a simple op-amp feedback current source (transimpedance amplifier), where the voltage over a current sense resistor is used to drive a power transistor or MOSFET which in turn provides current to the load [146–148]. This architecture is most commonly implemented as unipolar pulsatile current drives, and are often fed into an H-Bridge circuit to allow for polarity switching in a discontinuous manner.

Two factors cause the design of a low-power, continuous, current stimulator for human applications to be challenging beyond the pulsatile applications referenced above. First, driving small currents into large loads requires a very high output impedance current drive. Secondly, the load itself, two conductive electrodes attached across a limb, has a very large series resistive component at low frequencies, necessitating substantial

voltage compliance to drive current into the limb if an arbitrary signal is required. This substantial voltage compliance is not required in pulsatile applications that take advantage of the lower impedance at higher signal frequencies.

The possible magnitudes of the impedance connected to a current stimulator have a dramatic influence on the design specifications of the device. Bîrlea *et al.* performed a study that investigated participants who wore electrodes for seven days without removal and monitored the changes in impedance over time [139]. The impedance formed between the stimulation electrodes was modelled as a network of a single small resistor (r) in series with the parallel combination of a large resistor (R) and capacitor (C) (Figure 30). r is typically in the order of 2 kΩ, and can be thought to represent the resistance of the limb itself. R and C are usually in the order of 20 kΩ to 60 kΩ and 30 nF to 600 nF and represent the resistance and capacitance of the electrode connection to the skin respectively. This model of r, R and C accurately fits experimental impedance measures of different electrode types (see Chapter 4). At high frequencies and pulsatile applications, C effectively shorts out R and thus r dominates the impedance of the network. However, close to DC conditions, C is open circuit and R dominates, resulting in a high-impedance that requires large voltages to achieve the desired currents. An arbitrary signal current pump would need to be able to drive a worst-case load of 60 kΩ. To drive a 60 kΩ load, 60 V is needed for every mA of current, thus requiring 120 V in total to facilitate + 1 mA to -1 mA range.

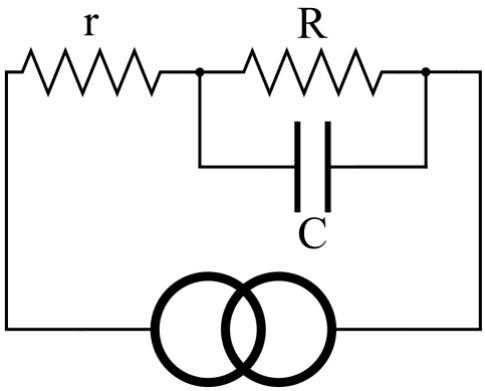

Figure 30. Effective network impedance of two electrodes connected to a human appendage driven by a current source. r is typically in the order of 2 k, and can be thought to roughly represent the resistance of the limb itself. R and C are usually in the order of 20 k to 60 k and 30 nF to 600 nF and represent the resistance and capacitance of the electrode connection to the skin.

The transimpedance amplifier architecture used in previous designs is adequate for low voltage bidirectional applications, or high voltage unidirectional applications. Standard

bidirectional transimpedance designs require that one side of the load be connected to the 0 V point of the circuit, or a virtual 0 V point. An improved Howland current generator [149] does not have this requirement, and allows for both sides of the load to be actively driven without compromising performance. This feature of the Howland current generator is used below (see 5.2.3) to double the compliance of the circuit.

The need for a high voltage power supply can be solved by using a switching boost converter to generate a high voltage power supply from a battery. High voltage op-amps can then be used in the design of the Howland current pump. However, switching converters, which often use inductors, are noisy, often draw excessive quiescent current, and are difficult to implement, often not producing the expected output. High voltage op-amps are expensive and draw larger quiescent currents than their low voltage counterparts.

Here, a solution to these problems, specifically tailored for continuous subthreshold transcutaneous neural stimulation, is presented.

5.2 Design of circuitry for a wearable current stimulator

5.2.1 Design specifications

The device needs to be sufficiently compact and lightweight so that it can be worn in every day circumstances. It should be able operate continuously for at least 10 hours without the need for recharging or replacing batteries, and it should be capable of applying electrical stimulation consistent with that used in previous studies (*e.g.* [31]). 10 hours was selected as this is the upper limit of the average workday, and would allow interventions to be investigated for continuous effect over the periods where improved sensation would have the most impact on function. Consequently, the proposed circuit needs the following attributes:

- Capable of driving a continuous current of +1 mA to -1 mA under worst-case load conditions.
- Have a frequency range of at least 0-1 kHz.
- Draw sufficiently little power so that 10 hours of operation can be achieved on a single battery charge, without the need for large cumbersome batteries.

- Consist of parts with sufficiently small form factors such that the overall device is compact and practical.
- Have a low manufacturing cost and be easy to implement.

The volume and weight of a "practically compact" device varies according to opinion and application, but a device as large or larger than the stimulator used in laboratory testing, the A-M Systems 2200 current stimulator, would certainly be considered to have failed the design requirements. The A-M Systems 2200 current stimulator measures 154 mm × 175 mm × 65 mm and weighs 1.27 kg. Similarly, the low manufacturing cost requirements, and ease of implementation are difficult to quantify. The device should be affordable, and thus should cost less than a premium cellular telephone (roughly 1000 USD). The device should be reproducible by other research laboratories, and thus all parts should be available from standard retailers, and the circuit able to be assembled by a standard Printed Circuit Board (PCB) manufacturer offering such a service.

5.2.2 Design of the High Voltage Power Supply Unit (HVPSU)

The worst-case load impedance can be estimated as 60 kΩ when driving DC currents. This necessitates a HVPSU voltage of at least -60 V to +60 V, given the minimum output current requirements of +1 mA to -1 mA. The "inverted-reference" design of the current pump presented below allows for half this voltage to be used to achieve the same output current, necessitating a HVPSU capable of producing 60 V when under load.

In theory, any boost converter with a sufficiently low quiescent current, capable of delivering more than 1 mA at 60 V from battery packs, would be appropriate. Of course, the HVPSU needs to supply additional current to power the subsequent circuitry.

Our design uses a cascaded series of TC962 voltage inverters to construct the desired HVPSU (Figure 31 and Figure 32). These inverters offer low quiescent current, are stable and efficient. The TC962 is a pin-for-pin replacement for the industry standard voltage inverter: the ICL7662. While the two chips are similar in most respects, the TC962 has a lower output impedance, which improves the performance of the circuit. In theory one could replace the TC962 with ICL7662 if low output impedance was not desired.

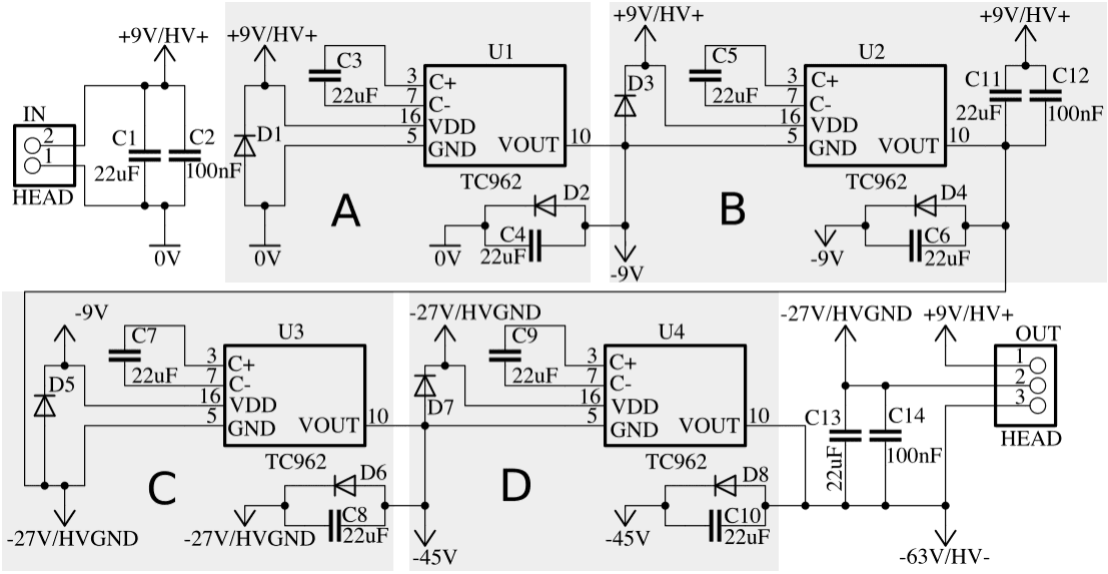

Figure 31. Design of a 9 V to 72 V converter using cascaded voltage inverters. The positive terminal of the input supply becomes the high voltage output, and the most negative output of the inverters, -63 V, is 72 V below the positive terminal and forms the negative output of the high voltage supply. The blocks A, B, C and D are each independent voltage inverters capable of inverting a maximum of 18 V.

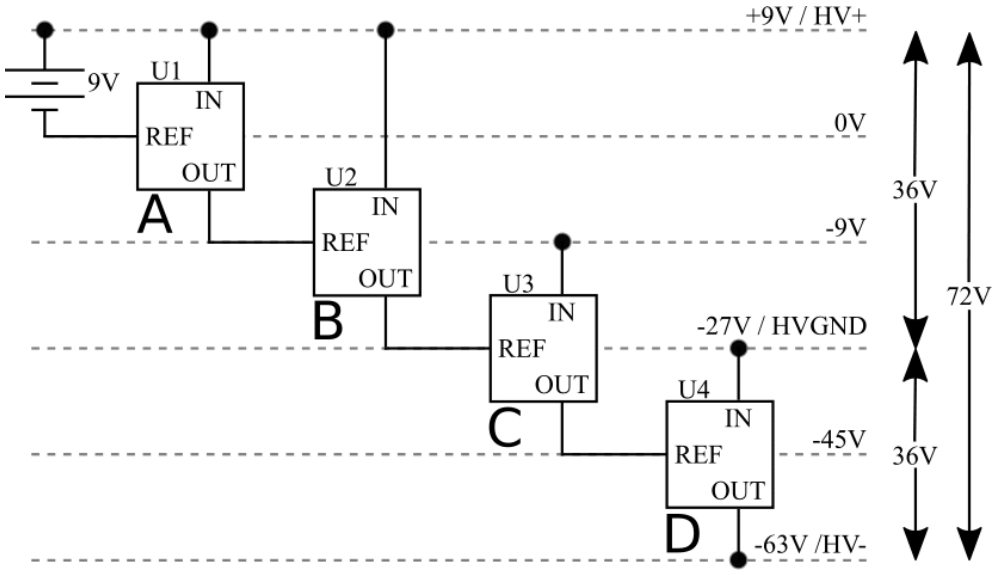

Figure 32. Explanatory diagram of the HVPSU. Four inverters, U1-U4, convert 9 V from the battery to a 72 V power supply with a midpoint tap at 36 V. Each inverter takes the difference between REF and IN as an input and inverts it below the REF input. The inverters can accept a maximum of 18 V as an input. The labels A, B, C and D correspond to the circuitry blocks with the same labels in Figure 31.

In this application, a 9 V battery and four inverters were used to achieve an HVPSU voltage of 72 V. A 9V battery was selected as it is a readily available battery voltage, is sufficiently small as to be wearable and requires less boost circuitry than lower voltage batteries to achieve the high voltage output. The 9 V battery is first inverted to create -9 V using a TC962 in its standard configuration (shown in block A of Figure 31

and Figure 32). The new total available voltage of 18 V above the -9 V rail is then inverted around the -9 V rail to create -27 V (shown in block B of Figure 31 and Figure 32). The total 36 V available is now too large to apply to a further TC962, which only allows an input voltage of 18 V. The next stage inverts the -9 V rail around the lowest available rail of -27 V to create -45 V (shown in block C of Figure 31 and Figure 32). Finally, the -27 V rail is inverted around the -45 V rail to create -63 V (shown in block D of Figure 31 and Figure 32). Treating the positive terminal of the battery as V+ and the most negative voltage available as V-, a total of 72 V is now available (9 V - (-63 V) = 72 V). The -27 V rail is midway between V+ and V- and can act as a pseudo split-rail 0 V for subsequent circuitry (9 V - (-27 V) = 36 V).

The actual voltage achieved will depend on the current drawn by the subsequent current pump due to the output impedance of the HVPSU. 22 µF capacitors, as opposed to the standard design using 10 µF capacitors, were used throughout the design to reduce the final output impedance. Protection diodes were also added to each stage to prevent over-voltage inputs.

As the output voltage is now eight times the input, and power is conserved throughout, the current drawn from the output of the HVPSU will be scaled up when traced back to the battery. If 1 mA is drawn from the HVPSU, then 8 mA will be drawn from the battery. This emphasises the importance of the low quiescent current in the current drive circuitry. This will hold true for any boost HVPSU.

5.2.3 Current source design

Figure 33 shows the design of the High Voltage Current Pump (HVCP). A differential input voltage applied to the positive and negative inputs of OA1 (via a differential low-pass filter, block A in Figure 33), at the "IN" header, and is converted to a proportional current via the gain control resistor R_{gain}:

$$I_{load} = \frac{V_{in+} - V_{in-}}{R_{gain}} \quad 4$$

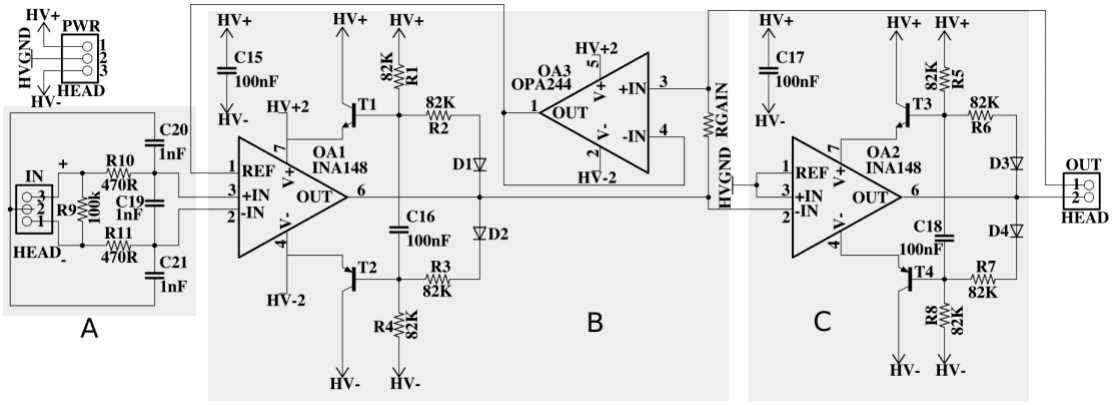

Figure 33. Schematic for a high-voltage, low-power transcutaneous current stimulator for wearable applications. Block A is a differential low-pass filter. Block B is a modified Howland current pump. The circuit takes advantage of bootstrapping transistors to enable low voltage differential amplifiers to operate at high voltage. Furthermore, the addition of an inverting amplifier (Block C) driving the reference electrode, allows the full supply voltage to be applied over the load in both directions, halving the requirement for the supply voltage.

This current is output via one electrode connection at pin 1 of the "OUT" header, and returns at electrode connection pin 2 of the "OUT" header. OA1 is a difference amplifier with internal laser-trimmed resistors and OA3 is a voltage follower, such that OA1 and OA3 form the modified Howland current pump covered in detail in [149] (block B in Figure 33). The differential low-pass filter is added to reduce high frequency steps created by digital controllers potentially used to drive the HVCP.

The electrode connection at pin 2 of the "OUT" header would typically just be kept at 0 V, or in this case HVGND. Since the current pump does not require feedback from this reference electrode, its voltage is free to be manipulated to improve compliance. Here the positive drive signal has been inverted via OA2 and the signal is applied to the reference electrode (block C in Figure 33). This allows the full voltage of the power supply to be applied positively and negatively over the load in a similar fashion to an H-bridge motor driver. This halves the maximum voltage required from the HVPSU for the circuit to achieve a desired alternating current through a specific load. OA2 is a unity gain inverter.

T1 to T4 bootstrap the op-amps' power supplies as described in [150] and [151]. The op-amps' power rails are adjusted as needed by the circuit and only ever see the portion of the supply voltage they require at that instant, linking their output voltage to the supply voltage. This allows the use of low voltage op-amps for high voltage applications simply by adding low-cost, high-voltage transistors (in this case BC546

and BC556 transistors). Any transistors with sufficient frequency, current gain, and voltage tolerances will suffice.

The bootstrapping solution creates a new problem in that the inputs of the op-amp can now fall well outside the power supply at any one time, even though the differential input voltage may be small.

Consequently, both OA1 and OA2 need to be specialised differential amplifiers capable of handling common mode inputs beyond their supply rails. Various commercially available amplifiers exist with this feature. Here a Texas Instruments INA148 is used. The device can handle ±200 V common-mode difference and draws a quiescent current of only 260 µA, making it ideal for this application. In contrast, a high-voltage op-amp such as the OPA454, which operates to 100 V, draws 3 mA to 4 mA quiescent current.

OA3 provides the required feedback voltage for the HVCP without drawing current from the load. It is vital that this op-amp has a high input impedance and it is preferable that the op-amp draws low quiescent current and has similar supply rail limitations to OA1 (in this case an OPA244). OA3 does not need independent bootstrapping, nor does it need to handle common-mode signals beyond its rails, as its input is only slightly different to OA1's output, so OA3 can share OA1's floating supply.

5.3 Results

The HVPSU and HVCP test circuits were designed as two separate printed circuit boards (PCB's), each with additional voltage test points and ammeter insertion points included in the design (Figure 34 and Figure 35). No attempt was made to minimise the size of these circuits in this initial test stage, as ease of access to signals was required for characterisation. The schematic and PCB files for these circuits are available within the digital appendix, in the folder "Prototype PCBs", and can be viewed using the free version of eagle CAD available online: www.autodesk.com/products/eagle/overview.

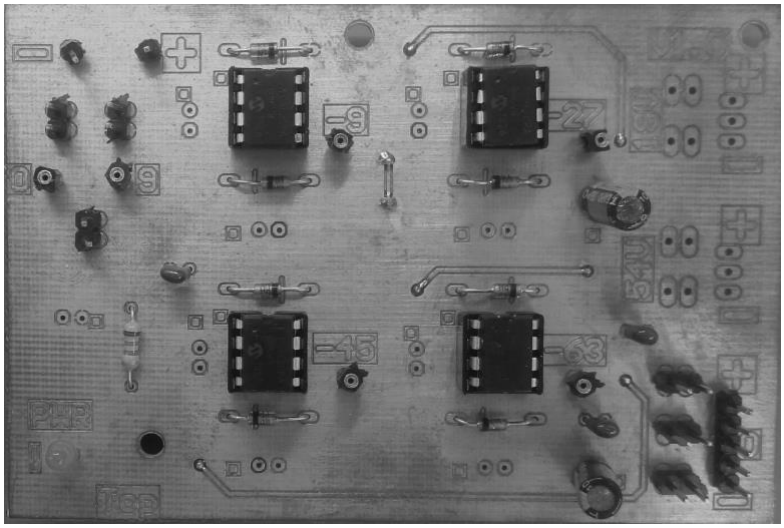

Figure 34. Photo of the HVPSU prototype PCB. Limited surface mount components are on the underside of the PCB.

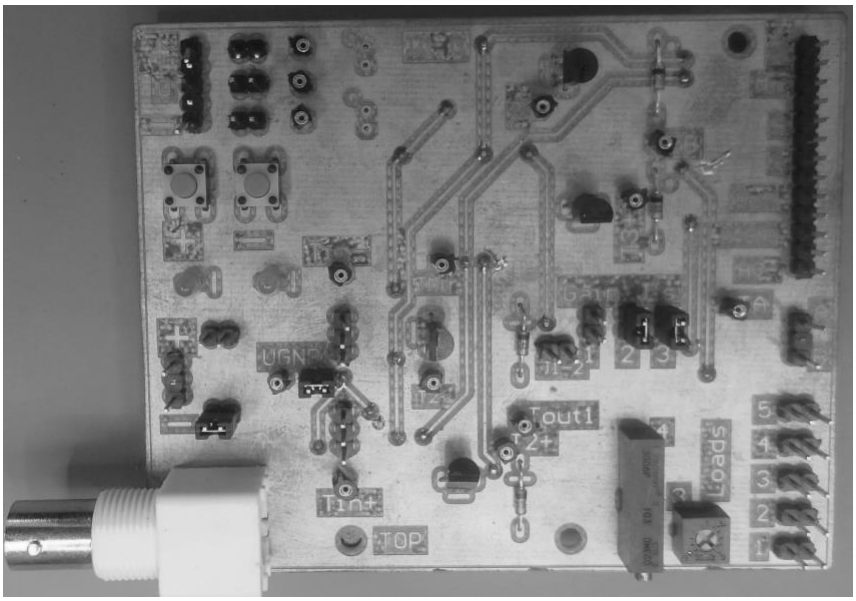

Figure 35. Photo of the HVCP prototype PCB. Limited surface mount components are on the underside of the PCB.

5.3.1 High Voltage Power Supply Unit (HVPSU) results

Figure 36 shows the output voltage of the HVPSU, when supplied with 9 V from a benchtop power supply, at various current draws. Current draw and efficiency are also plotted.

When drawing 20 mA from the HVPSU, the current output of the first voltage inverter is 80 mA, the maximum rated current for a TC962. The circuit was not tested beyond this limiting point.

The HVPSU produced 71.7 V with no load. Progressively increasing the current load on the HVPSU up to 20 mA showed a near linear reduction in voltage consistent with a constant output impedance of 1.470 kΩ.

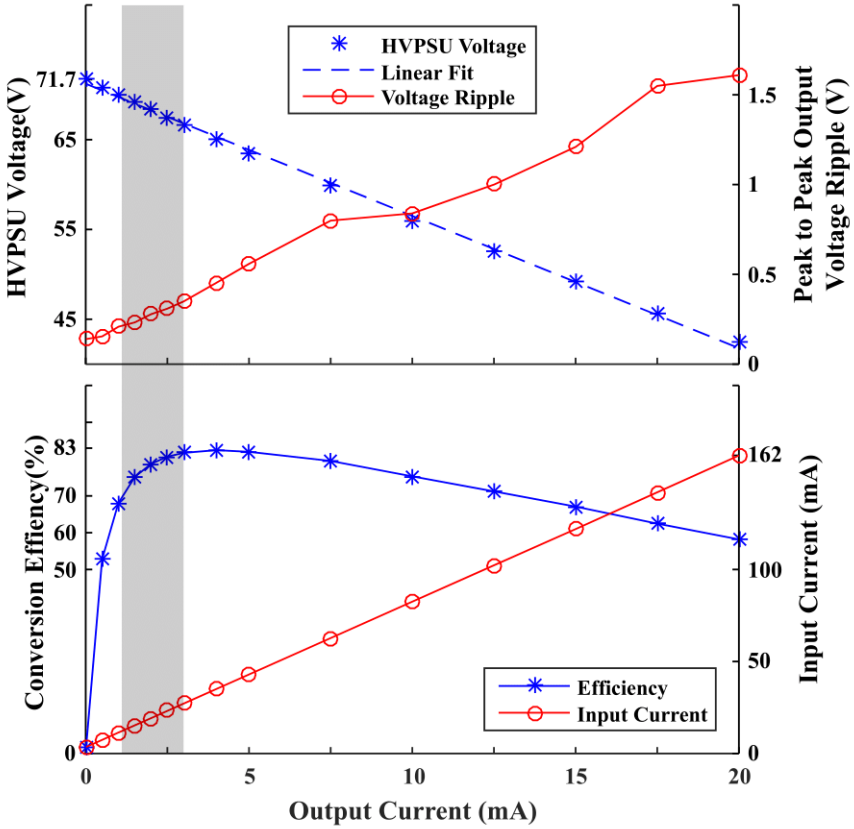

Figure 36. Various HVPSU parameters plotted against output current. Top: shows how the output voltage drops linearly with current draw, consistent with an output impedance of 1.47 kΩ. The linear fit has an R^2> 0.998. The switching converters produce voltage ripple on the output that increases with current drawn. Bottom: shows the efficiency of the circuit with respect to output current. For low currents the quiescent current of the circuit dominates the output power. At higher currents the loss over the effective output impedance dominates. Current drawn from the battery is also shown to rise at approximately 8 times the high voltage output current in accordance with theory. The typical operating current range of the subsequent HVCP is shown as the shaded region.

5.3.2 High Voltage Current Pump (HVCP) results

The HVCP, supplied by the HVPSU, was evaluated using both a 60 kΩ resistive load as a worst-case impedance test, and a complex load in the same form as Figure 30. with R = 58 kΩ, r = 2 kΩ, and C = 30 nF. Figure 37 shows the output gain amplitude and phase offset at various frequencies when driving a maximum of +1 mA to -1 mA sinusoid. The circuit was also tested using various simple resistive loads down to short circuit conditions.

The circuit was able to drive the required current over the entire frequency range with negligible phase offset and no clipping, in accordance with Equation 4 under all load conditions.

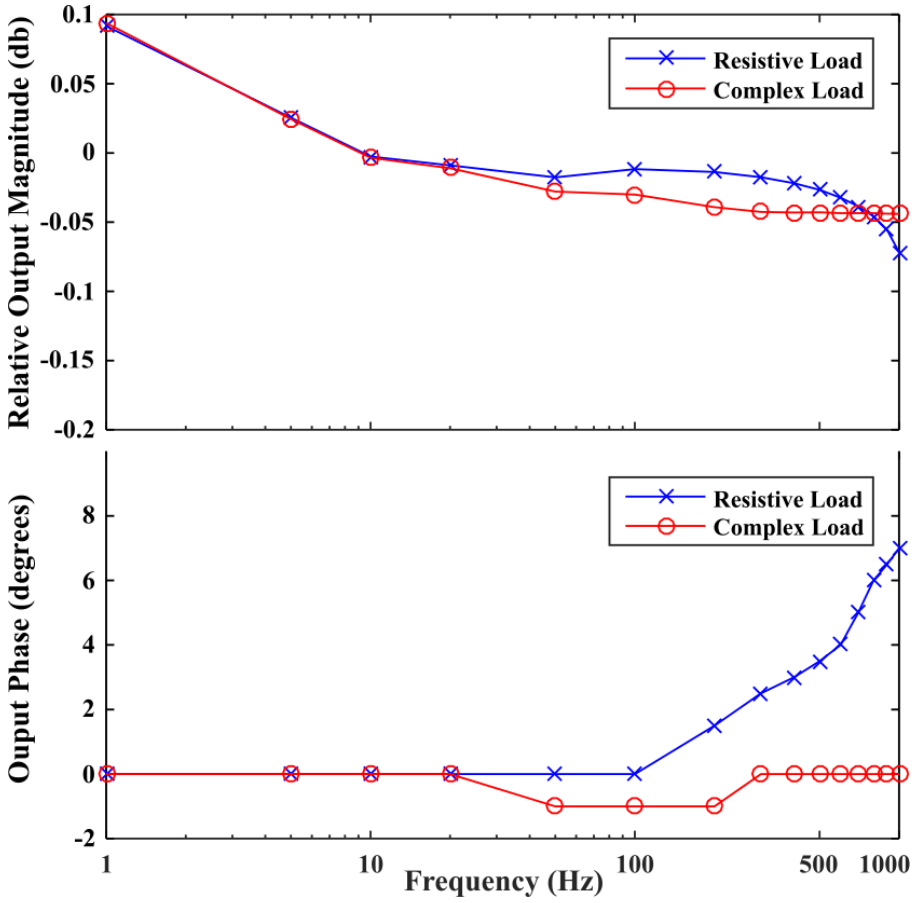

Figure 37. Graphs of relative output magnitude and output phase shift at various frequencies. The resistive load was 60 KΩ. The complex load was a 58 kΩ resistor with a 30 nF capacitor in parallel, both in series with a 2 kΩ resistor in the configuration of Figure 30. Both loads were tested for a constant drive amplitude of 2 mA peak to peak. $\boldsymbol{relative\ output\ magnitude = 10log_{10}\left(\frac{Amplitude}{Amplutude\ at\ 10\ Hz}\right)}$**. The output had minimal attenuation and phase response, especially at lower frequencies.**

The current consumption of the circuit was measured under various conditions and is shown in Table 14.

Table 14. HVPSU and HVCP current draw under various signal drive conditions for a load of 60 kΩ.

Load Current	0 mA DC	1 mA DC	-1 mA DC	2 mA[a] 100 Hz	2 mA[a] 1 kHz
HVCP only (mA)	1.02	2.53	3.07	2.15	2.14
9 V supply Current (mA)	11.69	25.6	25.9	20.6	20.5

[a]peak to peak

Figure 38 shows the output of OA1 driving a sinusoidal signal of 60 V peak to peak, without its supply rails exceeding the maximum rating for that chip of 36 V difference. It further shows the full + 60 V and -60 V being applied across the load terminals.

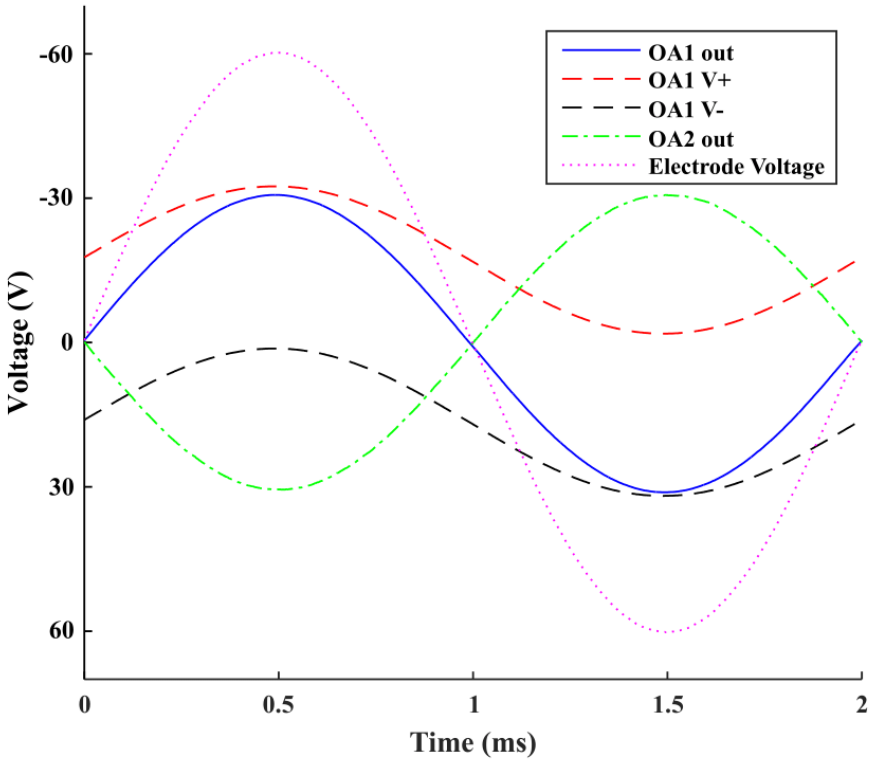

Figure 38. Test voltages of HVCP. The traces demonstrate: 1) how the bootstrapping of OA1's supply lines allow it to output a range beyond its usual limits, and 2) how inverting the current pump output onto the second electrode allows for the full 60 V to be applied bidirectionally over the electrodes. Test conditions were driving a 2 mA peak to peak sinusoidal current into a 60 kΩ load at 500 Hz.

The two circuits were redesigned as a single small form factor, two-layer PCB (Figure 39). In this design the smallest package component versions available were

used, and all test points were removed. The final PCB design measured 46 mm x 21 mm. This circuit performed as expected, with the change in form factor having no impact on performance. The schematic and PCB files for this circuit are available within the digital appendix, in the folder "Prototype PCBs", and can be viewed using the free version of eagle CAD available online:
www.autodesk.com/products/eagle/overview.

The total cost of the parts for this small version from online vendors is less than 35 USD when purchased in low quantities.

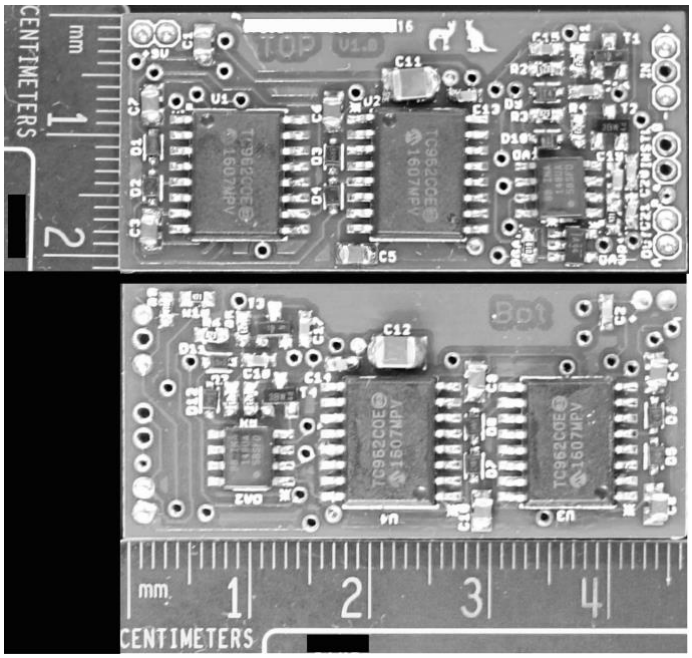

Figure 39. Top and bottom views of the compact version of low-power transcutaneous current stimulator for wearable applications.

5.4 Discussion

The HVPSU had poor efficiency for currents below 0.5 mA, but had efficiencies above 75% for currents between 1.5 mA and 10 mA. It is important to consider quiescent current when looking at the efficiency outcomes. The circuit only draws a quiescent current of ~3.6 mA when under no load. Consequently, when supplying power in the same range of the quiescent power, the subsequent efficiency calculation will be very poor, around 50%. This improves as more power is drawn, but will peak when the load reaches the internal impedance of the HVPSU.

One can subtract the quiescent power before calculating efficiency to get a metric of conversion efficacy alone. Doing this, the efficiency is then 100% at no load and

steadily decreases to 91.7% at 4 mA and 78% at 10 mA and then follows the original efficiency curve.

The HVPSU showed an increase in voltage ripple with current draw. As more current is drawn this voltage ripple would act to reduce minimum guaranteed output voltage of the HVPSU, and thus compliance of the HVCP. The operating range of the subsequent HVCP however keeps the HVPSU voltage ripple under 0.5 V, which allows the HVCP to operate unaffected.

The HVCP only draws 1.02 mA when under no load, far superior when compared to the current draw of just one high voltage op-amp. The worst 9 V (battery) current consumption of 25.9 mA occurred when driving a DC current of -1 mA into the load. The full circuit would therefore require a battery of at least 260 mAh at 9 V in order to operate for 10 hours without recharging or replacement under worst-case conditions. A standard 9 V battery has a capacity of between 300 mAh and 500 mAh. Dividing this by the worst-case current consumption of 25.9 mA yields a charge life of 11.6 hours to 19.3 hours.

The deviation in output magnitude and phase at frequencies above 500 Hz for the resistive load, did not occur when testing with small loads, or the complex load, requiring smaller voltages to drive the required currents. Changing the values of the stabilising capacitors C16 and C18 or the values of the transistor biasing resistors R1 to R8 had no effect on this phenomenon. The effect is likely caused by the op-amp supply bootstrapping. This creates very large common mode swings for both the supply voltage, and the relative input voltages to OA1 and OA2 under these conditions. The data-sheet for the INA148 indicates that both the common mode rejection ratio and the power supply rejection ratio start to fall as these signals approach 1 kHz. This problem is unlikely to affect actual stimulation applications, as the impedance of a typical skin electrode pair drops quickly with frequency. This means that the high frequency components will not induce these large common mode swings.

The “inverted reference” design was shown to be stable and did not impede the performance of the Howland current pump. However, for small loads bellow 2 kΩ high frequency oscillations may occur. While this is unlikely to occur in practice, the problem can be solved by inserting low pass filter in-line with the input of OA2. This inverted reference configuration also improves the safety of the circuit, as the largest

voltage in the device is now 72 V as opposed to at least 120 V if electrode B were held at HVGND as a constant reference voltage.

To our knowledge, no Application Specific Integrated Circuits (ASICs) exist that would achieve the design requirements of this application, and the only example of a stimulator designed with similar application in mind was created by Yamamoto *et al.* [152–154]. Three wireless stimulators which have similar design constraints to those used here are also compared [146–148]. While there are many differences created through differing needs of the end application, it is vital to note that these wireless stimulators are designed for pulsatile applications. These are much more common, but cannot be used for continuous signal stimulation needed for subthreshold interventions.

It is important to consider the power consumption of control circuitry not included in our design. Many appropriate microcontrollers are available that do not consume significant power, and have a small form factor. For example, the PIC24FJ128GC006, which has built in Digital to Analog Converters (DAC's), Analog to Digital Converters (ADC's) and analogue circuitry. This chip consumes less than 13 mW at 8 MHz. The results of the comparison are contained in Table 15. The weight and dimensions of a standard 9 V battery (46 g and 48.8 mm x 26 mm x 16.9 mm) have been added to our design in the figures of Table 15.

Table 15. Comparison to designs with similar constraints in the literature.

	This work	Yamamoto *et al.* [152–154]	Wang *et al.* [146]	Farahmand *et al.* [147]	Jovičić *et al.* [148]
Voltage compliance (V)	±72	±10[a]	±60	23	85
Power Consumption (mW)	233	312[a]	720	51.2	>700
Use Duration (hours)	>10	>24[a]	8	Unknown	Unknown
Current Output (mA)	±1	±1	60	0.4	70
Volume (cm^3)	28.2	210.1	127.5	90	52.5
Weight (g)	52	200	85	60	45
Signal Type	Continuous	Continuous	Pulsatile	Pulsatile	Pulsatile

[a] Approximate values based on information directly from the author.

The table indicates that our design has a smaller form factor and higher compliance than those with which it is compared. The power consumption of the circuit is also superior to those designs with higher compliance (greater than 23 V).

5.5 Conclusion

Here a current stimulator designed to overcome the challenges associated with continuous, low-power transcutaneous current stimulation for the improvement of peripheral sensitivity is presented. It has been shown that the circuit performs within specifications under worst-case load conditions. What makes the design most unique is its low power consumption, high voltage compliance, and small form factor making it specifically appropriate for wearable applications.

To the best of our knowledge, this is the first work to demonstrate a full design specifically targeting subthreshold electrical stochastic stimulation in wearable applications, with high voltage compliance, continuous-signal output, and sufficiently low power operation to be used in wearable applications. A list of specifications to be met in this application is proposed. The design adds to previous work by including an inverting reference to double the voltage compliance, a differential input filter to reduce noise from DAC's, a change of various components to reduce current consumption and ensure the circuit is appropriate for the application, and the inclusion of a low quiescent current HVPSU that is compact and simple to construct. Finally, a characterisation specifically focusing on aspects that apply to the intended application is presented.

The next step is to allow for the driving and instrumentation of the circuit using additional low power analogue and digital circuitry. Finally, the circuit must be tested on human participants.

6

A COMPLETE CONTINUOUS-CURRENT STIMULATOR FOR TRANSCUTANEOUS WEARABLE APPLICATIONS

Chapter 5 demonstrates a design that fulfils the basic requirements of a device to be used for the applications of Subsensory Electrical Nerve Stimulation (SENS), however, several limitations were noted. Firstly, the circuit is simply a voltage to current converter; there is a need for microprocessor-based waveform generation to allow the circuit to be a stand-alone device. Secondly, the circuit requires a means to monitor the current outputs accurately, both for functional and safety reasons. Finally, the circuit still requires *in vivo* testing to establish that the characterisation performed on artificial loads persists when stimulating human participants.

The work in this chapter has been submitted to be published in IEEE Transactions on Biomedical Circuits and Systems (TBioCAS):

Karpul D, Jayarathna T, Cohen GK, Gargiulo GD, van Schaik A, Breen PP. Continuous-current stimulator for transcutaneous wearable applications. Submitted to TBioCAS 2018

6.1 Background

Millions of people suffer from conditions that cause peripheral desensitisation such as diabetes [5], ageing [10] and HIV [11]. Currently there is little to no treatment that improves peripheral sensitivity in these populations [30]. Chapters 1 and 2 discusses the problem further and highlights a class of potential interventions seeking to improve tactile sensitivity using Subsensory Electrical Noise Stimulation (SENS).

No studies to date have conducted long term investigations using these interventions, possibly because the technology to apply the required signals in a wearable fashion has not been developed. Chapter 5 provides a list of criteria such a device would require based on the reviewed literature, "The device should be:

- Capable of driving a continuous current of + 1 to − 1 mA under worst-case load conditions.
- Have a frequency range of at least 0–1 kHz.
- Draw sufficiently little power so that 10 hours of operation can be achieved on a single battery charge, without the need for large cumbersome batteries.
- Consist of parts with sufficiently small form factors such that the overall device is compact and practical.
- Have a low manufacturing cost and be easy to implement."

The impedance of the skin at low frequencies (~20 kΩ to 60 kΩ, see Chapter 4 and [138]) necessitates operating voltages in the order of ±60 V to achieve the desired ±1 mA at DC. Pulsatile stimulators that use waveforms that penetrate the skin's effective capacitance more easily, transmit through a much lower effective impedance and thus require much lower operating voltages than arbitrary waveform stimulators with low frequency components.

The primary difficulty in designing a high voltage continuous current stimulator or high voltage current pump (HVCP) is power consumption. Generating the high voltage itself is often highly inefficient, and further, the analogue amplifiers that can operate at high voltages often have large quiescent currents.

The primary purpose of this chapter is to address the limitations noted by Chapter 5 and produce a tool that is ready for research requiring a wearable device.

The final design presented here further makes necessary improvements to the power supply and adds a variety of safety and interface features not present in the previous design.

6.2 Methods and Materials

6.2.1 High voltage power supply design

In Chapter 5 we achieved the required high voltage power supply (HVPSU) using a cascaded series of Microchip TC962 capacitive voltage inverters to generate 72 V from a 9 V alkaline battery. This design was compact, low-power and efficient. In practice, the design had one significant shortcoming.

The design offers no voltage regulation and relies on a constant 9 V from the battery: as the battery discharges from 9 V, the HVPSU voltage tracks it proportionally and the high compliance of the subsequent HVCP is lost. Both Lithium-Polymer (Li-Po) batteries and Alkaline 9 V batteries lose approximately 25% of their output voltage over their discharge curve, which results in at least 25% loss in compliance of the HVPSU.

The design of a small form factor boost supply that is both regulated and efficient for output currents in the range of 1 to 3 mA (0.072 to 0.36 watts) is not trivial.

For comparison, off-the-shelf module solutions like the Econoline DC/DC converter R1D**-xx24 [155], and the Kylinchip XL6009 [156] boast high efficiencies (74-84% and 94% respectively). This only occurs for output power in the order of 1 watt. For lower output power, with output currents of 1 to 3 mA, efficiencies are typically in the order of 50% or lower. Inductive switching boost converters do not efficiently produce high output voltages at low currents.

Using the switched capacitor inverters from the previous design is the most energy efficient way to solve the problem, but these are not regulated, or versions that include internal regulation sacrifice efficiency (*e.g.* MAX868). Regulation would need to be introduced and would need to be done using a switching regulator instead of a linear regulator to achieve high efficiency.

The paradox of requiring high output current for a switching regulator to operate efficiently, but only needing a low current at the HVPSU output, is solved by using the switching regulator only at the battery, to produce a low, but regulated bucked or boosted voltage. While we draw low currents (1-3 mA) from the high-voltage side of

the power supply, we are drawing high currents from the low voltage side (for a 3.6 V Li-Po battery at least 20 to 60 mA). Many parts offer high efficiency regulation from the full input range from a Li-Po battery (3 V to 4.2 V) for this output current range if producing low voltages. The TPS61028 by Texas Instruments offers efficiencies in excess of 90%.

The subsequent architecture of switched capacitor doublers and inverters must carefully balance multiple trade-offs. The ultimate output impedance of the HVPSU and each part affects regulation and efficiency. The quantity and quiescent power of parts used affects the total quiescent power of the HVPSU. Finally, the form factor in which each part is available affects the physical size of the HVPSU.

Not only can many potential voltage converters perform these tasks, each carrying a trade-off of some kind, but they can be connected in a multitude of configurations to achieve the high-voltage output. These parts are not readily available in libraries for modelling software such as SPICE [157,158]. Consequently, to investigate different architectures and optimise the design, we created a circuit-modelling framework in Matlab (See Appendix B for a full description of the modelling framework developed, and the results of power supplies simulated).

The framework allows the creation of any buck, boost, or voltage-inverter part based on its datasheet, and its connection into an HVPSU architecture. Correctly modelling the flow of the quiescent and output currents [159] was essential to modelling the efficiency of multiple interacting chips. We could then simulate connecting various parts together in feasible configurations to investigate the effect of different parts, different system architectures, different battery discharge-voltages and different numbers of cells on total battery life.

The dominant design goal was to reduce the battery capacity required to run the high voltage current pump (HVCP) circuit for the required 10 hours under worst-case conditions.

Figure 40 is an explanatory diagram of the various voltage inversion and boost stages in the final design. The TPS61028 at “A” regulates the Li-Po battery voltage from between 3 and 4.2 V to 4.5 V with high efficiency.

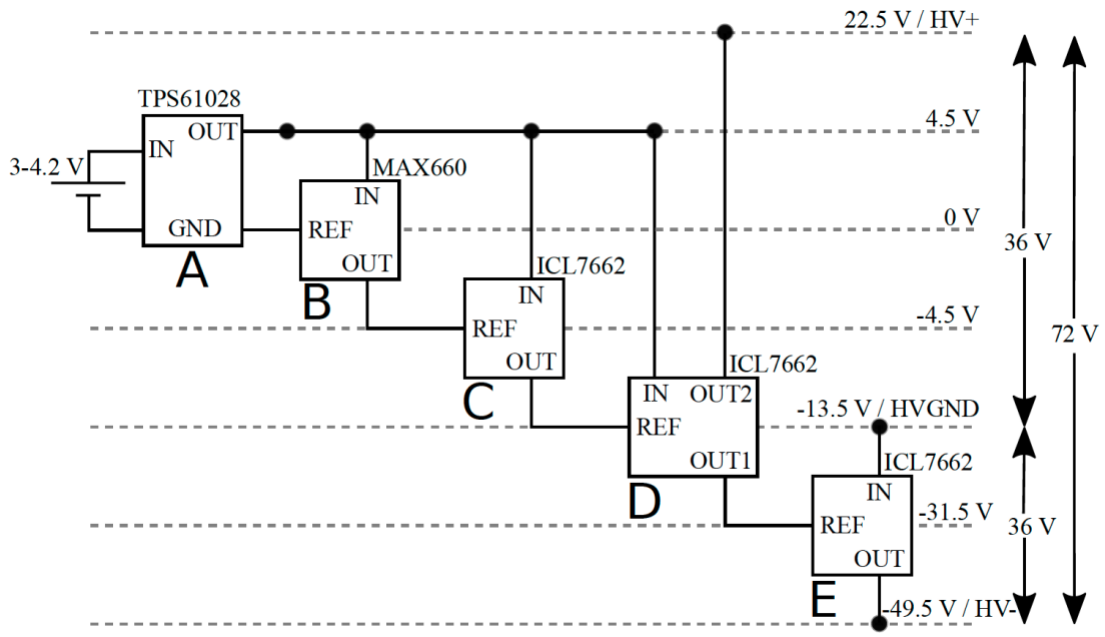

Figure 40. Explanatory diagram of a high efficiency power supply that regulates a 3 to 4.2 V battery output to +36 V and -36 V supply. The part at "D" uses the ICL7662 in both its doubling mode and inverting mode.

The 4.5 V is then inverted at "B" to create -4.5 V by a MAX660, which has superior output impedance and quiescent current draw than most capacitive inverters, but can only operate at low voltages. The total available voltage of 9 V (4.5 – -4.5) is now too large to invert using a second MAX660.

The +4.5 V is now inverted around the -4.5 V at "C" to create -13.5 V using an ICL7662. The total available voltage is now 18 V (4.5 – -13.5 = 18 V). The ICL7662 has superior quiescent current and form factor to the previously used TC962 but has poor output impedance. Simulation showed once the output voltage had reached 18 V, the output current had dropped sufficiently that output impedance was not a significant contributing factor to performance.

The 18 V is then inverted and doubled in one step ("D") with another ICL7662 to create 4.5 + 18 = 22.5 V and -13.5 – 18 = -31.5 V. The doubling mode of the ICL7662 comes at the cost of two forward-voltage diode drops, which reduces both efficiency and final output voltage. Using low forward-voltage Schottky diodes reduces this impact. Further, doubling and inverting in one step comes at the cost of increased output impedance compared to using two chips to perform each operation separately. Simulation indicated that using a single part for both the doubling and inversion significantly improved the circuit's performance over using two cascaded inverters despite the diode drops and increased impedance. This is partly due to powering a

reduced number of chips, but it also reduces the “depth” of the cascade, which has a multiplicative effect on output impedance.

Finally, the -13.5 V is inverted around the -31.5 V at “E” using another ICL7662 to create -49.5 V and a total voltage of 22.5 - -49.5 = 72 V with -13.5 V at the midway between the two extremes, 36 V from the highest and lowest voltages.

The final output voltage (72 V) is proportional to the output voltage at “A” (4.5 V). The output voltage of the TPS1028 can be manually increased from 4.5 V to compensate for the voltage losses at the final output when the subsequent current pump is drawing its quiescent current of 1 mA. An output of 4.7 V is typically what is needed to produce a final output of 72 V.

6.2.2 Instrumentation of the High Voltage Current Pump (HVCP)

It is desirable, but not essential to instrument the outputs of the HVCP. Bench-top stimulators like the Digitimer DS5 Bipolar Constant Current Stimulator include outputs that allow for the monitoring of the output current and voltage.

Monitoring the output current allows the driving hardware to check if the circuit is functioning properly. The most likely fault is current or voltage “clipping” when the circuit fails to have sufficient compliance to drive a given load. Table 15 shows the compliance of designs with similar applications. Several of these have less than the required supply voltage. These circuits do not report clipping, but also do not monitor the output and so are unable to detect voltage saturation. Clipping can be considered undesirable or even dangerous simply because the desired current is not flowing in the tissue.

Error states that cause a difference between the desired current and the achieved current are unsafe. Monitoring the achieved current with accuracy in the order of 2 μA allows the driving circuitry to monitor the HVCP for accurate operation.

Current being diverted away from the stimulator to other parts of the body can be extremely dangerous. As little as 100 μA across the heart is enough to cause micro-electric shock [160]. Monitoring the current on both stimulation-leads separately would improve the safety of the circuit further (Figure 41). The circuit should be able to determine if the current on both leads match to within 50 μA.

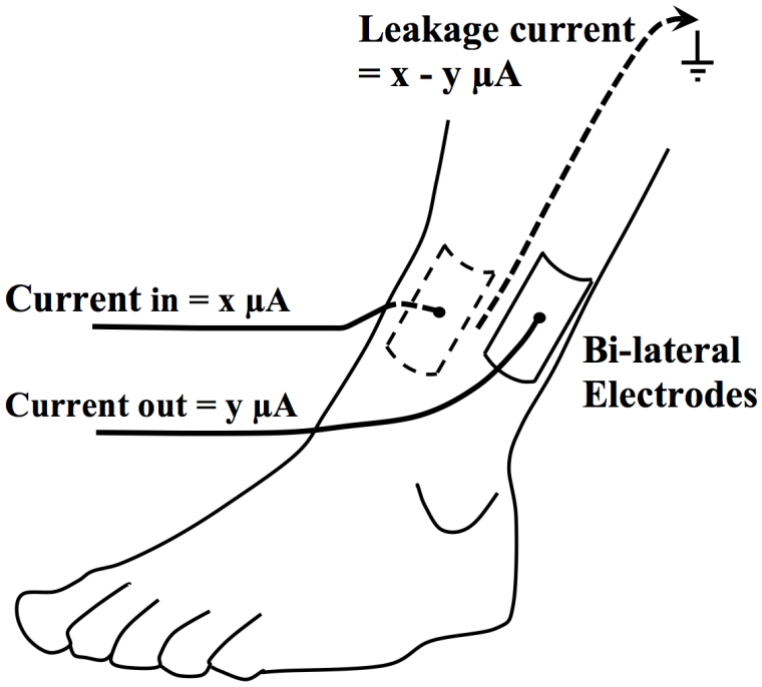

Figure 41. Diagram depicting the dangerous diversion of current to elsewhere in the body. The magnitude of the diverted current can be calculated by the difference in current between the two stimulation leads.

Unlike laboratory settings, in wearable applications it is expected that the quality of the electrode connections will change considerably over time [139]. The HVCP will adjust its drive accordingly, but having feedback information about the impedance of the electrode connection would further improve safety. The electrode impedance can be calculated by monitoring the drive voltage as well as the drive current.

In order to measure the current in each lead and the voltage applied to the participant, a relatively small resistor is placed in series with the leads and the voltage on either side is buffered (Figure 42). Signals a, b, c and d are all voltage-buffered signals, and drawing small currents from these points does not affect the current drive into the participant. OA1, OA2, BUFF1 and SENSE1 form the modified Howland current pump described in Chapter 5. Only BUFF2 is added to the previous design so as not to draw current from c* when monitoring the voltage at this point.

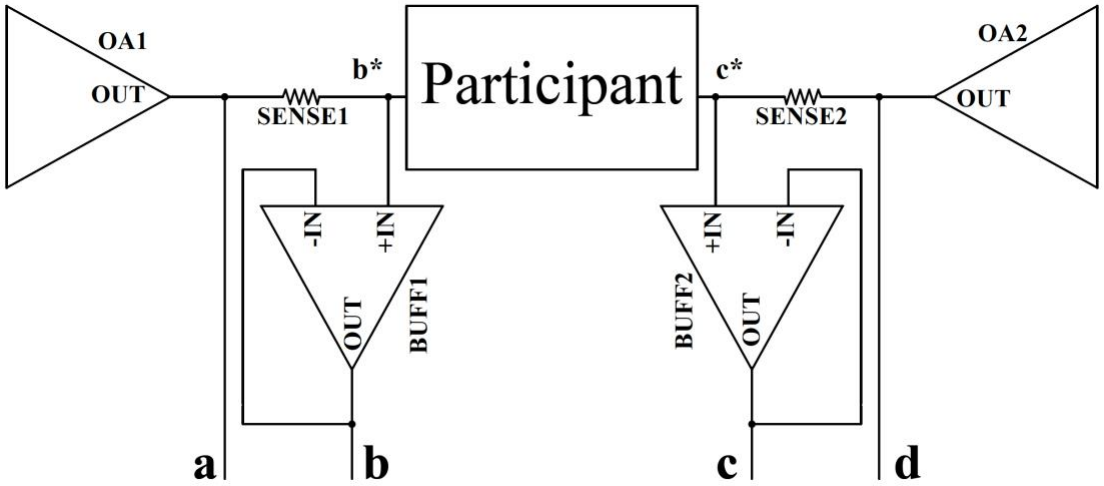

Figure 42. Representative schematic showing how the various currents and voltage signals are made available for instrumentation. OA1, OA2, BUFF1 and SENSE1 form the modified Howland current pump described in Chapter 5.

The current in each stimulation lead connected to the participant can be measured by the differential voltages $V_{a\text{-}b}$ and $V_{c\text{-}d}$. The voltage applied to the participant is given by $V_{b\text{-}c}$.

Measuring these voltage differences and conditioning the signals for analogue-to-digital conversion is not trivial. All of these signals draw their power from the HVPSU and they have a significant effect on battery life. Thus, the input impedance of any circuitry used is critical to reducing power consumption. Further, very high common mode rejection is required since $V_{a\text{-}b}$ and $V_{c\text{-}d}$ have a maximum of a 50 V common mode signal relative to the battery voltage, and a minimum differential resolution of 3 mV for 1 µA drive current if a 3 kΩ sensing resistor is used.

To measure the three voltage differences required we step each voltage (a, b, c and d) down to the range of the battery voltage / microcontroller supply using a standard resistor-divider circuit (Figure 43). The differences are then measured using ultra-low-power instrumentation amplifiers (INA333) powered directly from the battery and not the HVPSU. Gains G1, G2 and G3 are set to rescale the outputs to achieve maximum resolution on the subsequent Analogue to Digital Converter (ADC).

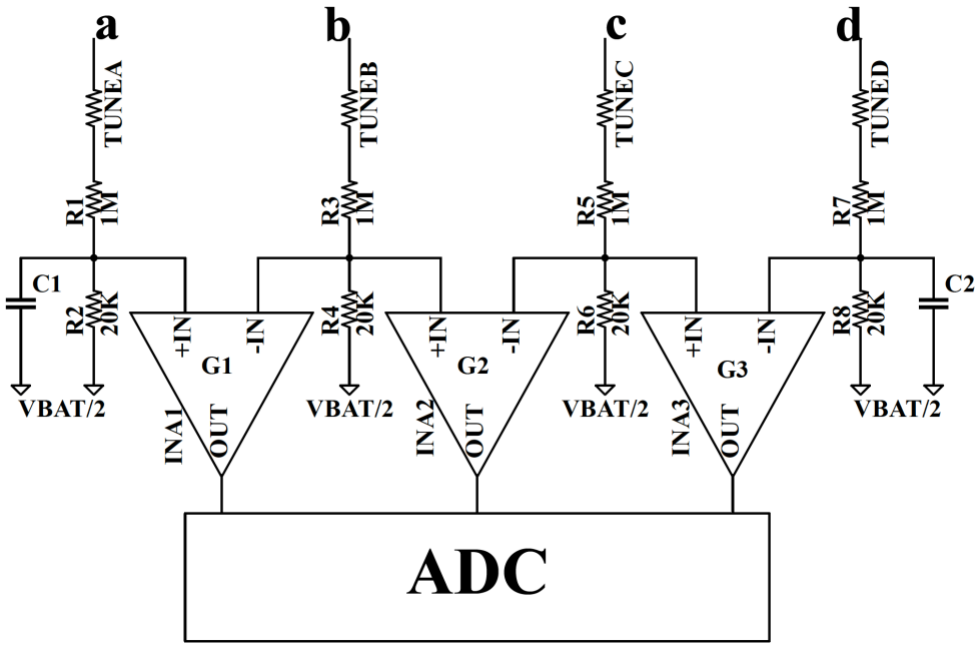

Figure 43. Representative schematic of instrumentation circuitry to monitor the current into and out of the participant, as well as the voltage applied to the participant. a, b, c, d represent the same signals as in Figure 42. G1, G2 and G3 are gains set to scale the voltage to maximise resolution.

This solution is more power efficient than using high common-mode voltage difference amplifiers such as the INA148 or the LT6375. These amplifiers would need supply voltages greater than the battery voltage in order to operate and an additional circuitry stage transferring their outputs to the microprocessor ADC would be required. They have higher quiescent current than the INA333 and often worse input impedance than the resistor divider that is used here.

The challenge is that any imbalance in the resistor-dividers creates large common mode gain at the output. Using the best commercially available precision resistors (0.1% 1 MΩ and 0.05% 20 KΩ) limits the imbalance, but tuning is still required. Four tuning resistors inserted during a calibration stage bring the DC common mode measurement error down to less than 1 µA output. Two capacitors (C1 and C2), in the order of 1-20 pF, adjust for capacitive mismatch, largely created by the inputs of INA2. (See Appendix C for more details on the calculations and process of balancing the resistor dividers.)

6.2.3 Microprocessor and interfacing

The final device is controlled by a Texas Instruments CC2640F128R Bluetooth® low energy Wireless MCU. The chip has a powerful ARM® Cortex®-M3 core processor and a second ultra-low-power independent “Sensor Controller”.

The chip’s primary purpose is to drive a precision 12-bit dual Digital to Analogue Converter (DAC) (AD5687) to generate the differential signal required by the HVCP. Driving differentially has three benefits over using a single channel: the common mode noise is not transferred to the output of the HVCP, an additional bit of resolution is achieved, and negative signals can be generated without the need for a known zero reference voltage.

Seven ADC lines monitor the three instrumented analogue outputs from the HVCP, as well as the mid-supply reference voltage used by the instrumentation as a zero point, a precision 3 V reference used by the DAC, and the voltage on a potentiometer which can be used by the user to make adjustments as needed.

The microprocessor has Bluetooth® low energy wireless capabilities that were not used in this design but could be added at a later stage for user interfacing and data transfer.

An SD cardholder is connected to allow the saving of recorded data and time stamps, as well as reading of pre-loaded drive signals if they are not to be algorithmically generated in real-time.

Logic lines control two status LEDs and can activate the shutdown logic of the TPS61028 disabling the entire high voltage side of the circuitry. Logic lines also control two solid-state relays (LH1525) (Figure 44), one disconnects the participant from one of the stimulation-leads preventing drive current into the participant. The second can short circuit the two drive leads, either discharging voltage on the participant if connected, or allowing current to pass from one lead to the other when the participant is not connected. This current bypass allows the circuit to perform a system check prior to connecting the participant. The relays can handle voltages up to 400 V on their outputs and only require 330 μA to remain powered.

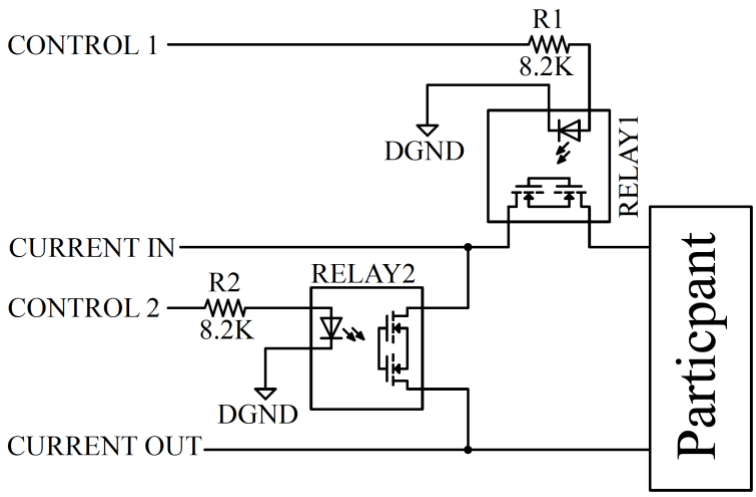

Figure 44. Schematic of output solid-state relays that can disconnect the participant from the device, discharge charge from the participant and allow current from the drive circuitry to circulate internally.

Finally, the circuit also has built-in USB charging for the Li-Po battery with indicator LEDs. Built in charging is more than just a convenience, it enables the circuit to be sealed in its enclosure with no need to have a removable battery.

The USB charging cable presents a potential risk to the participant as it may provide an earth reference to the circuit if the cable is connected while the participant is being stimulated. To mitigate this risk the circuit employs three safety measures. Firstly, the USB power is only physically connected to the charging circuitry when the main power switch is in the "off" position, thus the battery will never be charged while the device is in operation. Secondly, even in the "on" position, the 5 V from the USB directly drives a transistor that activates the shutdown pin of the HVPSU. Finally, this shutdown signal also activates an interrupt routine on the microprocessor allowing further shutdown actions to be taken, including disconnecting the participant via the solid-state relays.

6.2.4 Human testing

In Chapter 5 the HVCP was tested using purely resistive loads and a complex load that approximated the impedance of the limb-electrode combination. In order to ensure the circuit operates correctly on human participants, which present a more complicated and possible active load to the circuit, 5 participants were recruited and required to sign informed consent. This work was approved by the Human Research Ethics Committee of Western Sydney University (ref: H10922).

Two Axelgaard UltraStim® Snap SN2020 5 cm × 5 cm square adhesive electrodes were applied medially and laterally, proximal to the malleoli of the right leg of the 5 participants. The electrode site was not prepared using abrasion, cleaning or shaving in order to deliberately create an inferior connection.

Currents of +1 mA DC, -1 mA DC, 500 µA RMS at 500 Hz sine wave, and white noise low-pass filtered to 100 Hz with an RMS amplitude of 100 µA were tested. 100 Hz low-pass-filtered white noise of this amplitude is commonly used for SENS-type experiments.

6.3 Results

The workings of the HVCP are not changed from Chapter 5 and will not be characterised here.

6.3.1 High Voltage Power Supply Unit (HVPSU) results

The HVPSU was designed onto a two-layer Printed Circuit Board (PCB) (Figure 45). The test PCB (100 mm × 27 mm) was more spread out than the final version allowing more extensive testing and debugging of internal signals. The schematic and PCB files for the test PCB are available in the digital appendix, in the folder "Prototype PCBs".

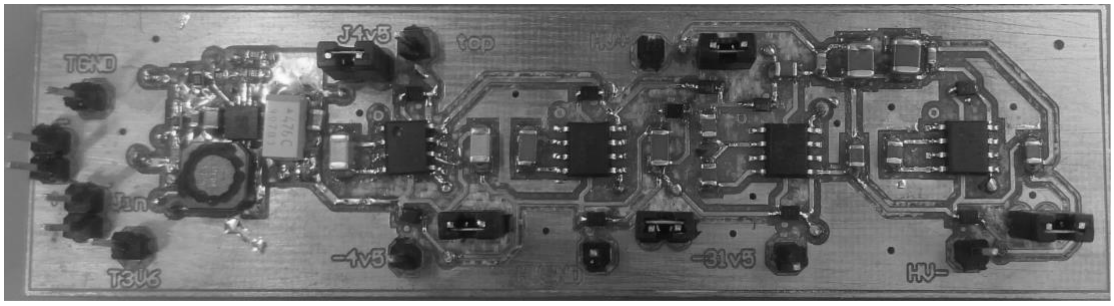

Figure 45. HVPSU testing PCB showing the various voltage conversion stages. The testing PCB allowed easy access to all the output voltage stages and currents flowing in the circuit.

The HVPSU produced a voltage of 72.75 V without load and regulated to within 50 mV for an input battery voltage range of 3 to 4.2 V.

The output voltage dropped linearly as more current was drawn consistent with an output impedance of 1956 Ω (linear fit $R^2 = 0.997$) compared to a simulated value of 1834 Ω using typical component values. The output voltage was 66.42 V under worst-case load conditions, a current draw of 3.17 mA.

Figure 46 shows power conversion efficiencies of the HVPSU for the two extreme battery voltages and current output conditions.

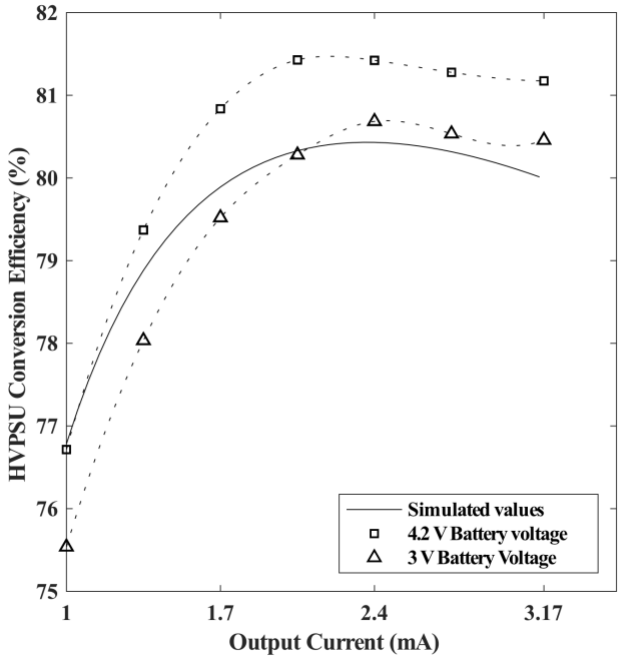

Figure 46. Power conversion efficiency for HVPSU at various output currents and battery voltages. The simulated values for battery voltages of 3 V and 4.2 V are indistinguishable at this scale.

The improvement in battery current consumption over a typical off-the-shelf module with an efficiency of 50% in this output current range can be calculated. The HVPSU uses between 34% and 39% less battery current than off-the-shelf solutions (see 6.2.1 and [155,156]), over the tested battery voltage and output current ranges from Figure 46.

6.3.2 High Voltage Current Pump (HVCP) instrumentation testing

The balancing of the instrumentation circuitry was challenging. The circuit would not function correctly when prototyped on breadboard due to capacitive mismatched in the breadboard tracks. The circuit was then tested and shown to work correctly on a separate 2-layer PCB connected by wires to the HVCP signals. More extensive testing was then conducted on a larger PCB which included all the circuit components, except the microprocessor, which allowed for simple signal driving using an external signal generator. The larger PCB allowed the performance of the instrumentation to be assessed when all the circuitry components where operating in concert, but to still allow

access to individual signals which would be difficult once the circuit was miniaturised. The final testing was performed on the full miniaturised device, discussed in 6.3.4.

In Chapter 5, the current consumption of the HVCP when driving -1 mA into a 60 kΩ load was 3.07 mA. With instrumentation circuitry added, the peak current draw was also during maximal DC operation, and was 3.17 mA.

The outputs of INA1, INA2 and INA3 (Figure 43) were measured directly using a bench-top multi-meter to establish the accuracy of the analogue instrumentation circuitry. Figure 47 shows the output error of the three instrumented signals for a variety of amplitude and frequency conditions. Current line A and current line B refer to the current flowing in the two stimulation leads.

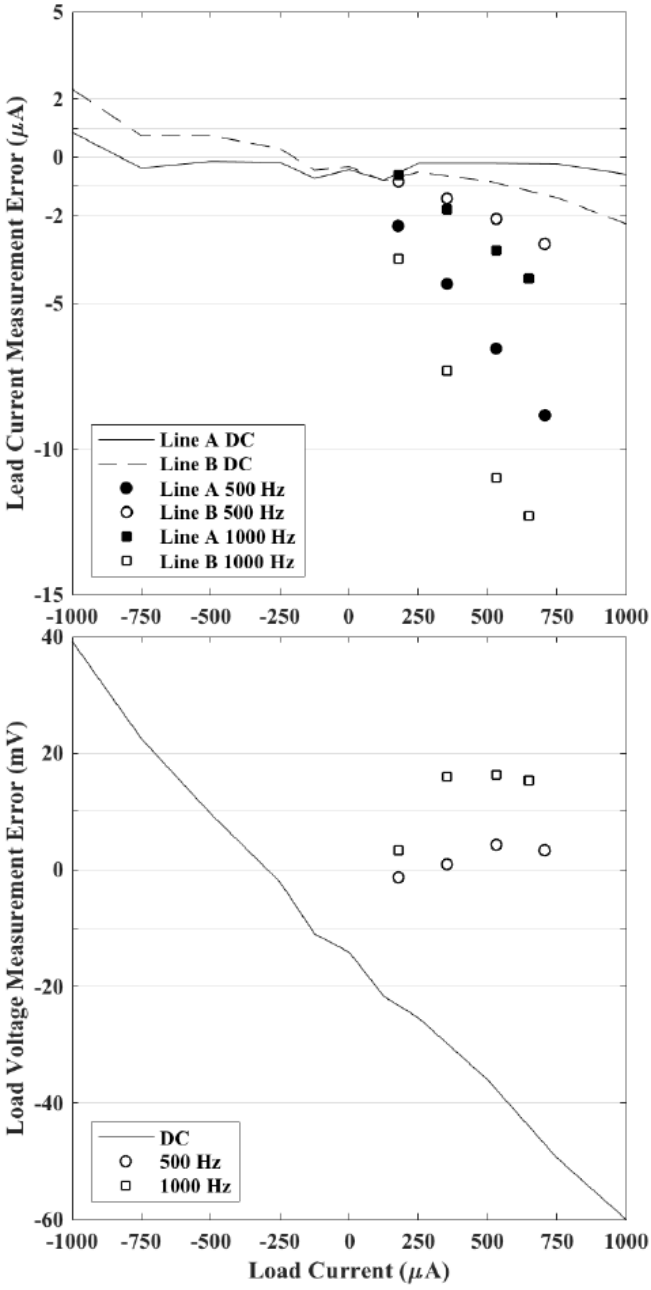

Figure 47. Output error in instrumentation circuitry over full range of output current and frequency. Top: error in the instrumentation of the current flowing into (Line A) and out of (Line B) the load. Bottom: error in instrumentation of voltage applied to the load. AC signals are measured as RMS and consequently cannot be negative. The four AC load current values measured roughly correspond to peak-to-peak load currents of 0.5 mA, 1 mA, 1.5 mA and 2 mA.

The maximum measurement error was 1.34% on line A and 2.08% on line B. The voltage measurement over the load never exceeded 0.31% error.

The actual difference in current between line A and line B is zero. Any difference in the measurements is thus the error in measurement of leakage current. The largest such difference occurs for maximal current at 1000 Hz and is less than 8.2 µA. The sum of

the worst error magnitudes is a conservative estimate of how bad this error could get if the circuit were built multiple times. This also occurs for maximal current at 1000 Hz and is less than 16.5 µA.

6.3.3 Battery testing

The final circuit (see Chapter 6.3.4) was tested using a 60 kΩ load running from a fully charged 1000 mAh battery. The large resistive load is selected to force the device to operate under worst-case power conditions.

When driving the worst-case -1 mA DC current into the load, the circuit operated for more than 15 hours. However, this waveform is not representative of a signal likely to be used in practice. A second test using a 1 kHz, ±1 mA peak-to-peak signal is more representative of a practical worst-case scenario. Under these conditions the circuit operated for more than 18 hours from a single charge.

As a best-case scenario, a DC current of 2 µA was driven. A non-zero DC current was chosen so that failure of the device was clearly apparent. Under these conditions the device operated for more than 33 hours.

The datasheet of the particular battery used does not specify cycle life. However, datasheets for similar batteries indicate that Li-Po batteries have more than 80% capacity after 300 cycles, which equates to more than 1 year of use at 10 hours per day. Even at 80 percent capacity, the battery can be expected to last 12 hours under worst case conditions.

6.3.4 Final device

The final device (Figure 48) was designed on a 6-layer PCB populated with parts placed on both surfaces. The circuit was designed to have similar dimensions to a standard 1000 mAh Li-Po battery and together they measured 33 mm × 55 mm × 15 mm and weighed less than 37 g. For comparison, the weight and dimensions of the benchtop currents sources used in Chapter 3 and Chapter 4 were measured. The Digitimer DS5 bipolar constant current stimulator measured 225 mm × 253 mm × 98 mm and weights 3.2 kg. The A-M Systems 2200 current stimulator measured 154 mm × 175 mm × 65 mm and weighs 1.27 kg. The schematic and PCB files for the full circuit is available in the digital appendix, in the folder “Prototype PCBs”.

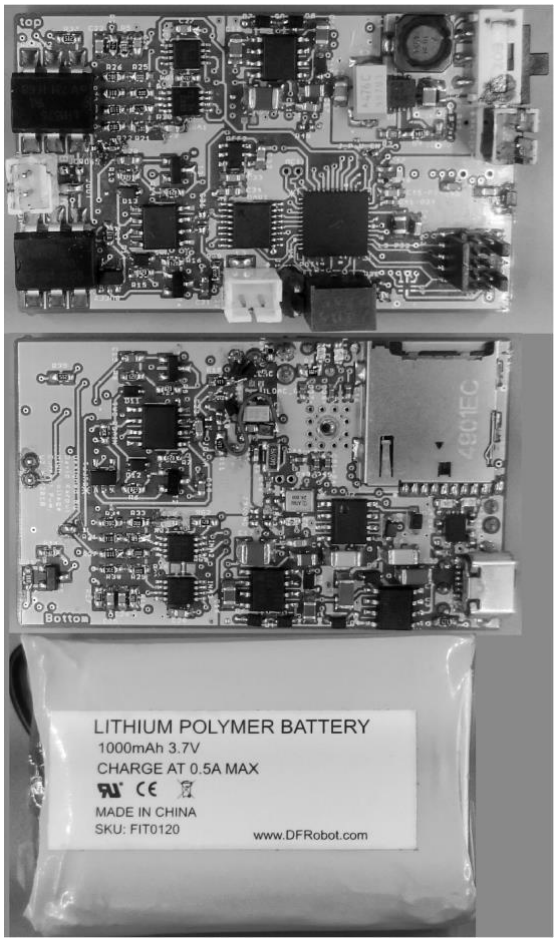

Figure 48. The topside (top) and underside (centre) of the assembled PCB, as well as the battery (bottom) used in testing. Together the PCB and battery measure 33 mm by 55 mm by 15 mm and weigh less than 37 g when the battery is placed on top of the PCB.

The indicator LEDs, output solid state relays, USB charging, HVPSU shut down control and interrupts, and the micro-SD card reading and writing were all tested to function as designed.

6.3.5 Human testing

The five participants recruited were all male. The device drove +1 and -1 mA DC, as well as 500 µA RMS at 500 Hz into the right leg of all participants with less than 2% error.

Figure 49 shows the recorded current signals when driving the same arbitrary white noise signal (100 µA RMS low-pass-filtered to 100 Hz) into each participant. Each signal overlaps making it difficult to distinguish between them, however, the figure inset shows the variation in the measured current signals. With the circuit disconnected the baseline noise amplitude and offset on the oscilloscope used to measure these waveforms was established. The amplitude of this measurement noise and offset was

large enough to account for most of the variability between recorded signals and the offset between recorded signals and the desired current.

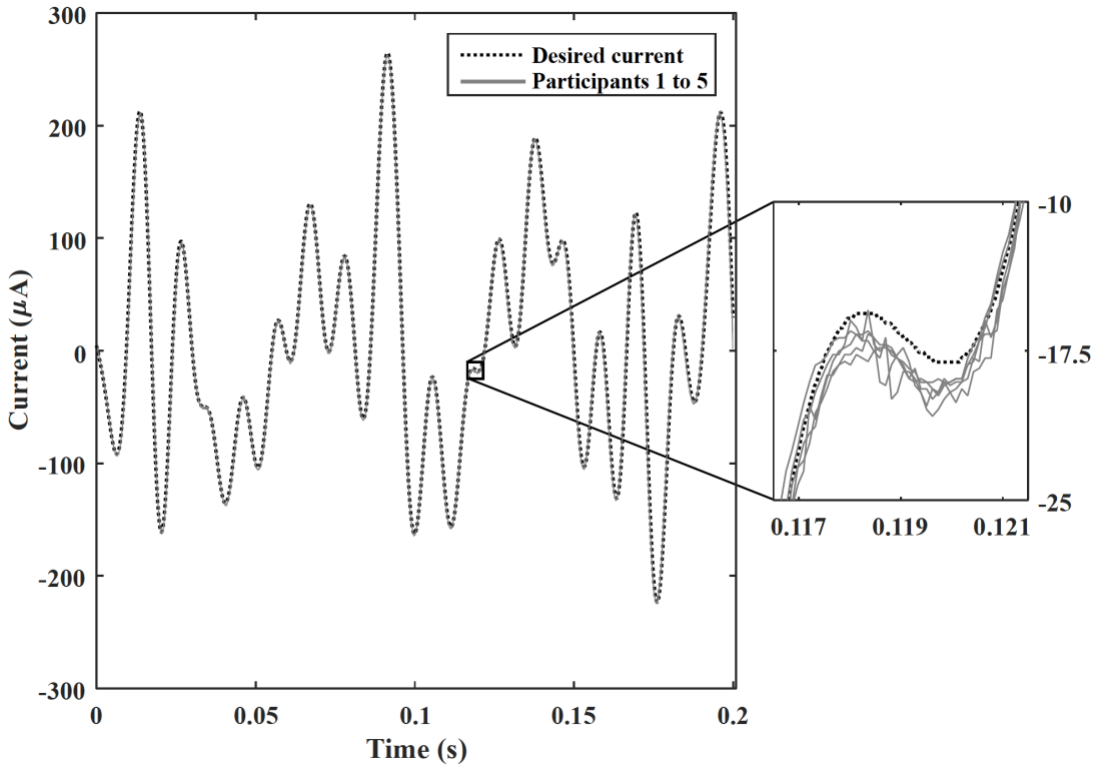

Figure 49. Desired current and achieved current plotted over time when stimulating 5 participants with the same white noise stimulus. The 6 signals lie over each other. Inset: A portion of the signals scaled so as to see the small variability between the 6 signals. Testing indicated that this variability could largely be attributed to measurement noise.

6.4 Discussion

The HVPSU was able to produce the required output voltage from a standard Li-Po battery for the full range of battery outputs produced as the battery discharges. Even though some output voltage is lost as a consequence of the internal resistance of the HVPSU, the worst-case conditions still offer sufficient compliance to drive ±1 mA through the impedance of the worst-case electrode connection.

The HVPSU circuit's performance was consistent with simulations. The small deviation in output impedance is likely a consequence of individual part output impedances being stipulated as ranges in the datasheets, whereas the simulation made use of only the typical values for each part.

The improvement in the efficiency of the HVPSU over simulated values, especially for higher input voltages is most likely a consequence of the TPS61028 being simulated

with a constant conversion efficiency (92%), whereas the datasheet does indicate the efficiency improves for higher input voltages. The exact efficiency values for the voltages and currents used in our design cannot be practically extracted from the datasheet, and a lower simulated efficiency was used regardless of input voltage.

The HVPSU is substantially more efficient than commercially available power supply modules facilitating a battery that is 34% smaller to achieve the same battery life (see [155,156]). Using a larger battery, to account for the power difference between the commercial solutions and the HVPSU presented here, is a feasible option. A 2000 mAh battery would increase the mass of the device by at least 14 g (an increase of 38% of the device weight), and the volume of the device by 8.9 cm^3 (an increase of 33% of the device volume). These values, while not the best solution, are not prohibitive.

The instrumentation circuitry produced accurate outputs in both AC and DC conditions. A key concern in the design of this circuitry was drawing current from the high voltage circuitry, which has a significant effect on battery life. The added current draw was in accordance with predicted values and is lower than what would be expected in simpler designs using high-voltage difference amplifiers.

The current measurement in the second electrode lead is only implemented to improve safety by monitoring for a condition where the current in the electrode leads differ more than 50 µA. The sum of the worst-case errors in the measurement of both currents was 16 µA, which guarantees that the error in the measured difference between the two electrodes will always be less than 50 µA.

Battery-life tests successfully demonstrated that the device can be used at full output power for an entire working day without the need for recharging.

It is not common to design portable stimulators for continuous application of current as opposed to pulsatile stimulation. Table 16 compares the design presented in this chapter to the design presented Chapter 5, as well as the only other known design for a similar application by Yamamoto *et al.* [152–154]. Three wireless stimulators are included, which have similar design constraints, but are designed for pulsatile applications and thus should be compared with caution.

Table 16. Comparison to designs with similar constraints.

	This work	Karpul *et al.* [4]	Yamamoto *et al.* [152–154]	Wang *et al.* [146]	Farahmand *et al.* [147]	Jovičić *et al.* [148]
Voltage compliance (V)	±72	±72	±10[a]	±60	23	85
Power consumption (mW)	123 - 272	106 - 233	312[a]	720	51.2	>700
Use duration (h)	15 to 33	>10	>24[a]	8	Unknown	Unknown
Current output (mA)	±1	±1	±1	60	0.4	70
Volume (cm^3)	27.3	28.2	210.1	127.5	90	52.5
Weight (g)	37	52	200	85	60	45
Signal type	Continuous	Continuous	Continuous	Pulsatile	Pulsatile	Pulsatile
Self – instrumentation	Yes	No	Yes	No	No	No
Control signal	Digital Internal / Wireless[b]	Analogue External	Digital Internal	Digital Internal / Wireless	Digital Internal / Wireless	Digital Wireless

[a] Approximate values based on information directly from the author

[b] Device has Bluetooth® low energy wireless capabilities but this functionality was not implemented as part of this work.

Despite the addition of multiple additional circuitry blocks, device weight and volume are lower than all other designs. This reduction in weight and volume is partially a consequence of using a much more energy dense Li-Po battery technology, which is both lighter and smaller for the same capacity as alkaline batteries.

The circuit accurately drove a variety of current waveforms into 5 participants. Until now, the HVCP has been tested extensively with artificial loads. The results of the human testing validate that these results transfer to using the circuit to apply currents to participants in *vivo*.

6.5 Conclusion

This chapter presents a novel stimulator specifically targeted at subthreshold continuous current stimulation for wearable applications. The research extends the work in Chapter 5, adding on-board device and signal control, instrumentation, safety and battery charging circuitry. Further, updates to the circuit's power supply mean the circuit is lighter and smaller than all known published designs with similar constraints. This is achieved without compromising battery life or high voltage compliance.

This work also presents the first instance where this design architecture has been tested *in vivo*. Human experiments indicated that the device is ready to be used in research applications. Research into the use of SENS-type interventions has previously been limited to short-term experiments, primarily due to the lack of a suitable wearable stimulator. This novel design opens new research opportunities. Future work should focus on exploiting this technology to perform long-term validation studies of interventions previously constrained to the research laboratory.

7

CONCLUSIONS

Each of the chapters of this thesis make important contributions to the current body of literature.

Chapter 1 presents the first numerical analysis of the outcomes of studies using subthreshold interventions similar to Subsensory Electrical Nerve Stimulation (SENS). The review provides a cohesive picture of this field of research, and offers some considered guidance as to where it should head. Aside from identifying short fallings of the current body of work and making recommendations for future research, the review identifies 3 gaps in knowledge that are addressed in this thesis.

First, no studies investigating the effect of this type of intervention on patients with HIV-related peripheral sensory neuropathy (HIV-PN) were found, and none of the studies reviewed reported on measures of pain. Second, none of the studies investigated participants' Electrical Perception Thresholds (EPTs) to electrical noise stimuli. While EPT has often been used as a means of determining the appropriate amplitude of SENS to apply, the reliability of this EPTs was unknown. Finally, none of the studies made use of, or researched, a device that could apply SENS-type interventions in a wearable fashion outside of a laboratory setting.

Chapters 2 and 3 address the first gap. Chapter 2 presents the first quantitative, double blind measurement of Vibration Perception Threshold (VPT) in patients with HIV-PN at different vibration frequencies. The adverse effects of HIV-PN on VPT are evidenced, which both justifies the need for an intervention, and validates the extensive VPT protocol used. An unexpected result was that outcomes of tests for interaction with vibration frequency suggest that the pathology of HIV-PN and its treatment may not affect all mechanoreceptors similarly.

Chapter 3 presents the first investigation into the effect of SENS on VPT and measures of pain in participants with HIV-PN. Beneficial outcomes similar to previous studies with other population groups were observed, however, likely because the protocol was more extensive than previous SENS work, several conditions where SENS was

ineffective or even detrimental were also observed. In this regard, the research raises important questions for the use of SENS as therapy, and more research is recommended. The analysis of pain outcomes did not indicate that SENS had a detrimental or beneficial effect. This is a very important outcome that can be used to justify future research with participants who experience higher levels of neuropathic pain, whereas previously this was avoided for ethical reasons, as the effect of SENS, or similar interventions, on pain was unknown.

Chapter 4 addresses the second gap in knowledge by providing the first investigation into participants' EPTs to noise stimuli under various conditions. Most subthreshold interventions claim to rely on the idea that the perceptual threshold of participants is stable with regard to the intervention signal. We show that this is not the case, and the perception thresholds are highly variable. This is an important finding because it either indicates that these interventions do not actually rely on applying the signal relative to threshold as claimed, or further research into how to adapt the signal for potentially dynamic thresholds is required. The results of Chapter 3 and Chapter 4 together present strong evidence that the mechanism of the beneficial effects seen with SENS specifically, are unlikely to occur through classic stochastic resonance, as is often claimed in the literature. This in itself is an important finding. Either way, the work strongly motivates that a better understanding of the effect of subthreshold interventions is required before proceeding.

The final gap is addressed in both Chapter 5 and Chapter 6 which together develop a constant current stimulator that is smaller, lighter and more powerful than designs presented in the literature. The device will facilitate future research into the long-term effects of SENS which are not understood, but vital for its development as potential therapy.

In addition to the gaps addressed in the main body of the thesis, Appendices A and B demonstrate the power of simulation to solve scientific questions in different contexts. Appendix A provides an uncommon statistical analysis that is vital to answer a valid scientific question regarding the "per-participant" optimal amplitude of SENS, without the false statistical bias seen in several previous works. Appendix B documents the implementation of a simulation framework which was then used to design a power supply with substantially improved characteristics over commercial solutions and previous designs.

7.1 Key findings

The key findings of this thesis are:

The body of literature regarding subthreshold interventions for the improvement of peripheral sensitivity is extensive and demonstrates this type of intervention to hold promise in reducing symptoms associated with peripheral sensory neuropathy. However, the literature lacks consistency and good quality scientific reporting, does not investigate the long-term effects of these interventions, may suffer from publication bias and does not properly understand the mechanisms by which these interventions interact with the underlying physiology. Further, we present evidence that SENS does not have beneficial effect though the mechanism of stochastic resonance, as is often claimed in the literature.

HIV-PN participants have reduced VPT compared to matched control participants, especially at 25 Hz. SENS improved VPT but only for 50 Hz vibration and only for certain amplitudes of SENS. SENS was not shown to have an effect on perceived measures of pain.

In contradiction to the manner in which it is treated in the literature, EPT is a highly variable measure and correlated little with potential explanatory variables when evaluated in a forced choice, double-blind manner.

Finally, the developed continuous current stimulator for wearable application of SENS is suitable for research into the long-term effect of SENS and similar subthreshold electrical stimulation interventions.

7.2 Future work

Each chapter makes specific recommendations of future work that should follow the conclusions made there, and should all be carried out in due course to progress this field. Here we answer the question more broadly: based on the whole thesis what should be done next?

The thesis as a whole demonstrates that the biggest barrier to developing SENS into a meaningful intervention for neuropathic populations is understanding the mechanism by which it has an effect on sensation. Understanding the mechanisms would allow the signal to be optimised and reduce the amount of exploratory work required.

Such investigations can take both a holistic and reductionist approach. Carefully designed studies that alter the location of the applied intervention can answer questions regarding where the intervention signal and sensory signal integrate: centrally, peripherally, or a combination. Studies carefully controlling and altering the nature of the intervention signal and its frequency spectrum, as well as the nature of the sensory signal to be detected, can answer questions regarding what physiological systems are involved and how to best interreact with them.

Reductionist approaches will also be essential. Studies looking at isolated nerve fibres *in vivo*, *in vitro* and in simulation will allow the perceptual component to be removed from the research. Finite element models can begin to answer questions of how individual nerves are affected, how bundles of nerves interact when exposed to a broad electric field and how the surrounding tissue influences the transmission of the signal to the axons. These models however must be based on realistic physiological data which does not currently exist for peripheral sensory nerves.

Ultimately, it is not necessary for the system to be treated as a "black box", where we "prod" the system and attempt to explain the outcomes. It may be technically more difficult and complex to open the box and understand how it works, but ultimately much more effective and efficient.

7.3 Final remarks

The results of this work demonstrate the potential viability of SENS as a therapy for HIV-PN, reveals the variability of electrical perception thresholds, explores the measures of pain for SENS interventions, and provides a complete and thoroughly tested design and implementation of an unparalleled electronic stimulator for non-laboratory environments. The conclusions of this work form both a strong theoretical and practical basis for future SENS intervention research.

APPENDIX A HYPOTHESIS TESTING FOR DATA THAT HAS UNDERGONE BIASED SELECTION

A.1 Background

In Chapter 3 we conducted a study that took a group of participants, tested them under four test-conditions and one control condition in an attempt to find a test condition that improved our outcome measure: vibrotactile sensitivity (Figure 50).

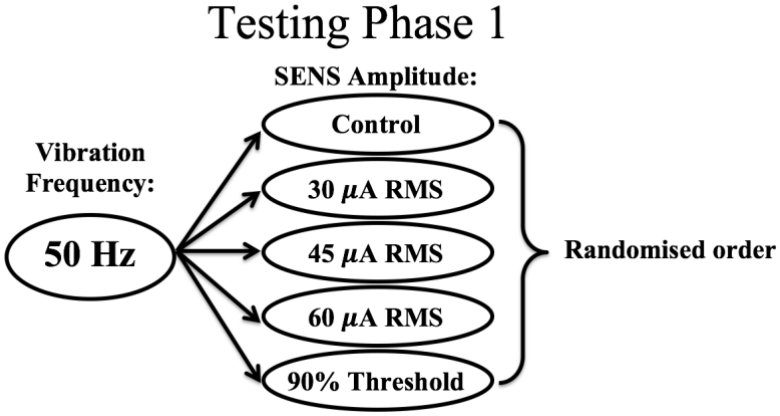

Figure 50. Diagram depicting the experimental design testing for improvement in 50 Hz VPT at various SENS amplitudes.

While analysing this data a very natural question arose: "What if each participant had an individualised test-condition that was optimal for sensitivity?", *i.e.* what if each person requires a different stimulation condition to get an effect? Then analysing the group response to each stimulation condition might weaken the effect sufficiently rendering the overall result null.

Standard test-statistics applied to intervention trials typically ask the simpler question: "Did '*this*' work or not?". Further, an ANOVA style analysis can ask: "Did one or more of the intervention categories have an effect on the group that distinguished it from rest?". We can check for the effect of *stimulation-condition* on the *outcome* and conclude if there was indeed a condition that had an effect on the group.

The question of individualised optimal treatment itself superficially seems very scientifically valid. Applying the common medical "dose-response" nomenclature, would we expect there to be a single *dose* that creates optimal *response* in every person? Testing a variety of conditions, matching participants to their optimal condition, and

creating theory to best predict what the optimal *dose* should be without difficult and costly testing, seems like a very reasonable way of developing any sort of treatment.

The simple numerical solution is to select the best response condition for each participant, create a new intervention category called "optimal", and compare the results for "optimal" to the control condition with an appropriate comparison test, such as a paired student's t-test. This often yields the desired positive result, but such 'cherry picking" is an invalid approach. However, research with this methodology has been published [69,73,77,92,94].

To demonstrate the bias this approach creates, we can plot the distribution of final outcomes, when selecting the best sub-outcome from "k" conditions, under the null condition when the difference is truly zero. We can calculate these distributions using statistical "extreme value theory" or simulate this condition in a Monte Carlo analysis (Figure 51). Extreme value theory derives for the probability distribution of outcomes x, when selecting the maximum from k selections from a normal distribution as:

$$P(x_k) = \mathrm{k}\Phi(x)^{k-1}.\Phi'(x)\ . \qquad 5$$

Where $\Phi(x)$ is the cumulative distribution function of a normal distribution, and $\Phi'(x)$ just returns the normal distribution.

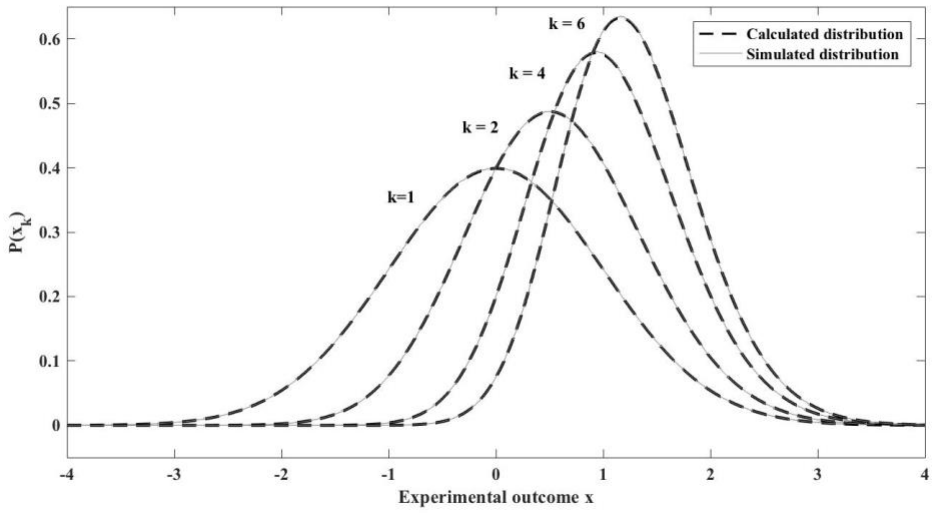

Figure 51. Plot of simulated and calculated probability, P(x), distribution functions for selecting the best outcome value from a set of k draws from a normal distribution. The two methods align with a high degree of accuracy.

In a hypothetical "t-test" like examination where the base control condition (k=1) is compared to the "optimal" condition (k>1), we can see the test will likely observe a difference in the data even when both datasets are generated from the same base distribution (*i.e.* the null condition).

A standard statistical test or correction factor is sought to answer the hypothesis regarding the "optimal" condition without the bias demonstrated above. Monte Carlo hypothesis testing can calculate test statistics against any null hypothesis that can be simulated and is consequently well suited to this situation [135–137].

A.2 Construction of the null hypothesis for cherry picked treatment amplitude

To apply the Monte Carlo hypothesis test, first we must construct our experiment's dataset under null conditions. In Chapter 3 we tested the "Optimal" SENS condition at a vibration frequency of 50 Hz for each participant against the no-SENS condition using the odds ratio of linear mixed effects models. This yields a p-value and an effect amplitude of percentage change from control. Table 17 summarises the result of the test on this skewed data.

Table 17. Summary of results for "Optimal" SENS condition for each participant for 50 Hz vibration.

	Effect of optimal SENS on VPT	p-value
HIV-PN	-17.8%	4.54e-13
Non-HIV	-24.3%	6.22e-15

To appropriately test the null-hypothesis we must construct a dataset that simulates our experiment, however with a known zero effect of SENS. We then run the dataset through the same statistical test and see if the results of the actual experiment lie outside of the distribution of many such null simulations.

To mimic the distribution of the participants more accurately, sub-datasets are generated for each participant with the same mean VPT as the average of the VPT from the no-SENS and the Optimal SENS conditions for that participant, and the same SD as the mean of the SD's from the two conditions for that participant. This is repeated five times for each participant in a cohort. The first of the five iterations acts as the no-SENS condition and the "Optimal SENS" condition is cherry picked from the

remaining four iterations. The data is saved to a separate file and the process repeated 10 000 times.

The statistical outcomes of the 10 000 files where we know there is no effect of SENS is then analysed. This can be done programmatically in the statistical package "R".

Figure 52 shows the distribution of the effect of Optimal SENS when we know there to be no effect. It demonstrates the extent of the bias created but also the limits of the bias. If the experimental data has a larger effect than the 95th percentile of this distribution we can say that the p-value for our data is less than 5%. Figure 53 shows the distributions of the p-values from the null hypothesis. Again, if the p-value from our dataset is lower than the 5th percentile of this distribution then we can then again state that the experimental data is indeed unlikely to come from the null distribution.

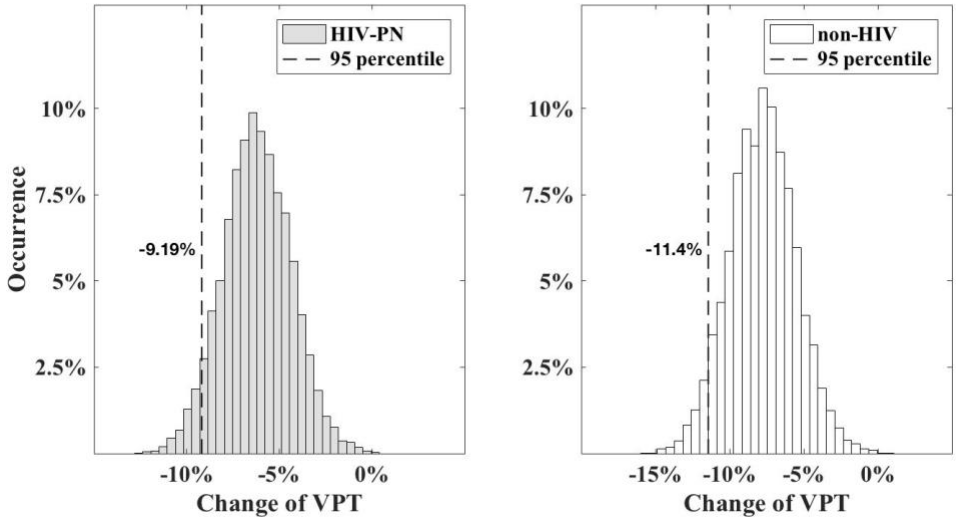

Figure 52. Distribution of the calculated effect of SENS in 10 000 simulated experiments under the null condition where the real effect of SENS is zero.

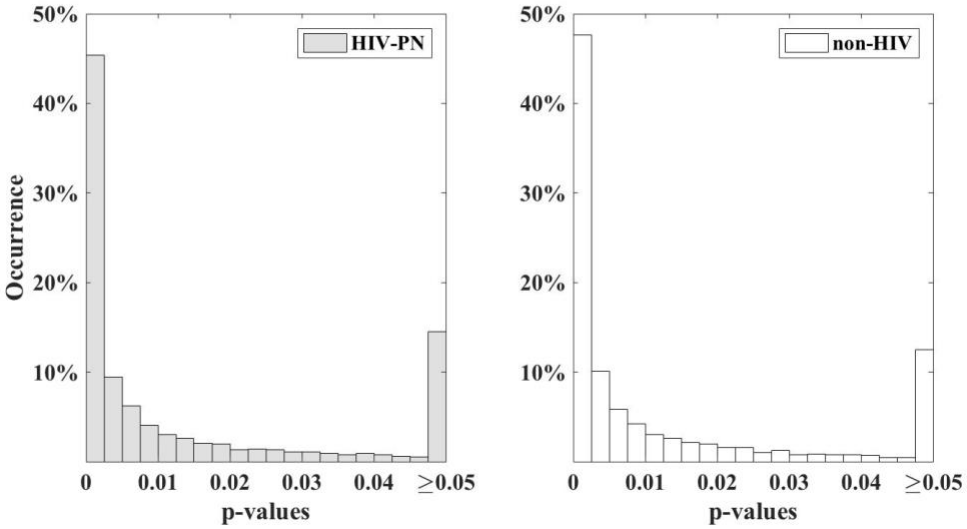

Figure 53. Distribution of the calculated p-value of the effect of SENS in 10 000 simulated experiments under the null condition where the real effect of SENS is zero. The 5th percentile for the HIV-PN null hypothesis is at p = 1.26e-5 and p = 8.93e-6 for the non-HIV group. Only ~15% of the p-values lie above the p = 0.05 mark, which demonstrates the extent of the p-deflation.

We can now extend Table 17 to include the outcomes from the simulation (Table 18).

Table 18. Experimental and simulated outcomes of statistical tests with the "optimal" SENS condition.

	Effect of optimal SENS on VPT	Simulated 95 percentile effect of optimal SENS on VPT	p-value	Simulated 5 percentile p-value
HIV-PN	-17.8%	-9.2%	4.54e-13	1.26e-5
Non-HIV	-24.3%	-11.4%	6.22e-15	8.93e-6

Table 18 clearly shows that the experimental data lies outside of the null distribution and thus can be considered statistically significantly different. We can go one step further and ask what percentile in the simulated data lies beyond the values of our experimental data. The data indicates that none of the 10 000 simulated experiments had data that exceeded the effects seen experimentally, indicating the true p-value is likely less than 0.0001.

A.3 Conclusion

The above work makes use of a Monte Carlo null hypothesis test to determine that the data presented in Chapter 3 is statistically significant, whereas conventional statistics would have led to a strongly biased outcome.

APPENDIX B SIMULATION OF MULTI-COMPONENT BUCK AND BOOST HIGH VOLTAGE POWER SUPPLIES

B.1 Background

Chapter 5.2.2 documents the design of a High Voltage Power Supply Unit (HVPSU) that cascaded several voltage inversion stages to generate 72 V (±36 V) from a 9 V battery. The design had a very low quiescent current and high efficiency for low output currents. During the development of the circuit, a bench-top 9 V supply was used, and in testing, a standard 9 V battery. However, after publishing the circuit [4], during further testing which involved discharging the battery, the assumption that the circuit would receive a constant 9 V failed as most battery technologies loose approximately 25% of their output voltage over their discharge curve. The HVPSU design had no regulation and consequently the output voltage would proportionally track the battery voltage as it discharged. This resulted in reduced compliance of the subsequent High Voltage Current Pump (HVCP) and may cause "voltage clipping" in practice, an undesirable output from the device.

This appendix deals with the design of the replacement HVPSU used in Chapter 6.2.1. First, the specifications and trade-offs in design architectures of this nature are discussed. Then, a Matlab framework, devised to simulate various HVPSU architectures, is presented. This framework enables the prediction of performance for various architectures and reduces time and cost in the design process. The results of several architectures are presented. Finally, the discussion focuses on design principles that emerged in the process and led to the final design.

B.2 Design specifications and trade-offs

The HVCP is required to drive ±1 mA into a worst-case 60 kΩ load. This requires an HVPSU voltage of at least ±60 V. Because the HVCP can invert the supply voltage, only a single sided +60 V or -60 V is required from the HVPSU. The HVCP however does not operate rail-to-rail and requires approximately 2.5 V additional "headroom" on each voltage rail. Thus, an HVPSU voltage of 65 V is required under maximum current draw. Due to the quiescent current of the HVCP and the circuit's conversion

efficiency, the maximum current drawn by the HVCP from the HVPSU is 3.17 mA, with a quiescent current of 1 mA when under no load.

The ultimate goal of the HVPSU and battery combination is to power the HVCP for the required minimum of 10 hours under worst-case operating conditions (3.17 mA). A more efficient power supply will allow for a smaller battery capacity to be used reducing the size and weight of the overall circuit. However, if a hypothetical circuit is more efficient, but the circuitry itself is large, the gains in reduction of battery size may be negated by the increase in physical circuitry size.

The design in Chapter 5, which uses a cascaded series of inverter chips produces a small, efficient circuit and forms the foundation of a potentially improved design. In making alterations, many trade-offs must be considered that influence the final efficiency and physical size of the circuitry.

B.2.1 Input voltage and battery selection

The input voltage of the circuit largely defines what types of batteries should be used. This can also be seen in reverse, which batteries offer the best trade-offs can define the input voltage of the subsequent HVPSU. Lithium-Polymer (Li-Po) batteries offer considerably superior energy density to alkaline batteries and are used in the vast majority of wearable devices available on the market [161]. Using a more energy dense battery technology would reduce battery size and weight for the same energy requirements. Single cell Li-Po batteries are easy to charge using USB power and small off the shelf chips. They also come in a multitude of capacities with various forms of protection circuitry built-in. However, the battery voltage available is limited by the battery chemistry and is generally between 2.7 V and 4.2 V depending on the technology and level of charge (most being between 3 V and 4.2 V).

Multiple battery cells can be placed in series to create higher voltages. For example, three cells stacked would create ~9 to 12 V (depending on the charge level of the batteries), which is similar to the original design which used a 9 V input. Charging multiple batteries in series is more difficult, and can result in suboptimal charge levels or damage to the Li-Po batteries if not controlled carefully. The advantage of using higher voltage batteries is that less “boost” is required by the HVPSU to get to the final output voltage. This would be more efficient.

Thus, there is a trade-off between the convenience of using a single cell and the efficiency of using multiple cells.

B.2.2 Placement of the reference voltage relative to the battery voltage

The initial HVPSU design multiplies the input voltage by a factor of minus eight. For every 1 mA of current drawn from the maximum HVPSU output, 8 mA is drawn from the battery. In the design, it was required that the control and instrumentation circuitry be 'placed near' the HVCP reference (~ -27 V). Simply connecting the control circuitry here will also draw several times its operation current from the battery. To combat this, a second battery can be used for the control circuitry, with the two references joined. This improves efficiency and has the added benefit of creating a certain amount of separation between the control circuitry and the HVCP.

However, if the HVPSU had a mid-supply reference that was 'close' to the battery voltage, then the effect of inserting the control circuitry at this point would no longer have a multiplicative effect on current consumption. A single battery could be used which would reduce the size and complexity of the circuit. Careful Printed Circuit Board (PCB) design would then be required to prevent the transfer of electrical noise between the low-voltage and high-voltage circuitry.

The benefits of using a single battery (system size) encourage the design of a supply that both boosts the voltage up from the battery and bucks the voltage negatively in order to maintain a mid-supply reference close to the battery voltage. This architecture is not a requirement, but simply a trade-off to be considered when evaluating architectures.

B.2.3 Conversion efficiency of each chip

The conversion efficiency of each chip in most architectures is multiplicative with the final efficiency always being lower than the worst chip in the sequence. Voltage conversion chips often have different efficiencies at different output currents. The required output current of each chip is defined by where in the circuit that chip is inserted. Chips with low output voltages will have higher output currents and *vice versa*. Few conversion technologies are efficient for low output currents in the range of 1-3 mA. Unregulated switched capacitor converters appear to be the most consistently

efficient for output currents in this range, whereas switched inductor converters appear to work well for regulated conversion requiring higher output currents.

B.2.4 Quiescent current of each chip

As stated above, drawing current from the high voltage stages of the HVPSU has a greater influence on battery life than drawing the same current from low voltage stages. Consequently, reducing the quiescent current of chips at the high voltage stages carries more weight than the same at low voltages.

Further, the number of chips used has an influence on power consumed. Again, this is less important at low voltages, but reducing the total number of chips required at higher voltages would improve the efficiency of the HVPSU design.

B.2.5 Output impedance of each chip

Each power conversion chip has an associated output impedance. The loss of power over the output impedance accounts for almost all of the conversion inefficiency in switched capacitor converters. In this case the power lost is: $P_{lost} = I^2 R_{output}$, where I is the current output by the chip and R_{output} is output impedance of that chip. From this we can see that it is very important that chips with higher output currents have lower output impedance. Further, the voltage lost over the output impedance is also greater for higher output currents and has an adverse effect on the final compliance of the circuit.

From this and from B.2.4 we can see that the design trade-offs dictate that chips near the final output stage of the cascade have low quiescent current, but consider output impedance as a less important factor, whereas chips near the battery voltage require lower output impedance and regard quiescent current as a less important factor.

B.3 Simulation of cascaded HVPSU architectures

The HVPSU architecture will fundamentally be created from three different forms of power converters: linear regulators, regulated buck/boost switched inductive converters, and unregulated switched capacitor converters. Each of these converters come in a wide variety of forms, each offering a trade-off of some kind with regards to the above factors. This is such a common problem that major manufacturers offer

design tools on their websites to aid with selection of parts. However, these tools were not able to provide any appropriate single chip solutions to the problem described here and are too simple to evaluate complex designs.

A second option is to use a circuit simulator package like SPICE [157,158]. While premade SPICE or SPICE-like parts are available for a multitude of electronic components, none could be found for the potential components of this design. Further, learning how to create parts and use them in SPICE is not straight forward and would potentially require more time than creating a custom, purpose-built simulator.

The Matlab objects outlined in the following sections were created to facilitate steady state simulation of any buck or boost circuit component based on information from the datasheet for that component. The components can then be connected together to simulate any architecture without the need to physically construct each circuit.

All simulated circuits are made of '*Parts*' which interact with the circuit's current and voltages through its '*Pins*'. '*Pins*' connect together outside of a part through a '*Net*' which transfers currents and voltages to other '*Pins*' and subsequently '*Parts*'. An overview of the structure is presented in Figure 54, and each object type is described in more detail in the following sections.

B.3.1 Pins

'*Pin*' objects are associated with a single *part* and a single *net* and are specified as either input or output. *Input pins* draw current from their connected *net*. How much current is drawn is defined by the associated *part*. While the *part* defines the current draw of the *input pin*, the *net* defines the voltage on the *input pin*. If the *part* updates the current draw of the *pin*, this triggers the update function of the attached *net* (see B.3.2).

Output pins have their voltage specified by the *part*, and impose their voltage onto the *net*. A change to the voltage of the *pin* causes an automatic update of the voltage on the *net* to which it is connected. Only one *output pin* can be connected to a *net* at a time (see B.3.2). The current drawn from an *output pin*, is defined by the *net* (and in turn the *input pins* connected to the *net*).

B.3.2 Nets

A *net* object stores a list of the *pins* connected to it. It has three main functions. Firstly, a 'connect' function which adds a specified *pin* to the *net*. The *pin* is checked for compliance before adding, *i.e.* it must be a *pin* object, and it may not be a second *output pin*.

The second function is to update the *net*. A *net* update causes the *net* to query the current requirements of all the *input pins* connected to it. It then updates the current draw from the *output pin* connected to it, it then queries the output voltage on the *output pin*, which may have been adjusted by the *part* based on the new current demands, and finally it sets the voltage at all the *input pins* based on the voltage output of the *output pin*.

Finally, a *pin* can be removed from *net*. If the *pin* specified in the function call is a valid *pin* that is part of the *net* then the *pin* is removed and the *net* update function is called. Otherwise an error is thrown.

B.3.3 Parts

Parts define a collection of input and output *pins* upon instantiation. Each *part* must define an update function which queries the required current on all *output pins*, the available voltage on all *input pins* and then calculates and updates the output voltage on *outputs pins* and the required current of all *input pins*, each of which triggers an update of the attached *nets*.

The manner in which the signals on the *pins* interact defines the behaviour of the *part*. This can range from a simple ideal battery which has two *output pins* whose voltages are not dependent upon any calculation, to a more complex battery whose voltage is dependent on the current drawn by the *net*, to extensively complex operation with multiple conditions and interactions between various *pins* and *part* properties.

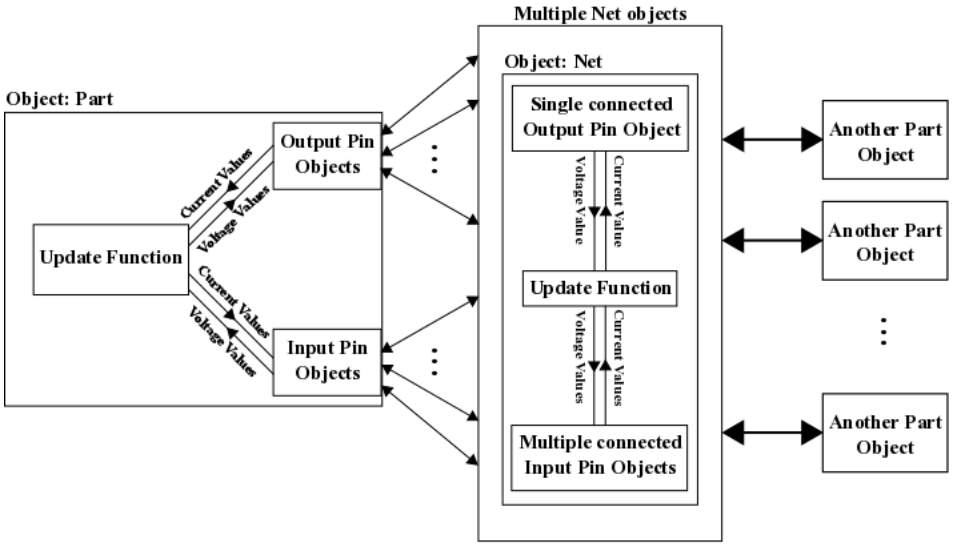

Figure 54. Diagram of the circuit simulation framework object relationships. Left, a generic *Part* object which defines an update function. The update function dictates the behaviour of the *Part* receiving information from and sending information to its associated *Pin* Objects (either input or output). Centre, each *Pin* object can connect to a single *Net* object. The structure of a *Net* object is shown in the diagram, allowing one *Output Pin* object to be connected, and multiple *Input Pin* objects. Right, multiple other *Part* objects can connect to the *nets* to model the flow of currents and voltages through complex interaction of *Parts* and *Nets*.

B.3.4 Simple simulation example

An example of a simple demonstrative simulation using this framework, which connects a resistor to a battery and measures the resulting current flow is as follows (all *parts* are predefined and available in the digital appendix in the folder 'HVPSU simulation code'):

Create two nets:

```
positive_rail = Net;

positive_rail.name = 'Positive Rail';

negative_rail = Net;

negative_rail.name = 'Negative Rail';
```

Create a predefined battery object with a battery voltage of 9 V:

```
my_battery = Battery(9);

my_battery.name = '9V battery';
```

Create a resistor with a value of 9 Ω:

```
my_resistor = Resistor(9);

my_resistor.name = 'The resistor';
```

Connect the resistor and the battery pins to the nets (the pins are predefined by the parts):

```
positive_rail.connect(my_battery.pins.V_plus);

positive_rail.connect(my_resistor.pins.pin_one);


negative_rail.connect(my_battery.pins.V_minus);

negative_rail.connect(my_resistor.pins.pin_two);
```

We then update the parts:

```
my_battery.update();

my_resistor.update();
```

“my_resisitor.pins.pin_one.current_sink” provides the current in the pin:

```
display(['The current flowing into pin 1 of the resistor is: ' num2str(
my_resistor.pins.pin_one.current_sink ) ' A.' ])
```

This generates the following console output:

```
Connected output pin: 9V battery_V_plus to net: Positive Rail.

Connected input pin: The resistor_pin_one to net: Positive Rail.

Connected output pin: 9V battery_V_minus to net: Negative Rail.

Connected input pin: The resistor_pin_two to net: Negative Rail.

The current flowing into pin 1 of the resistor is: 1 A.
```

We can change the resistance of the resistor to see the effect:

```
my_resistor.resistance = 18;
```

And then update the parts:

```
my_battery.update();

my_resistor.update();

display(['The current flowing into pin 1 of the resistor is: ' num2str(
my_resistor.pins.pin_one.current_sink ) ' A.' ])
```

This generates the following console output:

```
The current flowing into pin 1 of the resistor is: 0.5 A.
```

Naming the *parts* and *nets* with text labels is not necessary, but does increase the readability of the console output.

Provided the steady state interaction for the currents and voltages inside a *part* can be defined, we are now able to model the voltages and flow of current in a system of arbitrary complexity. That the system sits within a programing/scripting environment easily facilitates examining a circuit under a range of conditions.

Documenting how every *part* used was modeled is beyond the scope of this appendix, however, the following section presents one of the key components as an example. All *parts* are available in the digital appendix in the folder 'HVPSU simulation code'.

B.3.5 Simulating a generic switched capacitor voltage inverter

The most difficult *part* to simulate was a switched capacitator inverter required for the HVPSU architecture. Rather than defining a specific *part*, a generic *part* was created that can perform this function and model the flow of power and current accurately, allowing a whole family of parts to inherit from the object.

Understanding the flow of current as multiple inverters are cascaded is not intuitive. Application note AN051.1 from Intersil, which deals with the ICL7660 voltage inverter, provides a good model for the flow of load current and quiescent current when cascading devices [159]. We can adapt this formulation to demonstrate the current paths with cascaded inverters in general (Figure 55). The model also demonstrates how the load current and quiescent current increase as more stages are added between the battery and load.

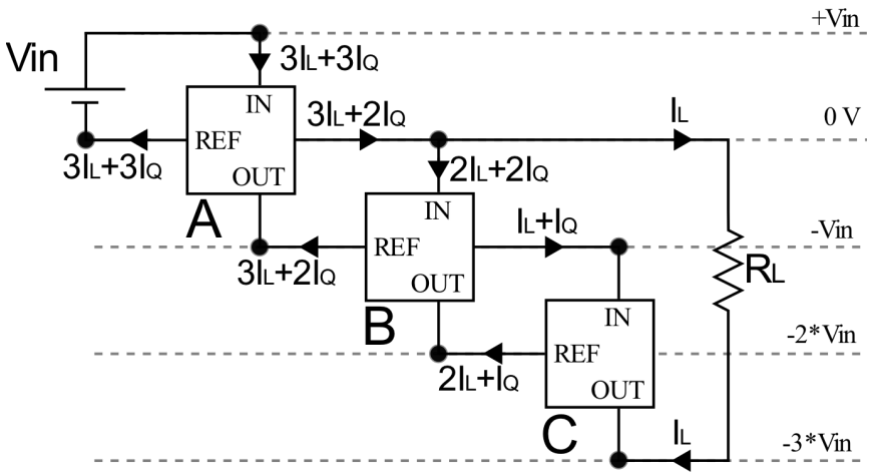

Figure 55. Representative diagram of three cascaded capacitive voltage inverters. Based on information from [159]. For each chip, the input (IN) and output (OUT) current match in magnitude, except an additional quiescent current is drawn into the input. Current out of the reference pin (REF) is then the sum of these two currents (in accordance with Kirchhoff's circuit laws). I_L is the current in the load (R_L) and I_Q is the quiescent current of each chip which is assumed to be the same for all the chips. The best way to trace the current flow in the diagram is to work backward from 'C'. Note that the REF pins of A and B have two connections each that supply current to both preceding parts and subsequent parts.

The generic inverter *part* has three *pins*, two *input pins*, 'IN' and 'REF', and one *output pin*, 'OUT'.

Using the *pin* names as subscripts and V and I denoting the voltage and current at the *pins*, we have available to the *part*'s update function from the connected *nets*: V_{IN}, V_{REF} and I_{OUT}. We need to define in the *part*'s update function the assignment of I_{IN}, I_{REF} and V_{OUT}. By convention, current directions are into *input pins* and out of *output pins*. In Figure 55 the current is depicted as flowing into the OUT pin, which is an *output pin*. Consequently, I_{OUT} in the equations below is always referred to as $-I_{OUT}$.

The ideal inverter, with no output impedance, perfect conversion efficiency and no quiescent current defines that

$$V_{OUT} = V_{REF} - (V_{IN} - V_{REF}), \quad 6$$

$$I_{IN} = -I_{OUT}, \quad 7$$

$$I_{REF} = -(I_{IN} + -I_{OUT}). \quad 8$$

The flow of current matching that in the model of Figure 55.

We can now adjust the ideal model to represent a more realistic inverter. The datasheet specifies a quiescent current (I_Q) and a Power Conversion Efficiency (PCE), thus:

$$I_{IN} = \frac{-I_{OUT}}{PCE} + I_Q. \quad (9)$$

If we wished, we could make I_Q and PCE values dependant on the input voltage as specified by the datasheet, but for our purposes single values will suffice.

Datasheets also define a Voltage Conversion Efficiency (VCE) and an output impedance (R_O). Therefore:

$$V_{OUT} = V_{REF} - (V_{IN} - V_{REF}) \times VCE + (-I_{OUT} \times R_O). \quad (10)$$

The part must therefore define: I_Q, PCE, VCE and R_O, and then input voltage limits and output current limits to be evaluated on each update. With these parameters most capacitive inverters can be simulated.

In practice, some inverters can also perform voltage doubling either as an independent function, or instead of an inversion. This can be added to the model in the similar way as above with an additional output pin. The final object was the most frequently used simulation component: a generic doubler/inverter which can be adjusted to model most switched capacitor inverters (see digital appendix folder 'HVPSU simulation code': DoublerInverter.m). The doubling mode can be ignored, or used, and when used, can include diode drop inefficiencies as specified in the datasheet. The diode model adjusts the forward voltage as a function of current in accordance with the datasheet of a Schottky rectifier diode.

B.4 Simulated architectures

Off-the-shelf solutions that boost battery voltages to produce high voltages in the range required, have efficiencies in the order of 50% for output currents in the required range (1-3.17 mA) (See Chapter 6.2.1). Any improvement beyond 50% would reduce the size of the battery required to operate the stimulator for a given period.

Many permutations of parts and configurations were simulated in an attempt to find a solution that appropriately balances the design trade-offs. Simulation results for four architectures (PSU-1, PSU-2, PSU-3 and PSU-4) are demonstrated. These designs were not selected for implementation, but demonstrate particular principles of this form of HVPSU design. Finally, simulation results for the original HVPSU from Chapter 5 (hereinafter referred to as PSU-5) and the replacement HVPSU from Chapter 6 (hereinafter referred to as PSU-6) are compared to empirical experimental data.

B.4.1 PSU-1

PSU-1 (Figure 56) attempts to make as few alterations to PSU-5 (Figure 31 and Figure 32 or Figure 60) as possible to gain the required voltage regulation. First the battery voltage which ranges from approximately 9.5 V to 6.5 V is regulated to 4.5 V by a high efficiency buck converter (TPS62122). That voltage is then doubled to generate a total available regulated voltage of 9 V by a MAX660. The MAX660 is an efficient voltage doubler for voltages and currents in this range, but is limited to multiplying a maximum of 5.5 V. From this regulated 9 V supply, the voltage is stepped up to 72 V using the same architecture as PSU-5.

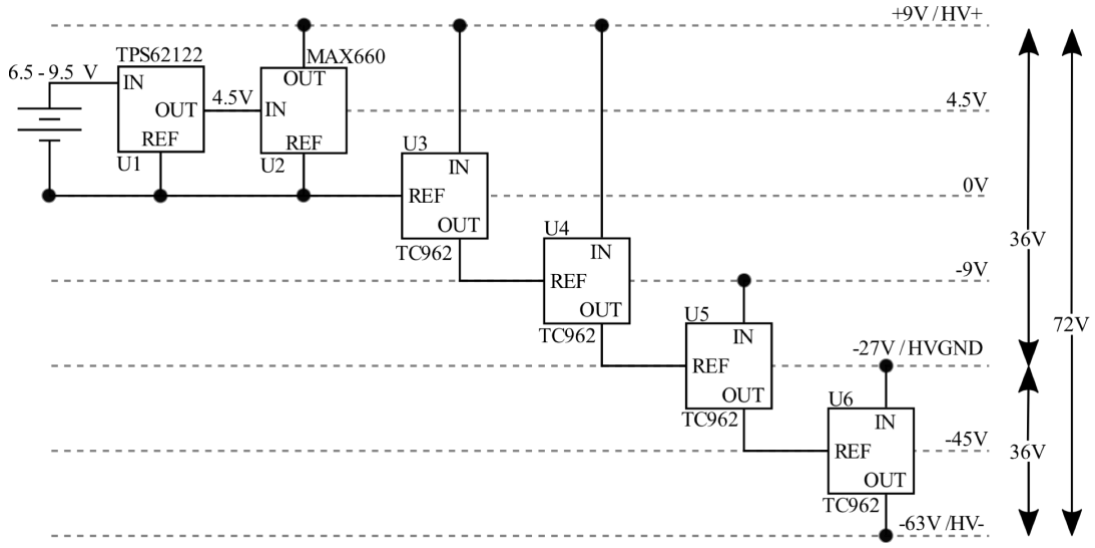

Figure 56. Representative diagram of PSU-1. U1 bucks the battery voltage to 4.5 V, U2 then doubles that voltage to a regulated 9 V. This is then used as the input for the architecture of PSU-5 (Figure 31 and Figure 32 or Figure 60).

B.4.2 PSU-2 and PSU-3

In PSU-2 (Figure 57) and PSU-3 (Figure 58) a combination of doublers and inverters in a ‘winged’ architecture is compared to a solution using the same number of parts, but only as voltage inverters. Not many parts perform efficient voltage doubling, and inputs are typically limited to lower voltages. The MAX660 performs well with low quiescent current and low output impedance. A Li-Po battery voltage of between 3 and 4.2 V is boosted to 5.15 V using an efficient boost converter (TPS61028). This voltage is then doubled and inverted as needed by a cascading series of inverters and doublers. Both designs produce the same relative outputs, and use the same parts, but the cascades have different depths.

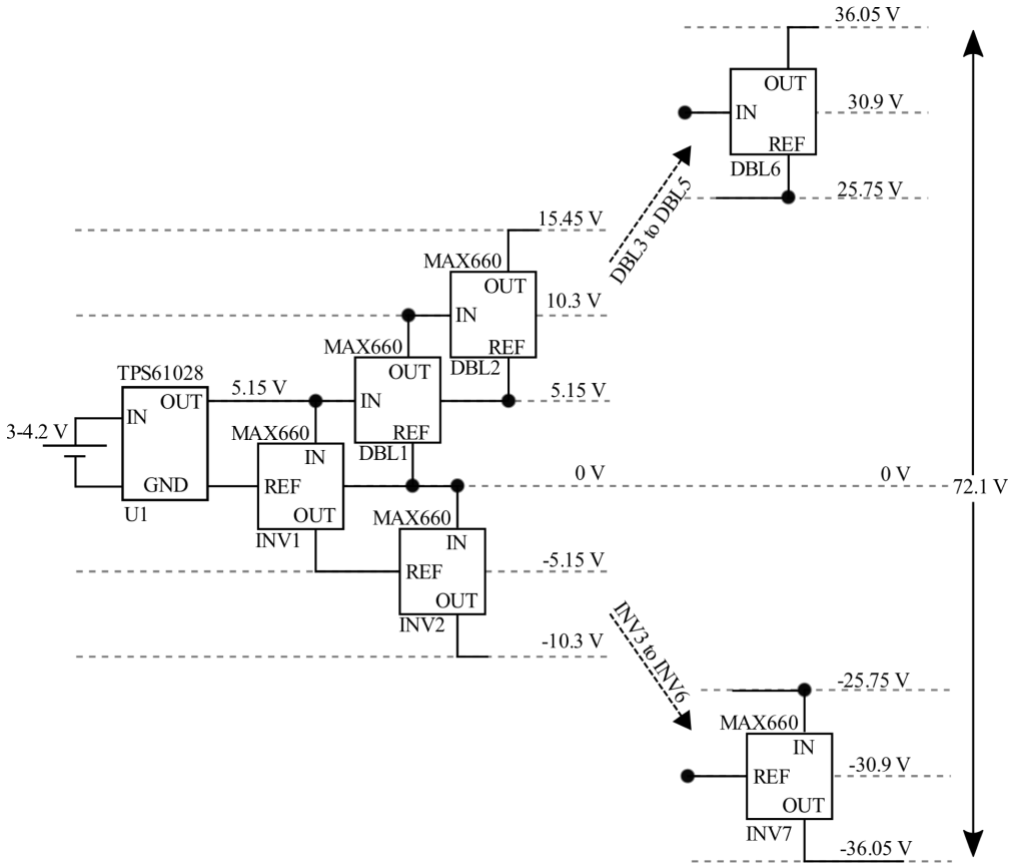

Figure 57. Representative diagram of PSU-2. U1 boosts the battery voltage to 5.15 V. From there DBL1 through DBL6 increase the voltage to 36.05 V. At the same time, INV1 through INV7 repeatedly invert the lowest available 5.15 V to finally produce -36.05 V.

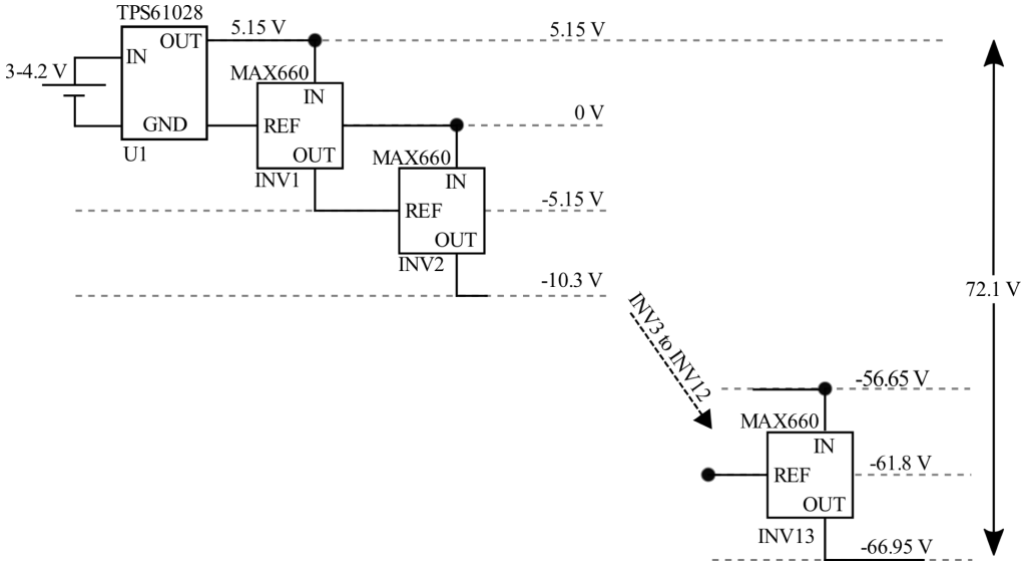

Figure 58. Representative diagram of PSU-3. U1 boosts the battery voltage to 5.15 V. That voltage is then inverted in steps of 5.15 V 13 times by INV1 through INV13 to ultimately produce a total voltage of 72.1 V. PSU-2 and PSU-3 produce the same relative voltage outputs and have the same circuit components, but in PSU-2 the depth of the cascade is 7 parts and in PSU-3 it is 13 parts.

B.4.3 PSU-4

PSU-4 (Figure 59) investigates using a high efficiency low voltage buck converter (MAX1920) from a single LiPo cell (3-4.2 V) to produce a very low regulated voltage (2.7 V). This voltage is then converted to produce the required output using several chips in various configurations. The hypothesis of this design being that the improved efficiency of using buck conversion at low voltages and therefore high currents may be sufficient to justify the additional multiplications required to attain the final output voltage. We will compare PSU-4 to PSU-6 (Figure 40 or Figure 61) which has a similar architecture but boosts the battery voltage instead of bucking it. PSU-4 and PSU-6 make use of ICL7662's instead of TC962's because they are available in a smaller package and can operate at higher voltages.

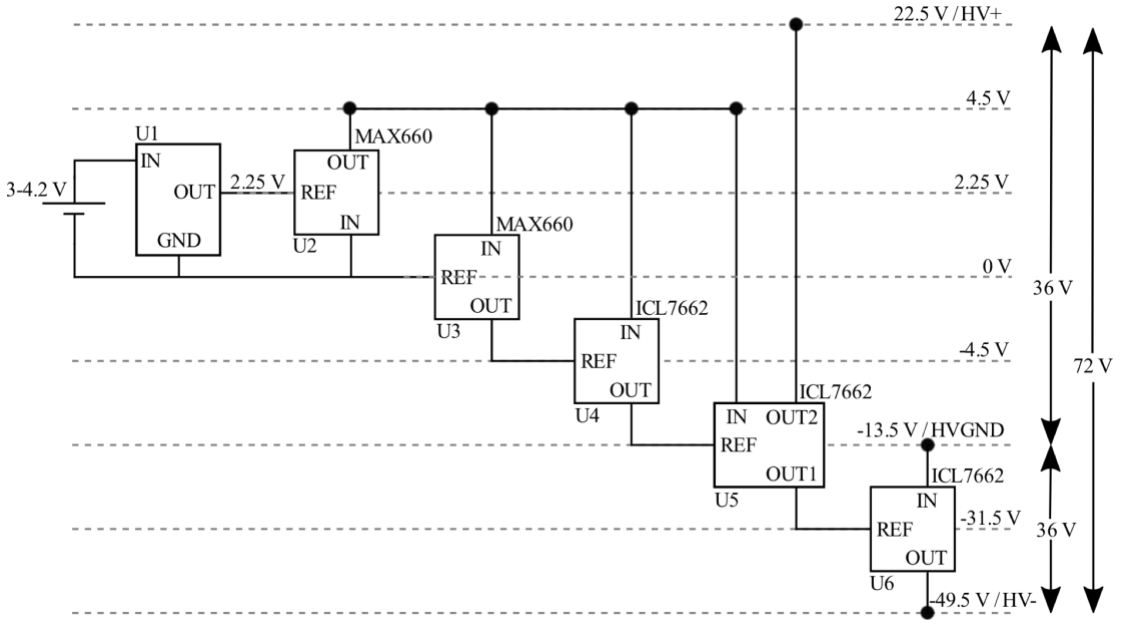

Figure 59. Representative diagram of PSU-4. The battery voltage is bucked to a regulated 2.25 V by U1. U2 then acts as a doubler to produce 4.5 V. U3, U4, U5 and U6 then act as inverters to produce -49.5 V. U5 also acts in its inefficient voltage doubling mode to produce a positive 22.5 V. This architecture is very similar to PSU-6 (Figure 40 or Figure 61) except the initial 4.5 V is generated in a different manner.

B.4.4 PSU-5 and PSU-6

Figure 60 and Figure 61 are representative diagrams of PSU-5 and PSU-6, repeated from Chapter 5 (Figure 32) and Chapter 6 (Figure 40) for convenience. For more detail regarding these designs please refer to the relevant chapters.

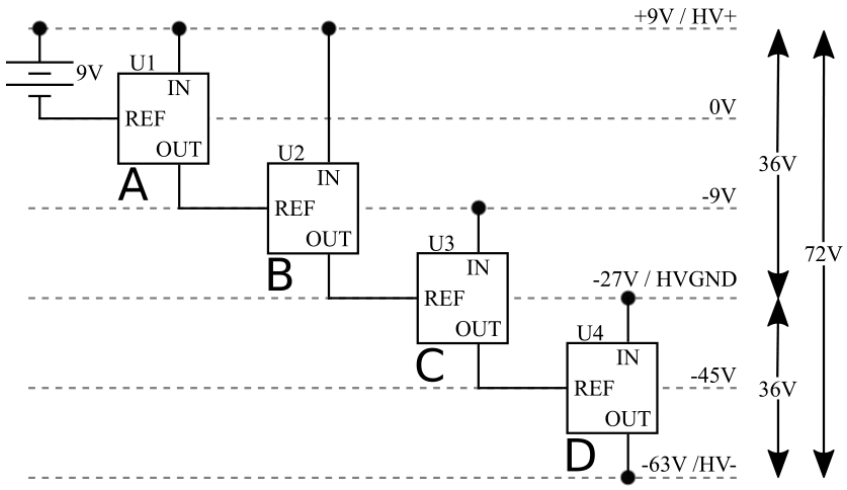

Figure 60. Explanatory diagram of the PSU-5 repeated from Figure 32. Four inverters, U1-U4, convert 9 V from the battery to a 72 V power supply with a midpoint tap at 36 V. Each inverter takes the difference between REF and IN as an input and inverts it below the REF input. The inverters can accept a maximum of 18 V as an input. The labels A, B, C and D correspond to the circuitry blocks with the same labels in Figure 31.

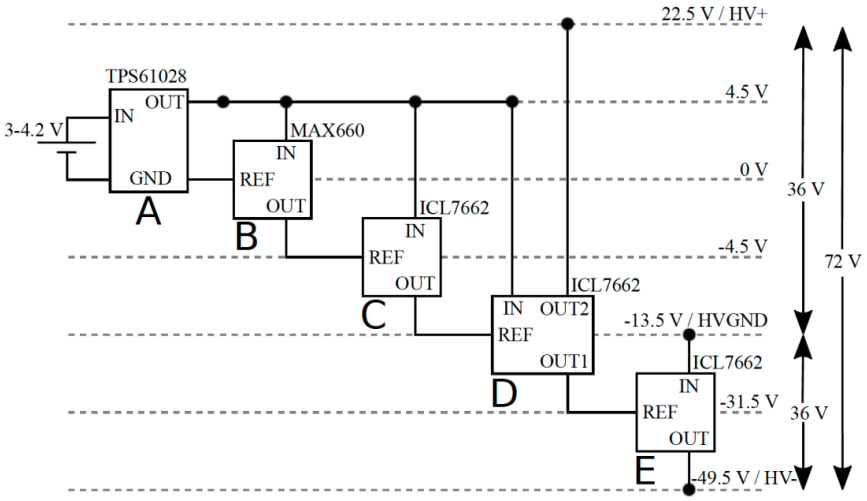

Figure 61. Explanatory diagram of PSU-6, repeated from Figure 40, a high efficiency power supply that regulates a 3 to 4.2 V battery output to +36 V and -36 V supply. The part at "D" uses the ICL7662 in both its doubling mode and inverting mode.

B.5 Simulation results

B.5.1 PSU-1

PSU-1 (Figure 56) seeks to implement the original HVPSU (PSU-5, Figure 32 or Figure 60) with as few changes as possible. Figure 62 shows the simulated efficiency and total voltage output of the two HVPSU designs for different battery voltages, and the range of output currents required by the HVCP. The maximum battery voltage of

9 V is used, as opposed to a more accurate 9.5 V since PSU-5 cannot operate above 9 V as this would exceed the voltage limits of the TC962.

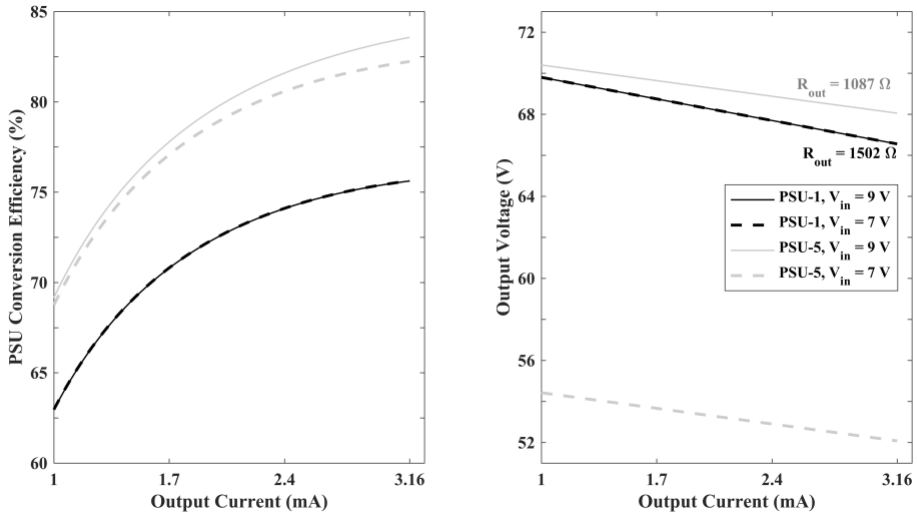

Figure 62. Graphs of the power conversion efficiency (left) and the total output voltage (right) of PSU-1 and PSU-5 for different input voltages and output currents required by the HVCP. The gradient of the voltage drop with current draw indicates the output impedance of the power supply and is indicated on the plot.

The voltage output graph strongly reflects the design flaw of HVPSU-5, showing a large reduction in compliance with falling battery voltage (~54 V output from ~68 V). This loss of compliance is not acceptable. The graphs indicate that the additional regulation in PSU-1 causes reduced efficiency. However, when the current draw is highest, and efficiency is most important, the efficiency is still substantially higher than commercially available solutions (~50% vs ~75%). Further, the additional two parts do not add significant physical bulk. Despite the efficiency loss, this is a feasible option to replace HVPSU-5.

B.5.2 PSU-2 and PSU-3

The purpose of simulating PSU-2 (Figure 57) and PSU-3 (Figure 58) was to investigate a particular principal of the design of this form of HVPSU rather than to find a specific replacement for HVPSU-5. Each uses the same 14 parts and produces the same relative output voltages in theory. The substantial bulk of using this many parts removes either as an option to replace PSU-5, but provides valuable insights into the trade-offs of such design architectures. The simulation indicates several unexpected results (Figure 63).

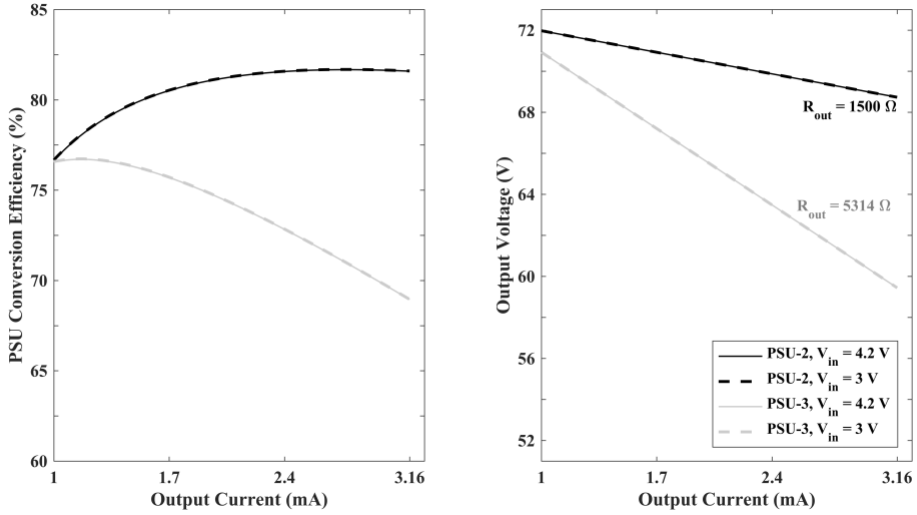

Figure 63. Graphs of the power conversion efficiency (left) and the total output voltage (right) of PSU-2 and PSU-3 for different input voltages and output currents required by the HVCP. The gradient of the voltage drop with current draw indicates the output impedance of the power supply (R_{out}).

Firstly, the detrimental effect of the additional quiescent current of cascading multiple devices is not as large as might be anticipated. Even though PSU-2 has 14 parts, it still attains a superior efficiency and output impedance to PSU-1. The results also indicate that the depth of the cascade has a large effect on the output impedance of the HVPSU. PSU-2 has a depth of only 7 parts, whereas PSU-3 has a depth of 13 parts, which is the cause of the more than three-fold increase in the output impedance of the supply and the subsequent substantial reduction in power conversion efficiency. This effect may be anticipated by the model presented in [159] and Figure 55.

If PSU-2 were not so physically large, its unexpected good performance justifies its use as a replacement for PSU-5. Also worth considering, is the financial cost of including so many inverter parts as a downside of this design. Parts capable of doubling larger voltages, thus reducing the part count in such an architecture, do not double voltages with similar efficiency to the MAX660, which can only operate up to 5.5 V. The principles demonstrated in this simulation, however, do indicate that using at least some voltage doubling is ultimately beneficial in such designs.

B.5.3 PSU-4

PSU-4 (Figure 59) attempts to use what we have learnt about regulated switching converters, (in that parts are more efficient for higher output currents that would occur in the HVPSU at lower voltages), and what we have learnt about the benefit of including

some voltage doubling in the architecture (see B.5.2). We compare in simulation PSU-4, which bucks the battery voltage to create a higher output current from the regulated stage, to PSU-6 (Figure 40) which has the same architecture but boosts the battery voltage (Figure 64).

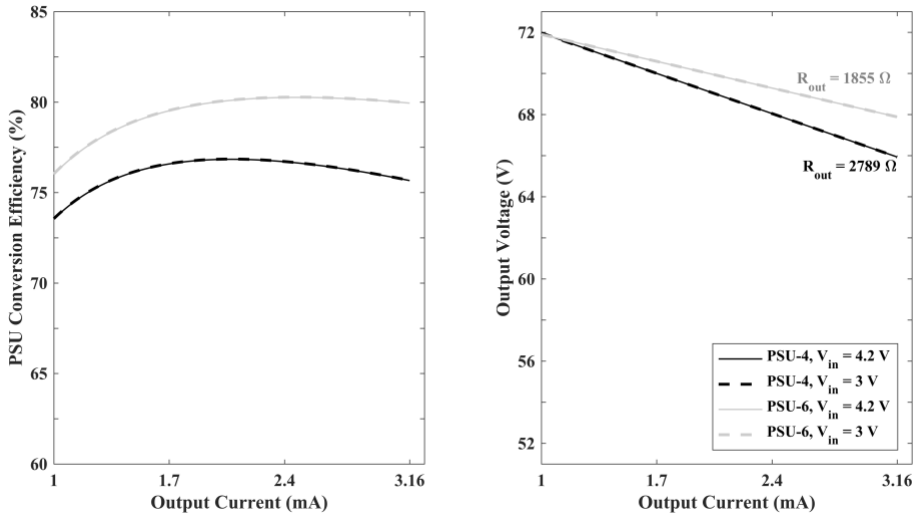

Figure 64. Graphs of the power conversion efficiency (left) and the total output voltage (right) of PSU-4 and PSU-6 for different input voltages and output currents required by the HVCP. The gradient of the voltage drop with current draw indicates the output impedance of the power supply (R_{out}).

Both PSU-4 and PSU-6 perform better than PSU-1 with improved efficiency and similar voltage compliance. The increased output impedance of PSU-4 over PSU-1 and PSU-6 is likely caused by adding the additional boost stage increasing the cascade depth. It is clear that the benefit of increased output current from stepping down the battery voltage is exceeded by the detriment of the additional voltage multiplication subsequently required over using the architecture of PSU-6.

PSU-6 appears to provide the best balance of output compliance, efficiency and physical size and is the best candidate of those examined to replace PSU-5 with an updated HVPSU that is still efficient but insensitive to battery voltage changes.

B.5.4 PSU-5 and PSU-6

Finally, PSU-6 (Figure 40 or Figure 61), the architecture that was selected for implementation in Chapter 6 is compared with the originally implemented HVPSU from Chapter 5 (Figure 32 or Figure 60). The simulated results are compared to actual values measured during testing of the circuits (Figure 65).

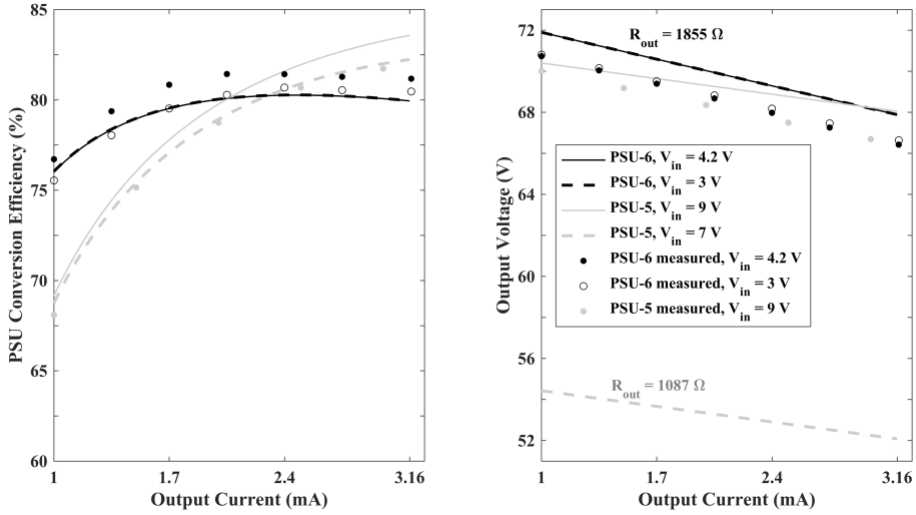

Figure 65. Graphs of the power conversion efficiency (left) and the total output voltage (right) of PSU-5 and PSU-6 for different input voltages and output currents required by the HVCP. The gradient of the voltage drop with current draw indicates the output impedance of the power supply and is indicated on the plot. The measured data of the physically constructed circuits is shown as individual data points.

The collected data follows very similar form and amplitude to the simulations thus validating the use of the tool for this design purpose. The deviations from the expected values can be ascribed to the ranges in possible values for the various parts' output impedance, efficiency and quiescent current. For the simulation only the "typical values" from the datasheet were used unless it provided an indication to adjust this value based on current draw or supply voltage.

PSU-6 has very similar efficiency and compliance to PSU-5. It maintains compliance with changes in the battery voltage whereas PSU-5 tracks the battery voltage proportionally without any regulation stage.

PSU-6 has the added benefit of being powered from a single cell Li-Po battery which has high energy density, is available in many different battery capacities which often include charge and discharge protection circuitry built in. Using a low voltage battery that is near the mid-supply voltage of the HVPSU also allows for a single battery to be used for the HVPSU and the control and instrumentation circuitry (which can be designed to run directly from a Li-Po battery).

B.6 Conclusion

This appendix outlines the design process of a battery powered High Voltage Power Supply (HVPSU) for a wearable current stimulator. Developed simulation software allows various types of power converter chips to be easily connected together in any configuration to examine the interaction of currents and energy losses regardless of the complexity of the design. All simulation software is available in the digital appendix folder "HVPSU simulation code". The software showed good agreement with empirical data from constructed circuits and is thus a useful tool for steady state simulations of this kind.

The simulations led to an improved understanding of these architectures which resulted in the design of an HVPSU that appropriately balances the design constraints. The updated HVPSU is more optimised than the previous version and ultimately sacrifices little in performance and physical size, but has multiple added benefits.

The updated HVPSU is physically small, makes use of high-density battery technology and produces an efficient and regulated output voltage sufficient in amplitude for all current draws required and battery voltages.

APPENDIX C COMMON MODE GAIN CALIBRATION OF HIGH VOLTAGE INSTRUMENTATION CIRCUITRY

The drawback of the self-instrumentation circuitry (see Chapter 6.2.2) is that to achieve the required CMRR the Wheatstone Bridges need to be balanced beyond the accuracy of commercially available resistors. What is required is that the ratio of the equivalents to R1:R2 is the same as R3:R4 regardless of the overall resistance or exact ratio (Figure 66). This must also be the case under AC conditions for reactive impedance. The "output voltage" measuring instrumentation amplifier (INA2 in Figure 43), creates imbalance in addition to the resistor tolerances, since it is connected to only one arm of each bridge. This adds an effective parallel resistance and capacitance that is hard to predict.

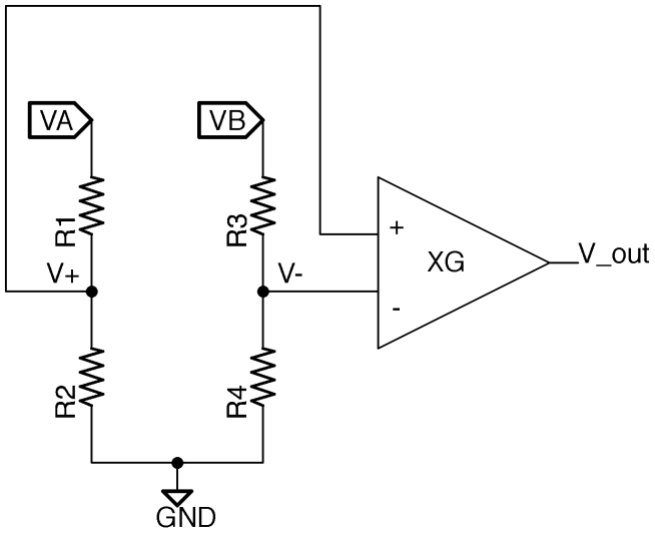

Figure 66. Diagram depicting a general Wheatstone Bridge connected to a difference amplifier with a gain of 'G'. The labels of R1, R2, R3 and R4 here do not correspond to values in other schematics and are used for generic calculations for circuits of this form. VA and VB are the two high voltage input voltages.

The process of balancing the Wheatstone Bridge has two steps: 1) Apply a common signal to both differential inputs, 2) Use the relative amplitudes of the input signal and the erroneous output signal to calculate the magnitude and location of the impedance mismatch. This process should first be conducted for DC mismatch (resistance only) and then for AC mismatch (capacitance only).

The circuit presented in Chapter 6 has jumpers that disconnect one side of each bridge and allows it to be connected to the complimentary bridge terminal, the equivalent of disconnecting VB from its source voltage and connecting it to the VA terminal.

The input signal is now completely common-mode and the desired output is zero. This common mode input voltage is referred to as V_{in}.

The imbalance is always either to the positive (R1/R2) or the negative arm (R3/R4), consequently the bridge can be balanced by adding resistance to R2 or R4 as required, or to R1 or R3. Thinking of it this way means that resistance never needs to be removed to attain balance. Adding to R1 or R3, being large 1 MΩ resistors, is the better choice, as the relative error will be less sensitive to small absolute resistance errors.

The equation for the DC offset resistance to add is derived as follows:

We assume that the imbalance seen is created by an added resistance ΔR to R1. Depending on the sign of V_{out} relative to V_{in}, ΔR may be positive or negative. A negative ΔR is the same as ΔR being added to R3. In either case, once the imbalance's location and magnitude are calculated, it must be added to the complimentary branch of the bridge to attain balance, *i.e.* positive ΔR, you must add to R3, negative ΔR you must add to R1.

Note that by design in our circuit R1 = R3 = 1 MΩ, and will hereinafter be referred to as capital R. Also, that R2 = R4 = 20 kΩ and will hereinafter be referred to as lower-case r. The voltage at the two output terminals is calculated as a standard resistor divider:

$$\boldsymbol{V_+ = V_{in}\left(\frac{r}{R + \Delta R + r}\right)} \quad \textbf{11}$$

$$\boldsymbol{V_- = V_{in}\left(\frac{r}{R + r}\right)} \quad \textbf{12}$$

The output of the difference amplifier is then the difference multiplied by a known gain:

$$\boldsymbol{V_{out} = G(V_+ - V_-)} \quad \textbf{13}$$

Substituting V_+ and V_-:

$$\boldsymbol{V_{out} = G\left(V_{in}\left(\frac{r}{R + \Delta R + r}\right) - V_{in}\left(\frac{r}{R + r}\right)\right)} \quad \textbf{14}$$

And solving for ΔR:

$$\mathbf{\frac{V_{out}}{G.V_{in}.r} + \frac{1}{R + r} = \frac{1}{R + \Delta R + r}} \quad \textbf{15}$$

$$\mathbf{R + \Delta R + r = \frac{G.V_{in}.r(R + r)}{V_{out}(R + r) + G.V_{in}.r}} \quad \textbf{16}$$

$$\mathbf{\Delta R = \frac{G.V_{in}.r.(R + r)}{V_{out}(R + r) + G.V_{in}.r} - (R + r)} \quad \textbf{17}$$

From this the required resistance to be added to the circuit, given a particular combination input values and output values, can be calculated. The know values are: R = 1 MΩ, r = 20 kΩ and G = 24.256 or 77.923 for the high side and low side currents sensing respectively (See Chapter 6). If a known calibration load is used on the current pump output then V_{in} is also known, and V_{out} can be measured with an oscilloscope or the microcontroller.

The most optimal way to balance the bridge is to set the output of the current pump to drive a slow sine wave signal (<10 Hz) at ±1 mA into a large load (≥ 60 kΩ). This creates a large common mode signal (±60 V), without the capacitive imbalance playing a significant role. Using an alternating signal allows us to use the peak to peak amplitude ignoring any zero offset errors.

After inserting the appropriate balancing resistor, which is typically an addition of a few hundred ohms to one of the 1 MΩ resistors, repeat the process and make a second adjustment combining the second calculated value with the first. Two correctly calculated adjustments are usually enough to bring the DC common mode error near to the measured noise amplitude of about 10 mV. This is equivalent of approximately ±0.35% DC common mode error.

Next a capacitor must be added to balance the AC common mode gain. The capacitive mismatch is dominated by the load of INA2's inputs (see Figure 43) on the bridge and is always placed at the same point in the bridge. For the high side current this is over the equivalent of R4 and for the low side current over R2. This is why there is only one option for location of the balancing capacitors, which are placed over the complimentary arms of the bridge (R2 for the high side and R4 for the low side).

To measure V_{out} for the AC mismatch drive a ±1 mA sine wave with a frequency >= 500 Hz into a large load (≥ 60 kΩ).

A similar derivation as above can be performed for Δc placed in parallel to R2 or R4. Here we will derive only for R2, the negative of the result will apply for placement

at R4. Note here that Δc will now be a complex impedance creating a phase offset at the output:

$$V_+ = V_{in}\left(\frac{\frac{r.X_c}{r+X_c}}{R+\frac{r.X_c}{r+X_c}}\right) \quad 18$$

where X_c is the complex impedance of the capacitive imbalance in parallel with R2.

$$X_c = \frac{1}{2\pi f j \Delta c} \quad 19$$

where f is the driving frequency and **j** is the complex unit vector.

$$V_+ = V_{in}\left(\frac{\frac{r}{2\pi f j \Delta c r + 1}}{R+\frac{r}{2\pi f j \Delta c r + 1}}\right) \quad 20$$

$$V_+ = V_{in}\left(\frac{r}{2\pi f j \Delta c r R + R + r}\right) \quad 21$$

$$V_- = V_{in}\left(\frac{r}{R+r}\right) \quad 22$$

$$V_{out} = G\left(V_{in}\left(\frac{r}{2\pi f j \Delta c r R + R + r}\right) - V_{in}\left(\frac{r}{R+r}\right)\right) \quad 23$$

And solving for jΔc:

$$\frac{V_{out}}{\mathrm{G.V_{in}}r} + \frac{1}{\mathrm{R+r}} = \frac{1}{2\pi f j \Delta c r R + R + r} \quad 24$$

$$2\pi f j \Delta c r R + R + r = \frac{\mathrm{G.V_{in}.r(R+r)}}{\mathrm{V_{out}(R+r)+G.V_{in}.r}} \quad 25$$

$$j\Delta c = \frac{\frac{\mathrm{G.V_{in}.r(R+r)}}{\mathrm{V_{out}(R+r)+G.V_{in}.r}} - (R+r)}{2\pi f r R} \quad 26$$

Which contains the same form as for ΔR above.

$$j\Delta c = \frac{\Delta \mathrm{R}}{2\pi \mathrm{f r R}} \quad 27$$

In practice the adjustment with the above result produces a good first approximation, usually in the order of 15 pF, but subsequent trial and error will reduce the imbalance close to the noise amplitude. In general, a helpful rule is that too much capacitance over R2 causes the output to phase lag the input and too little capacitance over R2 causes it to phase lead the output. The converse is true for capacitance over R4.

The discrepancy between the ideal ΔR or Δc and best values in practice, is likely due to the imbalance being caused in part due to resistance mismatch and stray capacitance as modelled, and in part due to leakage current into the difference amplifier, which is not modelled by the above equations.

In summary to perform the calibration for the specific circumstances of the designed stimulator:
Set the output amplitude to ±1 mA.

Attach an artificial output load of 60 kΩ.

To perform the resistive balancing:

Set the output frequency to 10 Hz.

Calculate ΔR or use a look up table and remember that V_{out}'s sign is measured relative to V_{in}:

$$\mathbf{\Delta R = \frac{5.93782 \times 10^7}{1.02V_{out} + 58.214} - 1.02 \times 10^6} \quad \textbf{28}$$

for high side current, or

$$\mathbf{\Delta R = \frac{1.90756 \times 10^8}{1.02V_{out} + 187.015} - 1.02 \times 10^6} \quad \textbf{29}$$

for low side current.

If ΔR is positive then place ΔR in series to the equivalent of R3 in the circuit. If ΔR is negative then place ΔR in series to the equivalent of R1 in the circuit.

Calculate ΔR again. Add the result to the previous result and make the necessary adjustment in the circuit.

To perform the capacitive balancing:

Set the output frequency to 500 Hz.

Calculate Δc or use a lookup table:

$$\Delta c = \frac{\frac{5.93782 \times 10^7}{1.02V_{out} + 58.214} - 1.02 \times 10^6}{6.2832 \times 10^{13}} \quad (30)$$

for high side current, or

$$\Delta c = \frac{\frac{1.90756 \times 10^8}{1.02V_{out} + 187.015} - 1.02 \times 10^6}{6.2832 \times 10^{13}} \quad (31)$$

for low side current.

Place Δc at C29 for high side current and C30 for low side current. Then adjust by trial and error.

If V_{out} is leading V_{in}: increase capacitance and *vice versa*.

While at first glance this process may seem overly complicated, in reality it takes just a few minutes to perform, and the benefits of instrumenting the circuit in this way outlined in Chapter 6 outweigh the detriment of having a circuit requiring physical calibration.

APPENDIX D FORMS

D.1 Participant information form

The details for each participant for the studies in Chapters 2 and 3 were recorded on the below form.

Participant Details UCT WSU SENS study 2016 HREC ref: 838/2015

Participant ID code:_____
First Name: _____

Surname (Family Name): _____

Gender:_____(eg Female, male, other)

Date of birth: DD / MMM / YYYY eg: 18 / SEP / 1984

ID number: _____

Contact number:_____(eg. 082 934 5572)

Email address:_____

HIV Positive: YES ☐ / NO ☐

Today's Date: DD / MMM / YYYY eg: 11 / SEP / 2016

Current Time: HH : MM eg: 14:58

Signed Participant Information Sheet: ☐

Assigned ref number: _____ eg: DK01

Added ID to Master List?: ☐

Added Participant to Database: ☐

Participant shoeless height: _____cm

Participant shoeless weight: _____Kg

Dominant foot: _____Right/Left

Self identified current stimulation threshold:_____(uA rms)

D.2 BPNS and TNSr tool (Page 1)

Revised V3 May 2015
SA BRIEF PERIPHERAL NEUROPATHY SCREENING/EXAM (UCT REC 221/2008)

Patient Number: _____ Date of Visit (DD/MM/YYYY) ____/____/20____

We are going to ask you a few questions about sensation in your legs. We will also briefly examine the nerves in your arms and legs. We may advise the clinic doctor on treatment.

BPNS : INSTRUCTIONS FOR RECORDING SYMPTOMS: *Ask subject to rate the severity of each symptom in 1a to 1c on a scale of 0 (absent) to 10 (most severe) for right and left feet, legs- worst in last week.* Enter the score for each symptom in the block marked Severity. Enter extent of symptoms eg Soles of feet/ toes (TNS=1); up to ankle (TNS=2); up to knee (TNS= 3) or above (TNS=4) on the TNS score overleaf.

1a. Pain, aching, burning in feet or legs. Ingaba iinyawo zakho zibuhlungu, ziyaqagamba, ziyatshisa kangangee-veki ezimbini?

Normal	Mild	→	→	→	→	→	→	→	→	Severe
0	1	2	3	4	5	6	7	8	9	10
Andinantlungu! →			→		→		→	Ndineentlungu ezigqithisileyo!		

Nn1 Score 1a	

1b. "Pins-and-Needles" in feet or legs. Ingaba iinhawo zakho zineenaliti noonotaka kangangee-veki ezimbini?

Normal	Mild	→	→	→	→	→	→	→	→	Severe
0	1	2	3	4	5	6	7	8	9	**10**
Andinantlungu! →			→		→		→	Ndineentlungu ezigqithisileyo!		

Nn2 score 1b	

1c. Numbness (lack of feeling) in feet or legs. Ingaba iinyawo zakho zinobundindisholo kangangee-veki ezimbini?

Abukho ubundindisholo		→	→	→	→	→	→	→	→	Andiva nto
0	1	2	3	4	5	6	7	8	9	**10**

Nn3 Score 1c	

TOTAL SENSORY PRESENCE/SEVERITY SCORE: Obtain the single highest severity score from 1-10 in 1(a - c) above:

0 = Grade 0 1-3 = Grade 1 4- 6 = Grade 2 7-8 = Grade 3 9-10 = Grade 4

Total sensory severity GRADE ____/4 nn4

1e. Do you have any other unpleasant symptoms in you legs such as cramps? Yes (1) No (0) nn6

1f. Has anything helped for the pain (medicine or other) ? _____ Yes (1) No (0) nn7

1i. If you have any of the abovementioned unpleasant symptoms in your feet, when did it start and for how long?
_____ N/A (0) ____ years nn10

2. INSTRUCTIONS FOR EVALUATING PERCEPTION OF VIBRATION:
Press the 2 ends together of a 128 Hz tuning fork, and release suddenly; place the vibrating tuning fork on the subject's clavicle; can they recognise the vibration or "buzzing" (ngcungcazela) of the tuning fork? Repeat and immediately place the vibrating tuning fork firmly on the interphalangeal bone (not nail) of one great toe and begin counting the seconds. Subject to tell you when the "buzzing" stops. Repeat on the other side.

Vibration Perception
(Take highest score but both R & L must be abnormal)

0- Vibration felt for >10 seconds (normal)
1- Vibration felt for 6-10 seconds (mild loss)
2- Vibration felt for 5 seconds or less (moderate loss)
3- No feeling of vibration (severe loss)

	Right	Left	
Great toe interphalangeal bone	___	___	(2) use highest value_____/3 nn11

D.3 BPNS and TNSr tool (Page 2)

Revised V3 May 2015

3. INSTRUCTIONS FOR EVALUATING DEEP TENDON REFLEXES:

With the subject seated, the examiner uses one hand to press upward on the ball of the foot, dorsiflexing the subject's ankle to 90 degrees. Using a reflex hammer (long-handled), the examiner strikes the Achilles tendon.

Reflexes
- 4- Absent
- 3- Reduced (difficult to elicit)
- 2- Normal deep tendon reflexes
- 1- Hyperactive deep tendon reflexes
- 0- Clonus

	Right	Left		
Ankle Reflexes: (Take highest score but both R & L must be abnormal)	_____	_____	(3) use highest value____/4	nn12

Final score for BPNS (1+2+3) ____/11 nn13

Reduced TNS score: tick in the box :

	0	1	2	3	4	
a. Sensory symptoms from 1a,b,c: Pain, burning pins or numbness	*none*	*Only in toes or soles of feet*	*Symptoms extend to ankle or wrist*	*Symptoms extend to knee or elbow*	*Symptoms knee or elbow or functionally disabling*	nn14
b. Pin sensibility	*normal*	*Reduced in fingers /toes*	*Reduced up to wrist/ ankles*	*Reduced up to elbow/ knee*	*Reduced above elbow/ knee*	nn15
c. Vibration sensibility (use normal as for BPNS)	*normal*	*Reduced in fingers /toes*	*Reduced up to wrist/ ankles*	*Reduced up to elbow/ knee*	*Reduced above elbow/ knee*	nn16
d. Deep tendon jerks	normal	Ankle reflexes reduced	Ankle reflexes absent	Ankle reflexes absent, other reduced	All reflexes absent	nn17
e. Strength- ankle and toes plantar & dorsi-flexion	normal	Mild weakness (MRC 4)	Moderate weakness (MRC 3)	Severe weakness (MRC2)	Paralysis (MRC 0-1)	nn18

Final score for rTNS (a+b+c+d+e) _____/20 nn19

Symptomatic DSP: a ≥1 and b≥1 or c≥1 or d≥1 yes 1/ no 0 _____ nn20

Asymptomatic DSP: a =0 yes 1/ no 0 _____ nn21

Proprioception in both toes Normal=0 reduced=1 absent=2 _____ nn25

Additional

f. Number of autonomic symptoms	*none*	*1 symptom*	2 symptoms	3 symptoms	4-5 symptoms	nn26

g. Autonomic symptom impact score	0		nn27

Do you fall easily? yes 1/ no 0 _____ nn28

8 REFERENCES

[1] Karpul D, McIntyre S, van Schaik A, Breen PP, Heckmann JM. Vibrotactile sensitivity of patients with HIV-related sensory neuropathy: An exploratory study. Brain Behav 2018:e01184. doi:10.1002/brb3.1184.

[2] Karpul D, McIntyre S, Heckmann JM, van Schaik A, Breen PP. On the Application of Subsensory Electrical Nerve Stimulation for the Improvement of Vibration Perception in Patients with HIV Related Peripheral Neuropathy. Australas. Neurosci. Soc. Annu. Sci. Meet. 2016 Abstr. Poster Present., 2016, p. 67.

[3] Karpul D, McIntyre S, Van Schaik A, Breen PP. Measurement of perception thresholds for electrical noise stimuli. Proc. Annu. Int. Conf. IEEE Eng. Med. Biol. Soc. EMBS, 2017, p. 2166–9. doi:10.1109/EMBC.2017.8037284.

[4] Karpul D, Cohen GK, Gargiulo GD, van Schaik A, McIntyre S, Breen PP. Low-power transcutaneous current stimulator for wearable applications. Biomed Eng Online 2017;16:118. doi:10.1186/s12938-017-0409-9.

[5] Said G. Diabetic neuropathy--a review. Nat Clin Pract Neurol 2007;3:331–40. doi:10.1038/ncpneuro0504.

[6] Kim JS, Choi-Kwon S. Discriminative sensory dysfunction after unilateral stroke. Stroke 1996;27:677–82. doi:10.1161/01.STR.27.4.677.

[7] Carey LM, Matyas TA. Training of somatosensory discrimination after stroke: facilitation of stimulus generalization. vol. 84. 2005. doi:10.1097/01.PHM.0000159971.12096.7F.

[8] Carey LM, Matyas TA. Frequency of discriminative sensory loss in the hand after stroke in a rehabilitation setting. J Rehabil Med 2011;43:257–63. doi:10.2340/16501977-0662.

[9] Connell L a, Lincoln NB, Radford K a. Somatosensory impairment after stroke: frequency of different deficits and their recovery. Clin Rehabil 2008;22:758–67. doi:10.1177/0269215508090674.

[10] Gescheider GA, Beiles EJ, Checkosky CM, Bolanowski SJ, Verrillo RT. The effects of aging on information-processing channels in the sense of touch: II. Temporal summation in the P channel. Somatosens Mot Res 1994;11:359–65. doi:10.3109/08990229409028879.

[11] Maritz J, Benatar M, Dave JA, Harrison TB, Badri M, Levitt NS, et al. HIV neuropathy in South Africans: Frequency, characteristics, and risk factors. Muscle Nerve 2010;41:599–606. doi:10.1002/mus.21535.

[12] Oyibo SO, Jude EB, Voyatzoglou D, Boulton AJM. Clinical characteristics of patients with diabetic foot problems : changing patterns of foot ulcer presentation. Diabet Foot 2002;19:10–2.

[13] Larsson J, Apelqvist J. Towards less amputations in diabetic patients. Incidence, causes, cost, treatment, and prevention--a review. Acta Orthop Scand 1995;66:181–92. doi:10.3109/17453679508995520.

[14] Menz HB, Morris ME, Lord SR. Foot and ankle characteristics associated with impaired balance and functional ability in older people. J Gerontol A Biol Sci Med Sci 2005;60:1546–52. doi:10.1093/gerona/60.12.1546.

[15] Gravelle DC, Laughton CA, Dhruv NT, Katdare KD, Niemi JB, Lipsitz LA, et al. Noise-enhanced balance control in older adults. Neuroreport 2002;13:1853–6. doi:10.1097/00001756-200210280-00004.

[16] Priplata A a., Niemi JB, Harry JD, Lipsitz L a., Collins JJ. Vibrating insoles and balance control in elderly people. Lancet 2003;362:1123–4. doi:10.1016/S0140-6736(03)14470-4.

[17] Priplata AA, Patritti BL, Niemi JB, Hughes R, Gravelle DC, Lipsitz LA, et al. Noise-enhanced balance control in patients with diabetes and patients with stroke. Ann Neurol 2006;59:4–12. doi:10.1002/ana.20670.

[18] Priplata AA, Niemi JB, Salen M, Harry JD, Lipsitz L a, Collins JJ. Noise-enhanced human balance control. Phys Rev Lett 2002;89:238101. doi:10.1103/PhysRevLett.89.238101.

[19] MacGilchrist C, Paul L, Ellis BM, Howe TE, Kennon B, Godwin J. Lower-limb risk factors for falls in people with diabetes mellitus. Diabet Med 2010;27:162–8. doi:10.1111/j.1464-5491.2009.02914.x.

[20] Hoyert DL, Arias E, Smith BL, Murphy SL, Kochanek KD. Deaths: final data for 1999. Natl Vital Stat Rep 2001;49:1–113.

[21] Collins JJ, Priplata AA, Gravelle DC, Niemi JB, Harry JD, Lipsitz LA. Noise-Enhanced Human Sensorimotor Function. IEEE Eng Med Biol Mag 2003;22:76–83. doi:10.1109/MEMB.2003.1195700.

[22] Pearson KG. Plasticity of neuronal networks in the spinal cord: modifications in response to altered sensory input. Prog Brain Res 2000;128:61–70. doi:10.1016/S0079-6123(00)28007-2.

[23] Edgerton VR, Leon RD, Harkema SJ, Hodgson JA, London N, Reinkensmeyer DJ, et al. Retraining the injured spinal cord. J Physiol 2001;533:15–22.

[24] Perez MA, Field-Fote EC, Floeter MK. Patterned sensory stimulation induces plasticity in reciprocal ia inhibition in humans. J Neurosci 2003;23:2014–8. doi:23/6/2014 [pii].

[25] Enders LR, Jin Seo N. Phalanx force magnitude and trajectory deviation increased during power grip with an increased coefficient of friction at the hand-object interface. J Biomech 2011;44:1447–53. doi:10.1016/j.jbiomech.2011.03.020.

[26] Seo NJ, Shim JK, Engel AK, Enders LR. Grip Surface Affects Maximum Pinch Force. Hum Factors J Hum Factors Ergon Soc 2011;53:740–8. doi:10.1177/0018720811420256.

[27] Hartman-Maeir A, Soroker N, Ring H, Avni N, Katz N. Activities, participation and satisfaction one-year post stroke. Disabil Rehabil 2007;29:559–66. doi:10.1080/09638280600924996.

[28] Carey LM, Matyas TA, Oke LE. Sensory loss in stroke patients: Effective training of tactile and proprioceptive discrimination. Arch Phys Med Rehabil 1993;74:602–11. doi:10.1016/0003-9993(93)90158-7.

[29] Pandya R, Krentz HB, Gill MJ, Power C. HIV-related neurological syndromes reduce health-related quality of life. Can J Neurol Sci 2005;32:201–4. doi:10.1017/S0317167100003978.

[30] Breen PP, ÓLaighin G, McIntosh C, O'Tuathail C, Quinlan LR, Dinneen SF, et al. Peripheral sensory function enhanced in younger and older adults using a novel electrical stimulation based technique. Sect Biomed Sci Annu Meet 2011, Irish J Med Sci 2011;180:294–5. doi:10.1007/s11845-011-0743-z.

[31] Breen PP, ÓLaighin G, McIntosh C, Dinneen SF, Quinlan LR, Serrador JM. A new paradigm of electrical stimulation to enhance sensory neural function. Med Eng Phys 2014;36:1088–91. doi:10.1016/j.medengphy.2014.04.010.

[32] McDougal RA, Morse TM, Carnevale T, Marenco L, Wang R, Migliore M, et al. Twenty years of ModelDB and beyond: building essential modeling tools for the future of neuroscience. J Comput Neurosci 2017;42:1–10. doi:10.1007/s10827-016-0623-7.

[33] Brill MH, Waxman SG, Moore JW, Joyner RW. Conduction velocity and spike configuration in myelinated fibres: computed dependence on internode distance. J Neurol Neurosurg Psychiatry 1977;40:769–74. doi:10.1136/jnnp.40.8.769.

[34] Moore JW, Joyner RW, Brill MH, Waxman SD, Najar-Joa M. Simulations of conduction in uniform myelinated fibers. Relative sensitivity to changes in nodal and internodal parameters. Biophys J 1978;21:147–60. doi:10.1016/S0006-3495(78)85515-5.

[35] Mulavara AP, Fiedler MJ, Kofman IS, Wood SJ, Serrador JM, Peters B, et al. Improving balance function using vestibular stochastic resonance: Optimizing stimulus characteristics. Exp Brain Res 2011;210:303–12. doi:10.1007/s00221-011-2633-z.

[36] Goel R, Kofman I, Jeevarajan J, De Dios Y, Cohen HS, Bloomberg JJ, et al. Using low levels of stochastic vestibular stimulation to improve balance function. PLoS One 2015;10:1–24. doi:10.1371/journal.pone.0136335.

[37] Mulavara AP, Kofman IS, De Dios YE, Miller C, Peters BT, Goel R, et al. Using low levels of stochastic vestibular stimulation to improve locomotor stability. Front Syst Neurosci 2015;9:1–14. doi:10.3389/fnsys.2015.00117.

[38] Zeng F-G, Fu Q-J, Morse R. Human hearing by noise. Brain Res 2000;869:251–5.

[39] Ward L, Desai S, Rootman D, Tata M, Moss F. Noise can help as well as hinder seeing and hearing. Bull Am Phys Soc 2001.

[40] Piana M, Canfora M, Riani M. Role of noise in image processing by the human perceptive system. Phys Rev E - Stat Physics, Plasmas, Fluids, Relat Interdiscip Top 2000;62:1104–9. doi:10.1103/PhysRevE.62.1104.

[41] Kitajo K, Nozaki D, Ward LM, Yamamoto Y. Behavioral stochastic resonance within the human brain. Phys Rev Lett 2003;90:218103. doi:10.1103/PhysRevLett.90.218103.

[42] Simonotto E, Riani M, Seife C, Roberts M, Twitty J, Moss F. Visual Perception of Stochastic Resonance. Phys Rev Lett 1997;78:1186–9. doi:10.1103/PhysRevLett.78.1186.

[43] Hidaka I, Nozaki D, Yamamoto Y. Functional stochastic resonance in the human brain: noise induced sensitization of baroreflex system. Phys Rev Lett 2000;85:3740–3. doi:10.1103/PhysRevLett.85.3740.

[44] Carroll D, Moore RA, McQuay HJ, Fairman F, Tramèr M, Leijon G. Transcutaneous electrical nerve stimulation (TENS) for chronic pain. Cochrane Database Syst Rev 2001. doi:10.1002/14651858.CD003222.

[45] Weiss T, Sens E, Teschner U, Meissner W, Preul C, Witte OW, et al. Deafferentation of the affected arm: A method to improve rehabilitation? Stroke 2011;42:1363–70. doi:10.1161/STROKEAHA.110.601138.

[46] Sens E, Teschner U, Meissner W, Preul C, Huonker R, Witte OW, et al. Effects of Temporary Functional Deafferentation on the Brain, Sensation, and Behavior of Stroke Patients. J Neurosci 2012;32:11773–9. doi:10.1523/JNEUROSCI.5912-11.2012.

[47] Collins JJ, Inglis TJ, Grigg P. Noise-enhanced tactile sensation. Nature 1996;383:770.

[48] Collins JJ, Imhoff TT, Grigg P. Noise-mediated enhancements and decrements in human tactile sensation. Phys Rev E 1997;56:923–6. doi:10.1103/PhysRevE.56.923.

[49] Cordo P, Inglis TJ, Verschueren S, Collins JJ, Merfeld DM, Rosenblum S, et al. Noise in human muscle spindles. Nature 1996;383:769–70.

[50] Hamer RD, Verrillo RT, Zwislocki JJ. Vibrotacile masking of Pacinian and non-Pacinian channels. J Acoust Soc Am 1983;73:1293–303. doi:10.1121/1.389278.

[51] Gescheider GA, Verrillo RT, Pelli DG. Effects of noise on detection of amplitude increments of sinusoidal vibration of the skin. J Acoust Soc Am 1992;91:348–53. doi:10.1121/1.402777.

[52] Verrillo RT, Gescheider GA, Calman BG, Van Doren CL. Vibrotactile masking: Effects of oneand two-site stimulation. Percept Psychophys 1983;33:379–87. doi:10.3758/BF03205886.

[53] Moss F, Ward LM, Sannita WG. Stochastic resonance and sensory information processing: a tutorial and review of application. Clin Neurophysiol 2004;115:267–81. doi:10.1016/j.clinph.2003.09.014.

[54] McDonnell MD, Abbott D. What is stochastic resonance? Definitions, misconceptions, debates, and its relevance to biology. PLoS Comput Biol 2009;5. doi:10.1371/journal.pcbi.1000348.

[55] McDonnell MD, Ward LM. The benefits of noise in neural systems: bridging theory and experiment. Nat Rev Neurosci 2011;12:415–26. doi:10.1038/nrn3061.

[56] Hoskins R, Wang J, Cao CGL. Use of stochastic resonance methods for improving laparoscopic surgery performance. Surg Endosc Other Interv Tech 2015:1–6. doi:10.1007/s00464-015-4730-8.

[57] Ross SE, Guskiewicz KM. Effect of Coordination Training With and Without Stochastic Resonance Stimulation on Dynamic Postural Stability of Subjects With Functional Ankle Instability and Subjects With Stable Ankles. Clin J Sport Med 2006;16:323–8. doi:10.1097/00042752-200607000-00007.

[58] Ross SE, Arnold BL, Blackburn JT, Brown CN, Guskiewicz KM. Enhanced balance associated with coordination training with stochastic resonance stimulation in subjects with functional ankle instability: An experimental trial. J Neuroeng Rehabil 2007;4:1–8. doi:10.1186/1743-0003-4-47.

[59] Collins AT, Blackburn JT, Olcott CW, Jordan JM, Yu B, Weinhold PS. The Assessment of Postural Control With Stochastic Resonance Electrical Stimulation and a Neoprene Knee Sleeve in the Osteoarthritic Knee. Arch Phys Med Rehabil 2012;93:1123–8. doi:10.1016/j.apmr.2011.12.006.

[60] Collins A, Blackburn JT, Olcott C, Yu B, Weinhold P. Clinical Biomechanics The impact of stochastic resonance electrical stimulation and knee sleeve on impulsive loading and muscle co-contraction during gait in knee osteoarthritis. JCLB 2011;26:853–8. doi:10.1016/j.clinbiomech.2011.04.011.

[61] Collins AT, Blackburn JT, Olcott CW, Miles J, Jordan J, Dirschl DR, et al. Stochastic resonance electrical stimulation to improve proprioception in knee osteoarthritis. Knee 2011;18:317–22. doi:10.1016/j.knee.2010.07.001.

[62] Collins A, Blackburn T, Olcott C, Jordan JM, Yu B, Weinhold P. A kinetic and kinematic analysis of the effect of stochastic resonance electrical stimulation and knee sleeve during gait in osteoarthritis of the knee. J Appl Biomech 2014;30:104–12. doi:10.1123/jab.2012-0257.

[63] Richardson KA, Imhoff TT, Grigg P, Collins JJ. Using electrical noise to enhance the ability of humans to detect subthreshold mechanical cutaneous stimuli. Chaos 1998;8:599–603. doi:10.1063/1.166341.

[64] Dhruv NT, Niemi JB, Harry JD, Lipsitz LA, Collins JJ. Enhancing tactile sensation in older adults with electrical noise stimulation. Neuroreport 2002;13:597–600. doi:10.1097/00001756-200204160-00012.

[65] Liu W, Lipsitz L a., Montero-Odasso M, Bean J, Kerrigan DC, Collins JJ. Noise-enhanced vibrotactile sensitivity in older adults, patients with stroke, and patients with diabetic neuropathy. Arch Phys Med Rehabil 2002;83:171–6. doi:10.1053/apmr.2002.28025.

[66] Khaodhiar L, Niemi JB, Earnest R, Lima C, Harry JD, Veves A. Enhancing Sensation in Diabetic Neuropathic Foot with Mechanical Noise. Diabetes Care 2003;26:3280–3. doi:10.2337/diacare.26.12.3280.

[67] Wells C, Ward LM, Chua R, Inglis TJ. Touch noise increases vibrotactile sensitivity in old and young. Psychol Sci 2005;16:313–20. doi:10.1111/j.0956-7976.2005.01533.x.

[68] Lee M-Y, Lin CF, Soon KS. New foot pressure activated sensory compensation posture-control enhancement in amputee. 2008 IEEE Int. Conf. Syst. Man Cybern., vol. 12, IEEE; 2007, p. 236–43. doi:10.1109/ICSMC.2008.4811682.

[69] Ross SE. Noise-enhanced postural stability in subjects with functional ankle instability. Br J Sports Med 2007;41:656–9. doi:10.1136/bjsm.2006.032912.

[70] Hijmans JM, Geertzen JHB, Zijlstra W, Hof AL, Postema K. Effects of vibrating insoles on standing balance in diabetic neuropathy. J Rehabil Res Dev 2008;45:1441–9. doi:10.1682/2008.02.0023.

[71] Collins AT, Blackburn JT, Olcott CW, Dirschl DR, Weinhold PS. The effects of stochastic resonance electrical stimulation and neoprene sleeve on knee proprioception. J Orthop Surg Res 2009;4:3. doi:10.1186/1749-799X-4-3.

[72] Galica AM, Kang HG, Priplata AA, D'Andrea SE, Starobinets O V., Sorond FA, et al. Subsensory vibrations to the feet reduce gait variability in elderly fallers. Gait Posture 2009;30:383–7. doi:10.1016/j.gaitpost.2009.07.005.

[73] Magalhães FH, Kohn AF. Imperceptible electrical noise attenuates isometric plantar flexion force fluctuations with correlated reductions in postural sway. Exp Brain Res 2012;217:175–86. doi:10.1007/s00221-011-2983-6.

[74] Kurita Y, Sueda Y, Tsuji T, Hattori M, Tokunaga M, Egi H, et al. Improvment of Tactile Sensitivity by Stochastic Resonance: Application to Vibrating Forceps. ASME 2012 5th Annu. Dyn. Syst. Control Conf. Jt. with JSME 2012 11th Motion Vib. Conf., 2012, p. 1–5. doi:DSCC2012-MOVIC2012-8811.

[75] Breen PP, Macefield VG. Proximally applied subsensory electrical noise stimulation reduces variance in action potential timing and enhances sensory perception. 2013 6th Int. IEEE/EMBS Conf. Neural Eng., IEEE; 2013, p. 267–70. doi:10.1109/NER.2013.6695923.

[76] Enders LR, Hur P, Johnson MJ, Seo NJ. Remote vibrotactile noise improves light touch sensation in stroke survivors' fingertips via stochastic resonance. J Neuroeng Rehabil 2013;10:105. doi:10.1186/1743-0003-10-105.

[77] Ross SE, Linens SW, Wright CJ, Arnold BL. Customized Noise-Stimulation Intensity for Bipedal Stability and Unipedal Balance Deficits Associated With Functional Ankle Instability. J Athl Train 2013;48:463–70. doi:10.4085/1062-6050-48.3.12.

[78] Sueda Y, Hattori M, Sawada H, Egi H, Ohdan H, Ueda J, et al. Improvement of tactile sensitivity by stochastic resonance effect - Applications to surgical grasping forceps -. 35th Annu. Int. Conf. IEEE EMBS Osaka, Japan, 3 - 7 July, 2013, 2013, p. 4601–4.

[79] Kurita Y, Shinohara M, Ueda J. Wearable Sensorimotor Enhancer for Fingertip Based on Stochastic Resonance Effect. IEEE Trans Human-Machine Syst 2013;43:333–7. doi:10.1109/TSMC.2013.2242886.

[80] Kurita Y, Shinohara M, Ueda J. Wearable sensorimotor enhancer for a fingertip based on stochastic resonance. 2011 IEEE Int. Conf. Robot. Autom., IEEE; 2011, p. 3790–5. doi:10.1109/ICRA.2011.5980283.

[81] Ribot-Ciscar E, Hospod V, Aimonetti J-M. Noise-enhanced kinaesthesia: a psychophysical and microneurographic study. Exp Brain Res 2013;228:503–11. doi:10.1007/s00221-013-3581-6.

[82] Hur P, Wan YH, Seo NJ. Investigating the role of vibrotactile noise in early response to perturbation. IEEE Trans Biomed Eng 2014;61:1628–33. doi:10.1109/TBME.2013.2294672.

[83] Iliopoulos F, Nierhaus T, Villringer A. Electrical noise modulates perception of electrical pulses in humans : sensation enhancement via stochastic resonance 2014:1238–48. doi:10.1152/jn.00392.2013.

[84] Magalhães FH, Kohn AF. Effectiveness of electrical noise in reducing postural sway: a comparison between imperceptible stimulation applied to the anterior and to the posterior leg muscles. Eur J Appl Physiol 2014;114:1129–41. doi:10.1007/s00421-014-2846-5.

[85] Seo NJ, Kosmopoulos ML, Enders LR, Hur P. Effect of Remote Sensory Noise on Hand Function Post Stroke. Front Hum Neurosci 2014;8:1–9. doi:10.3389/fnhum.2014.00934.

[86] Keshner EA, Slaboda JC, Day L, Darvish K. Visual conflict and cognitive load modify postural responses to vibrotactile noise. J Neuroeng Rehabil 2014;11:6. doi:10.1186/1743-0003-11-6.

[87] Lakshminarayanan K, Lauer AW, Ramakrishnan V, Webster JG, Seo NJ. Application of vibration to wrist and hand skin affects fingertip tactile sensation. Physiol Rep 2015;3:e12465. doi:10.14814/phy2.12465.

[88] Lipsitz LA, Lough M, Niemi J, Travison T, Howlett H, Manor B. A shoe insole delivering subsensory vibratory noise improves balance and gait in healthy elderly people. Arch Phys Med Rehabil 2015;96:432–9. doi:10.1016/j.apmr.2014.10.004.

[89] Ross SE, Linens SW, Wright CJ, Arnold BL. Noise-Enhanced Eversion Force Sense in Ankles With or Without Functional Instability. J Athl Train 2015;50:819–24. doi:10.4085/1062-6050-50.5.06.

[90] Dettmer M, Pourmoghaddam A, Lee B-C, Layne CS. Effects of aging and tactile stochastic resonance on postural performance and postural control in a sensory conflict task. Somat Mot Res 2015:1–8. doi:10.3109/08990220.2015.1004045.

[91] Wang F, Lakshminarayanan K, Slota GP, Seo NJ, Webster JG. An MRI-compatible hand sensory vibrotactile system. Physiol Meas 2015;36:N15-21. doi:10.1088/0967-3334/36/1/N15.

[92] Breen PP, Serrador JM, O'Tuathail C, Quinlan LR, McIntosh C, ÓLaighin G. Peripheral tactile sensory perception of older adults improved using subsensory electrical noise stimulation. Med Eng Phys 2016;38:822–5. doi:10.1016/j.medengphy.2016.05.015.

[93] Serrador J, OLaighin G, McIntosh C, OTuathail C, Quinlan LR, Dinneen SF, et al. Peripheral Sensory Function Enhanced Using Stochastic Noise Stimulation. FASEB J 2012;26:865.15-.

[94] Mendez-Balbuena I, Manjarrez E, Schulte-Monting J, Huethe F, Tapia JA, Hepp-Reymond M-C, et al. Improved Sensorimotor Performance via Stochastic Resonance. J Neurosci 2012;32:12612–8. doi:10.1523/JNEUROSCI.0680-12.2012.

[95] Review Manager (RevMan) [Computer program]. Version 5.3. Copenhagen: The Nordic Cochrane Centre, The Cochrane Collaboration 2014.

[96] Hirji KF, Fagerland MW. Calculating unreported confidence intervals for paired data. BMC Med Res Methodol 2011;11:66. doi:10.1186/1471-2288-11-66.

[97] Galica AM, Kang HG, Priplata A a., D'Andrea SE, Starobinets O V., Sorond F a., et al. Subsensory vibrations to the feet reduce gait variability in elderly fallers. Gait Posture 2009;30:383–7. doi:10.1016/j.gaitpost.2009.07.005.

[98] Seo NJ, Lakshminarayanan K, Bonilha L, Lauer AW, Schmit BD. Effect of imperceptible vibratory noise applied to wrist skin on fingertip touch evoked potentials – an EEG study. Physiol Rep 2015;3:e12624. doi:10.14814/phy2.12624.

[99] Manjarrez E, Rojas-Piloni G, Méndez I, Flores A. Stochastic resonance within the somatosensory system: effects of noise on evoked field potentials elicited by tactile stimuli. J Neurosci 2003;23:1997–2001.

[100] Magalhães FH, Kohn AF. Vibratory noise to the fingertip enhances balance improvement associated with light touch. Exp Brain Res 2011;209:139–51. doi:10.1007/s00221-010-2529-3.

[101] Kimura T, Kouzaki M, Masani K, Moritani T. Unperceivable noise to active light touch effects on fast postural sway. Neurosci Lett 2011;506:100–3. doi:10.1016/j.neulet.2011.10.058.

[102] Lugo E, Doti R, Faubert J. Ubiquitous Crossmodal Stochastic Resonance in Humans: Auditory Noise Facilitates Tactile, Visual and Proprioceptive Sensations. PLoS One 2008;3:e2860. doi:10.1371/journal.pone.0002860.

[103] Méndez-Balbuena I, Huidobro N, Silva M, Flores A, Trenado C, Quintanar L, et al. Effect of mechanical tactile noise on amplitude of visual evoked potentials: multisensory stochastic resonance. J Neurophysiol 2015;114:2132–43. doi:10.1152/jn.00457.2015.

[104] Trenado C, Mikulić A, Manjarrez E, Mendez-Balbuena I, Schulte-Mönting J, Huethe F, et al. Broad-band Gaussian noise is most effective in improving motor performance and is most pleasant. Front Hum Neurosci 2014;8:1–9. doi:10.3389/fnhum.2014.00022.

[105] Trenado C, Mendez-Balbuena I, Manjarrez E, Huethe F, Schulte-Mönting J, Feige B, et al. Enhanced corticomuscular coherence by external stochastic noise. Front Hum Neurosci 2014;8:325. doi:10.3389/fnhum.2014.00325.

[106] Hijmans JM, Geertzen JHB, Schokker B, Postema K. Development of vibrating insoles. Int J Rehabil Res 2007;30:343–5. doi:10.1097/MRR.0b013e3282f14469.

[107] UNAIDS World AIDS Day Report 2012. doi:QH 11.0408.

[108] Centner CM, Bateman KJ, Heckmann JM. Manifestations of HIV infection in the peripheral nervous system. Lancet Neurol 2013;12:295–309. doi:10.1016/S1474-4422(13)70002-4.

[109] Centner CM, Little F, Van Der Watt JJ, Vermaak J-R, Dave JA, Levitt NS, et al. Evolution of sensory neuropathy after initiation of antiretroviral therapy. Muscle Nerve 2018;57:371–9. doi:10.1002/mus.25710.

[110] Borkum MS, Heckmann JM, Manning K, Dave JA, Levitt NS, Rayner BL, et al. High prevalence of "non-dipping" blood pressure and vascular stiffness in HIV-infected South Africans on antiretrovirals. PLoS One 2017;12. doi:10.1371/journal.pone.0185003.

[111] Cherry CL, Wesselingh SL, Lal L, McArthur JC. Evaluation of a clinical screening tool for HIV-associated sensory neuropathies. Neurology 2005;65:1778–81. doi:10.1212/01.wnl.0000187119.33075.41.

[112] Malhotra R, Hoyo C, Østbye T, Hughes G, Schwartz D, Tsolekile L, et al. Determinants of obesity in an urban township of South Africa. South African J Clin Nutr 2008;21:315–20. doi:10.1080/16070658.2008.11734173.

[113] Tang AM, Forrester J, Spiegelman D, Knox TA, Tchetgen E, Gorbach SL. Weight Loss and Survival in HIV-Positive Patients in the Era of Highly Active Antiretroviral Therapy. JAIDS J Acquir Immune Defic Syndr 2002;31:230–6. doi:10.1097/00126334-200210010-00014.

[114] Phillips TJC, Brown M, Ramirez JD, Perkins J, Woldeamanuel YW, Williams ACDC, et al.

Sensory , psychological , and metabolic dysfunction in HIV-associated peripheral neuropathy : A cross-sectional deep profiling study. Pain 2014;155:1846–60. doi:10.1016/j.pain.2014.06.014.

[115] Simpson DM, Kitch D, Evans SR. HIV neuropathy natural history cohort study : Assessment measures and risk factors 2006. doi:10.1212/01.wnl.0000218303.48113.5d.

[116] Talbot WH, Darian-Smith I, Kornhuber HH, Mountcastle VB. The sense of flutter-vibration: comparison of the human capacity with response patterns of mechanoreceptive afferents from the monkey hand. J Neurophysiol 1968;31:301–34.

[117] Mold JW, Vesely SK, Keyl B a, Schenk JB, Roberts M. The prevalence, predictors, and consequences of peripheral sensory neuropathy in older patients. J Am Board Fam Pract 2004;17:309–18. doi:10.3122/jabfm.17.5.309.

[118] Deshpande N, Metter EJ, Ling S, Conwit R, Ferrucci L. Physiological correlates of age-related decline in vibrotactile sensitivity. Neurobiol Aging 2008;29:765–73. doi:10.1016/j.neurobiolaging.2006.12.002.

[119] Boles DB, Givens SM. Laterality and sex differences in tactile detection and two-point thresholds modified by body surface area and body fat ratio. Somatosens Mot Res 2011;28:102–9. doi:10.3109/08990220.2011.627068.

[120] Yümin ET, Şimşek TT, Sertel M, Ankaralı H. The effect of age and body mass index on plantar cutaneous sensation in healthy women. J Phys Ther Sci 2016;28:2587–95. doi:10.1589/jpts.28.2587.

[121] Shy ME, Frohman EM, So YT, Arezzo JC, Cornblath DR, Giuliani MJ, et al. Quantitative sensory testing: Report of the Therapeutics and Technology Assessment Subcommittee of the American Academy of Neurology. Neurology 2003;60:898–904. doi:10.1212/01.WNL.0000058546.16985.11.

[122] Pourhamidi K, Dahlin LB, Englund E, Rolandsson O. Evaluation of clinical tools and their diagnostic use in distal symmetric polyneuropathy. Prim Care Diabetes 2014;8:77–84. doi:10.1016/j.pcd.2013.04.004.

[123] Alanazy MH, Alfurayh NA, Almweisheer SN, Aljafen BN, Muayqil T. The conventional tuning fork as a quantitative tool for vibration threshold. Muscle Nerve 2018;57:49–53. doi:10.1002/mus.25680.

[124] Baron R, Binder A, Wasner G. Neuropathic pain: Diagnosis, pathophysiological mechanisms, and treatment. Lancet Neurol 2010;9:807–19. doi:10.1016/S1474-4422(10)70143-5.

[125] Ørstavik K, Namer B, Schmidt R, Schmelz M, Hilliges M, Weidner C, et al. Abnormal function of C-fibers in patients with diabetic neuropathy. J Neurosci 2006;26:11287–94. doi:10.1523/JNEUROSCI.2659-06.2006.

[126] Ørstavik K, Jørum E. Microneurographic findings of relevance to pain in patients with erythromelalgia and patients with diabetic neuropathy. Neurosci Lett 2010;470:180–4. doi:10.1016/j.neulet.2009.05.061.

[127] Ørstavik K, Weidner C, Schmidt R, Schmelz M, Hilliges M, Jørum E, et al. Pathological C-fibres in patients with a chronic painful condition. Brain 2003;126:567–78. doi:10.1093/brain/awg060.

[128] Moss F, Pierson D, O'Gorman D. Stochastic resonance: tutorial and update. Int J Bifurc Chaos 1994;04:1383–97. doi:10.1142/S0218127494001118.

[129] Benzi R, Sutera A, Vulpiani A. The mechanism of stochastic resonance. J Phys A Math Gen 1999;14:L453–7. doi:10.1088/0305-4470/14/11/006.

[130] Lai S, Ahmed U, Bollineni A, Lewis R, City K, Angeles L, et al. Diagnostic Accuracy of Qualitative vs. Quantitative Tuning Forks: Outcome Measure for Neuropathy. J Clin Neuromuscul Dis 2016;15:96–101. doi:10.1097.0000000000000019.

[131] Pavlik a E, Inglis JT, Lauk M, Oddsson L, Collins JJ. The effects of stochastic galvanic vestibular stimulation on human postural sway. Exp Brain Res 1999;124:273–80.

[132] Brockwell PJ DR. Time series: theory and methods. Springer, Berlin Heidelberg New York. Springer, Berlin Heidelberg New York; 1991.

[133] Yarnitsky D. Quantitative sensory testing. Muscle Nerve 1997;20:198–204.

[134] Karpul D, McIntyre S, van Schaik A, Breen PP. Measurement of Perception Thresholds for Electrical Noise Stimuli. Embc17 2017:2166–9.

[135] Barnard GA. Discussion of paper by M. S. Bartlett. J R Stat Soc n.d.;B 25:294.

[136] Besag J, Clifford P. Sequential Monte Carlo p-values. Biometrika 1991;78:301–4. doi:https://doi.org/10.1093/biomet/78.2.301.

[137] Turner R, Jeffs C. An extension of Monte Carlo hypothesis tests. Commun Stat - Simul Comput 2017;46:6545–58. doi:10.1080/03610918.2016.1208232.

[138] Rosell J, Colominas J, Riu P, Pallas-Areny R, Webster JG. Skin impedance from 1 Hz to 1 MHz. IEEE Trans Biomed Eng 1988;35:649–51. doi:10.1109/10.4599.

[139] Bîrlea SI, Breen PP, Corley GJ, Bîrlea NM, Quondamatteo F, ÓLaighin G. Changes in the electrical properties of the electrode-skin-underlying tissue composite during a week-long programme of neuromuscular electrical stimulation. Physiol Meas 2014;35:231–52. doi:10.1088/0967-3334/35/2/231.

[140] McAdams ET, Jossinet J, Lackermeier A, Risacher F. Factors affecting electrode-gel-skin interface impedance in electrical impedance tomography. Med Biol Eng Comput 1996;34:397–408. doi:10.1007/BF02523842.

[141] Watson AB, Pelli DG. QUEST: a Bayesian adaptive psychometric method. Percept Psychophys 1983;33:113–20. doi:10.3758/BF03202828.

[142] Sims JA, Pelli D. The ideal psychometric procedure. Investig Ophthalmol Vis Sci 1987;28:366.

[143] King-Smith PE, Grigsby SS, Vingrys AJ, Benes SC, Supowit A. Efficient and unbiased modifications of the QUEST threshold method: Theory, simulations, experimental evaluation and practical implementation. Vision Res 1994;34:885–912. doi:10.1016/0042-6989(94)90039-6.

[144] Brainard DH. The psychophysics toolbox. Spat Vis 1997;20:433–6.

[145] Schabrun S, Hillier S. Evidence for the retraining of sensation after stroke: a systematic review. Clin Rehabil 2009;23:27–39. doi:10.1177/0269215508098897.

[146] Wang H-P, Guo A-W, Zhou Y-X, Xia Y, Huang J, Xu C-Y, et al. A wireless wearable surface functional electrical stimulator. Int J Electron 2017;104:1514–26. doi:10.1080/00207217.2017.1312708.

[147] Farahmand S, Vahedian H, Abedinkhan Eslami M, Sodagar AM. Wearable, battery-powered, wireless, programmable 8-channel neural stimulator. Proc Annu Int Conf IEEE Eng Med Biol Soc EMBS 2012:6120–3. doi:10.1109/EMBC.2012.6347390.

[148] Jovičić NS, Saranovac L V, Popović DB. Wireless distributed functional electrical stimulation system. J Neuroeng Rehabil 2012;9:54. doi:10.1186/1743-0003-9-54.

[149] Pease RA. AN-1515 A Comprehensive Study of the Howland Current Pump. Texas Instruments 2013:1–17.

[150] King G, Watkins T. Bootstrapping your op amp yields wide voltage swings. Edn 1999;44:117–29.

[151] Caldwell J. A High-Voltage Bidirectional Current Source. Texas Instruments n.d.

[152] Yamamoto Y, Struzik ZR, Soma R, Ohashi K, Kwak S. Noisy vestibular stimulation improves autonomic and motor responsiveness in central neurodegenerative disorders. Ann Neurol 2005;58:175–81. doi:10.1002/ana.20574.

[153] Iwasaki S, Yamamoto Y, Togo F, Kinoshita M, Yoshifuji Y, Fujimoto C, et al. Noisy vestibular stimulation improves body balance in bilateral vestibulopathy. Neurology 2014;82:969–75. doi:10.1212/WNL.0000000000000215.

[154] Fujimoto C, Yamamoto Y, Kamogashira T, Kinoshita M, Egami N, Uemura Y, et al. Noisy galvanic vestibular stimulation induces a sustained improvement in body balance in elderly adults. Sci Rep 2016;6:37575. doi:10.1038/srep37575.

[155] Econoline DC/DC converter datasheet n.d. https://www.recom-power.com/pdf/Econoline/R1S_R1D.pdf (accessed June 20, 2018).

[156] Kylinchip XL6009 datasheet n.d. http://www.haoyuelectronics.com/Attachment/XL6009/XL6009-DC-DC-Converter-Datasheet.pdf (accessed June 20, 2018).

[157] Nagel LW. SPICE2: A Computer Program To Simulate Semiconductor Circuits. PhD Diss Univ California, Berkeley, CA, Available as Memo No ERL-M520, Electron Res Lab Coll Eng Univ California, Berkeley, CA 1975:431.

[158] Nagel LW, Pederson DO. Simulation Program with Integrated Circuit Emphasis (SPICE). 16th Midwest Symp. Circuit Theory, Ontario, Canada, 1973.

[159] Intersil. Principles and Applications of the ICL7660 CMOS Voltage Converter. Appl Note 1994;AN051.1:1–10.

[160] Olson W, Peura R, Webster JG, Clark J, Neuman M, Primiano F, et al. Medical Instrumentation: application and design. 4th ed. John Wiley & Sons Inc; 2010.

[161] Scrosati B, Garche J. Lithium batteries: Status, prospects and future. J Power Sources 2010;195:2419–30. doi:10.1016/j.jpowsour.2009.11.048.